1967

Neutron thermalization in water using spherical geometry

Mohamed Shawky Fahim Nassar
Iowa State University

NEUTRON THERMALIZATION IN WATER USING SPHERICAL GEOMETRY

by

Mohamed Shawky Fahim Nassar

A Dissertation Submitted to the
Graduate Faculty in Partial Fulfillment of
The Requirements for the Degree of
DOCTOR OF PHILOSOPHY

Major Subject: Nuclear Engineering

Approved:

Signature was redacted for privacy.
In Charge of Major Work

Signature was redacted for privacy.
Head of Major Department

Signature was redacted for privacy.
Dean of Graduate College

Iowa State University
Of Science and Technology
Ames, Iowa
1967

TABLE OF CONTENTS

I. INTRODUCTION

The subject of neutron thermalization concerns the manner in which the "neutron gas" comes into thermal equilibrium (if it ever does!) with the medium which contains it. Its analysis shows a nice interplay between theories of neutron transport and theories of the solid and liquid state, and is also reminiscent of the classical kinetic theory of gases. More precisely, it resembles the "foreign-gas" problem, where a small number of gas molecules is introduced into a large collection of molecules already in equilibrium at some temperature.

The thermalization problem might be compared with a particularly simple, linearized version of the kinetic theory of gases, were it not for the feature of chemical binding. In all but the simplest models, the atoms of the moderator interact with one another and the complicated motions which result produce a complex scattering pattern in the laboratory system.

Recently, the subject has assumed various and interesting fields of neutron physics. One of these, which received extensive theoretical and experimental considerations, is the field dealing with the integral part of the thermalization problem and which is the main interest of this thesis. In the integral experiments the concentration is on the temporal

change of the energy-integrated flux rather than on the details of neutron spectra.

The most eminent technique for these experiments is the pulsing technique introduced by Von Dardel (54). The theory behind the method is summarized in a consideration of a burst of fast neutrons injected in the moderator. When a sufficiently long time has elapsed after the initiation of the pulse the flux decays as $\exp(-\lambda t)$ where λ is the decay constant. A semi-log. plot of the flux, obtained by a "1/V" detector, versus time should give a straight line with a slope equal to $-\lambda$.

von Dardel and Sjöstrand (55) found that λ could be expressed in terms of power series of the square of the geometric buckling, B_g^2:

$$\lambda = \alpha + D_o B_g^2 + C B_g^4 + \text{---} \ldots$$

where α is the decay constant which would be observed in an infinite medium, D_o is the diffusion coefficient and C is the diffusion cooling constant that describes the cooling phenomenon due to the preferential leakage of the high-energy neutrons from a finite medium. Nelkin (38) has obtained these coefficients by a variational approach. He used the "neutron temperature" as a variational parameter. Singwi (48), and Purohit (43), applying the diffusion approximation, have determined D_o and C with the help of the Laguerre expansion.

The experimental values of α and D_o were obtained with good accuracy and the values measured by different experimenters are in agreement with each others and with the simplest model of diffusion theory. On the other hand, the data reported for C showed large discrepancies.

All pulse data available today have been obtained from multi-dimensional systems whose methods of analysis are, undoubtedly, complicated. To help in resolving the inconsistencies of the experimental values of the diffusion cooling constant, further work with spherical geometries is needed. This need has been emphasized by Gelbard et al. (24) because this shape would be amendable to theoretical interpretation and might yield more information on the thermalization parameters.

The purpose of this thesis is to study the feasibility of pulse experiments in spherical geometry. The study is based on both theoretical and experimental investigations. The former is treated in Chapter II while the latter is dealt with in Chapter V.

The theoretical model of the present work is the P_1-L_1 approximation developed in section II-A. In the next section the eigenvalue problem is defined and the behavior of the decay constants, as functions of the space eigenvalues, is studied. This study is felt to be of interest for two reasons. First, Travelli and Calame (52) pointed out that the plot of

the fundamental time-eigenvalue, as obtained by a 4-group P_1 approximation, versus the space eigenvalue gave a curve with a positive curvature at the origin in disagreement with the experimental results. The study is aimed to clarify the nature of this contradiction. Second, some understanding of the eigenvalue spectrum is needed to test the feasibility of the commonly used expansion of the decay constant in power series of the geometric buckling. The results inferred from this study are used in verifying the treatment in section II-C where the various diffusion parameters are derived.

In section II-D the space-energy dependence of the eigenfunctions is examined together with the concept of a unique buckling. Equations for the computation of the diffusion-cooled neutron spectra for the asymptotic and the transient distributions are developed. These equations are made use of, in section II-E, to calculate the spectrum-weighted average energy and effective buckling for a sphere.

The space-dependence of the extrapolation distances for a spherical geometry are compared with those of an "equivalent slab" in section II-F. The Marshak's boundary condition is used for the system-vacuum interface.

In the experimental part two different investigations of the die-away experiments are described. Section V-A deals with the determination of the diffusion parameters. The extrapolation distances for five spherical geometries are determined in section V-B.

II. GENERAL THEORY

A. The P_1-L_1 Equation in Spherical Geometry

1. The P_1 equation

The source-free integro-differential form of the Boltzmann transport equation describing the time, space, energy and angular dependence of neutron flux in a sphere of homogeneous materials is

$$\frac{1}{V}\frac{\partial\phi(r,E,\mu,t)}{\partial t} + \mu\frac{\partial\phi(r,E,\mu,t)}{\partial r} + \frac{(1-\mu^2)}{r}\frac{\partial\phi(r,E,\mu,t)}{\partial\mu}$$

$$+ \Sigma_T\phi(r,E,\mu,t) = 2\pi\int_{-1}^{1}\int_{E'}\Sigma_s(\mu_o,E'\rightarrow E)\phi(r,E',\mu',t)d\mu'dE' \qquad (2.1)$$

where

$\phi(r,E,\mu,t)$ = The angular flux

$\Sigma_s(\mu_o,E'\rightarrow E)$ = The scattering kernel

$= \Sigma_s(\mu'\rightarrow\mu,E'\rightarrow E)$

μ = Direction cosine

Σ_T = Total macroscopic cross section

The solution of 2.1 should be made to satisfy the usual boundary conditions of transport theory, namely:

a. The neutron flux must be finite and non-negative in all regions of the medium since the medium contains no sources.

b. At the outer boundary, which faces a vacuum, there must be no neutrons returning to the medium from

the vacuum.

Since $\phi(r,E,\mu,t)$ is time dependent, an initial condition must also be stated to solve the problem completely. However this study is concerned only with the relative behavior of the angular flux as a function of the system size and some reference time; hence the complete solution of the problem is not required.

The angular dimension of 2.1 may be removed in the usual manner by expanding the angular flux and the scattering kernel in Legendre polynomials

$$\phi(r,E,\mu,t) = \sum_m \frac{(2m+1)}{4\pi} \phi_m(r,E,t)P_m(\mu) \qquad (2.2.a)$$

$$\Sigma_s(\mu_o,E'\rightarrow E) = \sum_m \frac{(2m+1)}{4\pi} \Sigma_{sm}(E'\rightarrow E)P_m(\mu_o) \qquad (2.2.b)$$

This yields, after the insertion of the angular expansion, making use of the addition theorem of Legendre polynomials, multiplying through by $P_n(\mu)$ and integrating over $-1\leq\mu\leq 1$:

$$(n+1)[\frac{\partial}{\partial r} + \frac{(n+2)}{r}]\phi_{n+1}(r,E,t) + n[\frac{\partial}{\partial r} - \frac{(n-1)}{r}]\phi_{n-1}(r,E,t)$$

$$+ (2n+1)[(\Sigma_T + \frac{1}{V}\frac{\partial}{\partial t})\phi_n(r,E,t) - S_n\phi_n(r,E',t)] = 0 \qquad (2.3)$$

where $n = 0,1,2,\ldots N$ for an N^{th} order angular approximation,

$$S_n\phi_n(r,E',t) = \int_{E'=0}^{\infty} \Sigma_{sn}(E' \rightarrow E)\phi_n(r,E',t)dE' \qquad (2.4)$$

and

$$\phi_{-1}(r,E,t) = 0$$

By direct substitution, it can be shown that the solution of 2.3 is of the form

$$\phi_n(r,E,t) = F_n(B,E,\lambda)j_n(Br)e^{-\lambda t} + G_n(B,E,\lambda)n_n(Br)e^{-\lambda t} \qquad (2.5)$$

where $j_n(Br)$ and $n_n(Br)$ are the n^{th} order spherical Bessel functions of first and second type respectively. The parameter B is a space eigenvalue and λ is a time eigenvalue.

The asymptotic limits for spherical Bessel functions with small arguments are:

$$j_n(Br) \xrightarrow[r \rightarrow 0]{} \frac{(Br)^n}{1 \cdot 3 \cdot 5 \cdots (2n+1)}$$

$$n_n(Br) \xrightarrow[r \rightarrow 0]{} \frac{1 \cdot 3 \cdot 5 \cdots (2n+1)}{(Br)^{n+1}}$$

Since $n_n(Br)$ contains the argument in the denominator of its limit, it is seen that it would violate the first boundary condition, while j_n does not. Therefore the arbitrary constant $G_n(Br)$ must be set identically equal to zero and $\phi_n(r,E,t)$ becomes:

$$\phi_n(r,E,t) = F_n(B,E,\lambda)j_n(Br)e^{-\lambda t} \qquad (2.6)$$

The substitution of $\phi_n(r,E,t)$ as given by 2.6 into 2.3 gives a set of N + 1 homogeneous coupled equations relating the F_n's for an N^{th} order approximation:

$$(n+1)BF_{n+1}(B,E,\lambda) - nBF_{n-1}(B,E,\lambda) + (2n+1)[(\Sigma_T - \tfrac{\lambda}{V})F_n(B,E,\lambda) - S_nF_n(B,E',\lambda)] = 0 \qquad (2.7)$$

In the P_1 approximation, this set takes the form

$$BF_1(B,E,\lambda) + [(\Sigma_T - \tfrac{\lambda}{V})F_0(B,E,\lambda) - S_0F_0(B,E',\lambda)] = 0 \qquad (2.8.a)$$

$$-BF_0(B,E,\lambda) + 3[(\Sigma_T - \tfrac{\lambda}{V})F_1(B,E,\lambda) - S_1F_1(B,E',\lambda)] = 0 \qquad (2.8.b)$$

The P_1 component of the scattering kernel can be approximated by

$$\Sigma_{s1}(E'\rightarrow E) \simeq \bar{\mu}(E)\Sigma_{so}(E'\rightarrow E)\delta(E'-E)$$

where $\delta(E'-E)$ is the Dirac delta function and $\bar{\mu}$ is the average of the cosine of the scattering angle.

With the above approximation the integral S_1F_1 becomes

$$S_1F_1(B,E',\lambda) \simeq \Sigma_{so}(E)\bar{\mu}F_1(B,E,\lambda) \qquad (2.9)$$

The substitution of this expression into 2.8 gives

$$F_1(B,E,\lambda) = BF_0(B,E,\lambda)/3(\Sigma_{TR} - \tfrac{\lambda}{V}) \qquad (2.10.a)$$

$$[B^2/3(\Sigma_{TR} - \frac{\lambda}{V}) + \Sigma_T - \frac{\lambda}{V}]F_o(B,E,\lambda) = S_o F_o(B,E',\lambda) \qquad (2.10.b)$$

where

$$\Sigma_{TR}(E) = \Sigma_a(E) + \Sigma_{so}(E)[1 - \bar{\mu}(E)] \qquad (2.11)$$

The set 2.10 is closely related to that obtained by Nelkin (39) and Vértes (53) for an infinite slab using the Fourier transform. However, the above formalism has an advantage over Nelkin's; namely, the Fourier transform implies an infinite medium. By finding the set of eigenvalues of 2.10:

$$B_o, B_1, \text{-----} B_k$$

one can write down the total solution of 2.8 which will satisfy the boundary conditions of a finite sample.

2. Limiting value of the decay constant

According to Corngold and others (11-14) the discrete eigenvalues of the decay constant, λ, are limited by

$$\lambda_{lim.} = (V\Sigma_{s,in.})_{min.} \qquad 2.12)$$

where $\Sigma_{s,in.}$ is the macroscopic inelastic scattering cross section for neutrons of speed V. The minimum theoretical value of $V\Sigma_{s,in.}$ occurs for $V \to 0$, and for water it is close to 300,000 $sec.^{-1}$. As Corngold and Michael (14) pointed out, the experimental values of the fundamental decay constant

exceed this limit in many cases. This means that if the experimental points are correct, they stand in direct contradiction to rather direct consequences of the Boltzmann equation. It is perhaps more reasonable to look at the problem from a different point of view.

In 2.10.b, $F_0(B,E,\lambda)$ is recognized as the energy component of the scalar flux at a given B and λ. For this component to be real and finite the following should hold.

$$\lambda < [VB^2/3(\Sigma_{TR} - \frac{\lambda}{V}) + V(\Sigma_s + \Sigma_a)]_{E_o} = \lambda_{lim.} \qquad (2.13)$$

where E_o corresponds to the energy at which the quantities in brackets are at a minimum. Equation 2.13 explains why the experimental decay constant exceeds Corngold's limit in some cases. In case of water, however, both the absorption and the transport cross section behave like 1/V for small V and 2.13 would reduce to Corngold's limit as $V \to 0$ provided that $(V\Sigma_s)_{E_o}$ is recognized as $(V\Sigma_{s,in.})_{E_o}$.

From the foregoing one concludes that $\lambda_{lim.}$ is a separating point between two types of spectra:

a. A discrete set of eigenvalues and a corresponding discrete spectrum of eigenfunctions in the range

$$\lambda < \lambda_{lim.}$$

b. A continuum of eigenvalues in the range

$$\lambda > \lambda_{lim.}$$

The corresponding eigenfunctions are given by

$$F_0(B,E,\lambda) = P\left[\frac{\int_0^\infty \Sigma_{so}(E'\to E)F_0(B,E',\lambda)dE'}{(B^2/3(\Sigma_{TR} - \frac{\lambda}{V}) + \Sigma_T - \frac{\lambda}{V})}\right]$$

$$+ g(\lambda)\delta(\frac{\lambda}{V} - \Sigma_T + \frac{B^2}{3(\Sigma_{TR} - \frac{\lambda}{V})} \qquad (2.14)$$

where P implies the principal value of the integral when the denominator appears as the integrand. The delta functions give the contribution of singularities other than the poles.

By the principle of superposition, the solution of the P_1 equation becomes

$$\phi_n(r,E,t) = j_n(Br)[\sum_{i=0}^{M} F_{ni}(B,E,)e^{-\lambda_i t} + \int_{\lambda_{lim.}}^{\infty} F_n(B,E,\lambda)e^{-\lambda t}d\lambda]$$

$$;n = 1,2 \qquad (2.15)$$

where M stands for the number of the discrete eigenvalues and the integral gives the contribution of the continuum.

Only for a proton gas case does there exist a satisfactory discussion of the character of the time eigenvalues associated with the energy modes, as given by Corngold et al. (14).

According to these authors the number of discrete eigenvalues between zero and $\lambda_{lim.}$ is infinite for an infinite medium. Shapiro (47) has obtained extensive numerical results

for the existence and convergence of discrete eigenvalues for the monatomic gas model. Numerical results for the eigenvalues of the bound proton model have been obtained by Ohanian and Daitch (41) using the diffusion approximation. The quoted paper indicated that the first eigenvalue always exists for a finite medium. There are also strong indications that there is always at least a second eigenvalue even though it may lie close to the limiting decay constant. Recently the thermal neutron space-time eigenvalue spectrum of the multi-group P_N approximations were investigated numerically by Travelli et al. (52), for a modified form of Radkowsky kernel. Both discrete and continuous eigenvalues were found.

3. Expansion of energy eigenfunctions in orthogonal polynomials

Expansion of $F_n(B,E)$ in a complete set of orthogonal polynomials allows the solution of the eigenvalue problem. The choice of these polynomials is arbitrary. The Laguerre polynomials have been used widely, as they are the exact eigenfunctions of the Wilkin's heavy gas scattering operator. Let

$$F_n(B,E) = \sum_{k=0}^{\infty} M(E) F_n^{k}(B) L_k^{(1)}(E), \tag{2.16}$$

$$\Sigma_a(E) = \Sigma_{a_o}\sqrt{E} \text{ (1/V absorber)} \tag{2.17}$$

$$\Sigma_{TR}(E) = \Sigma_{TRo}/\sqrt{E} \text{ (1/V transport cross section)} \quad (2.18)$$

and

$$V = V_o\sqrt{E} \quad (2.19)$$

where E is a dimensionless energy variable expressed in units of KT,

$$M(E) = \text{Maxwellian neutron distribution} = E\, e^{-E} \quad (2.20)$$

$$L_k^{(1)}(E) = \text{Associated Laguerre polynomials of first order} = (k+1)\sum_{P=0}^{k} \frac{(-1)^P k!}{P!(1+P)!(k-1)!} E^P \quad (2.21)$$

Σ_{ao} = Absorption cross section at room temperature

Σ_{TRo} = Transport cross section at room temperature

V_o = Neutron speed at room temperature
$= 2.2 \times 10^5$ cm/sec.

By rewriting the scattering cross section in the integral form

$$\Sigma_{so}(E) = \int_0^\infty \Sigma_{so}(E' \to E)dE' \quad (2.22)$$

and substituting 2.16 through 2.22 into 2.10, one gets

$$\sum_{k=0} [(-V_o\sqrt{E}\, B^2/3(V_o\Sigma_{TRo} - \lambda) + (\lambda/V_o - \Sigma_{ao}))M(E)L_k^{(1)}(E)$$

$$+ \int_0^\infty (L^{(1)}_k(E')M(E')\Sigma_{so}(E'\to E) - L^{(1)}_k(E)M(E)\Sigma_{so}(E\ E'))dE']F_0^k(B)$$

$$= 0 \qquad (2.23.a)$$

$$\sum_{k=0}^{\infty} M(E)(F_1^k(B) - V_oBF_0^k(B)/3(V_o\Sigma_{TRo} - \lambda))L^{(1)}_k(E) = 0 \qquad (2.23.b)$$

According to the detailed balance theorem of statistical mechanics,

$$M(E')\Sigma_{so}(E'\to E) = \Sigma_{so}(E')M(E')H(E'\to E)$$

$$= \Sigma_{so}(E)M(E)H(E\to E') \qquad (2.24)$$

where $H(E'\to E)dE$ is the probability that a neutron suffering a scattering collision at E' shall have an energy E in dE. By expanding

$$L^{(1)}_k(E') = L^{(1)}_k(E) + \sum_{P=1} \frac{d^P L^{(1)}_k(E)}{dE^P} \frac{(E' - E)^P}{P!}$$

and using the above results, the scattering terms can be expressed as a sum of energy transfer moments:

$$\int_0^\infty [L^{(1)}_k(E')M(E')\Sigma_{so}(E'\to E) - L^{(1)}_k(E)M(E)\Sigma_{so}(E\to E')]dE'$$

$$= \sum_{P=1} \frac{1}{P!} \frac{d^P L^{(1)}_k(E)}{dE^P} M(E)\Sigma_{so}(E)A_P(E) \qquad (2.25.a)$$

$$A_p(E) = \int_0^\infty (E' - E)^P H(E' \to E) dE' \qquad (2.25b)$$

$= P^{th}$ energy transfer moment

By substituting 2.25 into 2.23, multiplying through by $L^{(1)}_i(E)$ and integrating over E, one gets

$$\sum_{k=0}^{\infty} [t_{ik} B^2/3 + (K/V_o) W_{ik} + F_{ik}] F_0{}^k(B) = 0 \qquad (2.26.a)$$

$$F_1{}^i(B) = \frac{B^2}{3} \sum_{k=0}^{\infty} t_{ik} F_0{}^k(B) \qquad (2.26.b)$$

where

$$t_{ik} = V_o \int_0^\infty [\sqrt{E}\, M(E) L^{(1)}_i(E) L^{(1)}_k(E) / (V_o \Sigma_{tro} - K)] dE$$

$$= V_o v_{ik} / (V_o \Sigma_{tro} - K), \qquad (2.27)$$

$$v_{ik} = \int_0^\infty \sqrt{E}\, M(E) L^{(1)}_i(E) L^{(1)}_k(E) dE$$

$$\Sigma_{tro} = \Sigma_{TRo} - \Sigma_{ao}$$

$=$ Transport cross section for zero absorption

$$= \Sigma_{so}(1 - \bar{\mu}) \qquad (2.28)$$

$$w_{ik} = \int_0^\infty (1/\sqrt{E}\,) M(E) L^{(1)}_i(E) L^{(1)}_k(E) dE \qquad (2.29)$$

$$K = \lambda - V_o \Sigma_{ao} \qquad (2.30)$$

$$F_{ik} = \sum_P \frac{1}{P!} \left[\int_0^\infty dE \frac{d^P L^{(1)}_i(E)}{dE^P} M(E) L^{(1)}_k(E) \Sigma_{so} A_P(E) \right] \qquad (2.31)$$

Some values for w_{ik} and v_{ik} are listed in Table 2.1 and 2.2 respectively.

Equation 2.26 is the P_l-L_k equation in spherical geometry. For the L_1 approximation it reduces to

$$(t_{00}B^2/3 - Kw_{00}/V_o)F_0^0(B) + (t_{01}B^2/3 - Kw_{01}/V_o)F_0^1(B) = 0 \qquad (2.32.a)$$

$$(t_{10}B^2/3 - Kw_{01}/V_o)F_0^0 + (t_{11}B^2/3 - Kw_{11}/V_o + |F_{11}|)F_0^1(B) = 0 \qquad (2.32.b)$$

$$F_1^0(B) = \frac{B}{3}(t_{00}F_0^0(B) + t_{01}F_0^1(B) \qquad (2.33.a)$$

$$F_1^1(B) = \frac{B}{3}(t_{01}F_0^0(B) + t_{11}F_0^1(B) \qquad (2.33.b)$$

where

$$F_{11} = -M_2/4 \ , \qquad (2.34.a)$$

$$M_2 = \int_0^\infty \int_0^\infty (E' - E)^2 \Sigma_{so}^{(E)} M(E) H(E \to E') dE' dE \qquad (2.34.b)$$

= Second energy transfer moment.

Equation 2.32 is a set of homogeneous equations. The roots of the characteristic equation are the possible values of B^2.

Table 2.1. Values[a] of w_{ik}

w_{00}	w_{01}	w_{02}	w_{03}	w_{11}	w_{12}	w_{13}	w_{22}
0.8862	0.3134	0.1919	0.1384	0.7754	0.3392	0.2252	0.7061

[a]From Purohit (43).

Table 2.2. Values of v_{ik}

v_{00}	v_{01}	v_{11}
1.330	-0.471	1.828

For other values of v_{ik} use is made of the relations

$$v_{ik} = v_{00}[(w_{ik}/w_{00}) - T_{ik}],\ T_{ik} = [(w_{ik}/w_{00}) - (v_{ik}/v_{00})]$$

Table 2.3. Values[a] of T_{ik}

T_{00}	T_{01}	T_{02}	T_{03}	T_{11}	T_{12}	T_{13}
0.0	0.7071	0.2887	0.1882	-0.5505	0.8674	0.3540

[a]From Perez (42).

4. Matrix elements and associated integrals

The success of the P_l-L_k equation in interpreting the experimental data depends on how accurately the matrix elements F_{ik} of the scattering operator are determined. For P_1-L_1, only the element F_{11} is required.

The elements can be obtained from the related energy transfer moments M_{kp} or their associated integrals.

Nelkin (38) was the first to introduce M_{20} or (M_2) in estimating the thermalization parameters, by the use of variational principles. Using the detailed balance theorem, Purohit (44) gave recurrence formulas.

The values of the energy transfer moments depend on the scattering model used. For water, four models are tried in this thesis. These are:

a. Hydrogen gas: The motions of the protons in water are like a free gas (58) with no binding between protons and oxygen.

b. Mass-18 gas: The water molecules are considered as rigid structures and replaced by a gas of point particles with mass 18.

c. Brown-St.John (6): The water molecules are treated as rigid structures free to rotate. The rotator is then replaced by a free point particle with an "effective rotational mass" of 1.88. The model utilizes a trial cross section that contains adjustable

parameters so that the computed scattering cross section can be fitted to the experimental cross section.

d. The Nelkin water (40): The dynamics of protons in water are described by three harmonic oscillators, two for the vibrational levels at 0.205 ev and 0.48 ev and one for the hindered rotation at 0.06 ev. The motions of the molecules are described by a mass-18 gas.

The second energy transfer moment, M_2, for the above mentioned models is listed in Table 2.4. In all these cases a free gas kernel with mass 16 was considered to approximate the scattering from oxygen.

Throughout the remainder of this work, whenever there is a choice among the above models, the Nelkin water model will be the one selected. This is justified on the basis that this kernel predicts infinite medium spectra in good agreement with spectra measured by Beyster (5) over a wide range of poison types and concentrations. The kernel also gives diffusion coefficients and cooling coefficients in good agreement with values measured by Star and Koppel (49). Detailed comparisons of the Nelkin kernel with measurements by Eglestaff et al. (21) have been made by Goldman and Federighi (25). They found reasonable agreement between the theoretical predictions of the model and the experimental results at

Table 2.4. Second energy moment of the isotropic scattering kernel[a]

$$M_2 = \int_0^\infty \int_0^\infty M(E')\Sigma_{so}(E')H(E' \rightarrow E)(E - E')^2 dE dE'$$

Kernel	$M_2(cm^{-1})$
H gas	3.85
Mass 18	0.67
Brown & St.John	5.23
Nelkin	3.34

[a]From Honeck (27).

all but small values of energy and moment transfer. Fortunately this region contributes little to the total cross section or to the energy transfer moments. Finally, the Nelkin water gives a total cross section over the entire thermal energy range.

B. Time Eigenvalues

A study of the eigenvalue spectra in the multigroup P_N approximations (15, 52) indicated the possibility of a traveling wave phenomenon at large bucklings. This work is extended here to the P_1-L_1 approximation for two reasons. First, Travelli and Calame (52) pointed out that the fundamental eigenvalue curve in the (λ, B^2) plane, in a 4-group P_1 approxi-

mation, contradicts the experimental results in having a positive curvature at the origin. This study will explain the nature of this contradiction. Second, the split of energy into few groups does not reflect the usual diffusion cooling phenomena (15). The diffusion cooling is obtained in the continuous energy representation by expanding the lowest eigenvalue in power series of B^2. The radius of convergence of this expansion is evaluated by a knowledge of the eigenvalue spectra.

The eigenvalue problem relevant to this study is

$$\begin{bmatrix} (t_{00}B^2/3 - Kw_{00}/V_o) & (t_{01}B^2/3 - Kw_{01}/V_o) \\ (t_{10}B^2/3 - Kw_{01}/V_o) & (T_{11}B^2/3 - Kw_{11}/V_o + |F_{11}|) \end{bmatrix} \begin{bmatrix} F_0^0(B) \\ F_0^1(B) \end{bmatrix} = 0 \tag{2.35}$$

Since equation 2.35 consists of two linear homogeneous equations, the eigenvalues are fixed by the condition that the determinant of the coefficients must vanish, i.e., by the equation

$$Q(K,B^2) = (t_{00}B^2/3 - Kw_{00}/V_o)(t_{11}B^2/3 - Kw_{11}/V_o + |F_{11}|) - (t_{10}B^2/3 - Kw_{01}/V_o)^2 = 0 \tag{2.36}$$

where K is related to λ by 2.30.

The function $Q(K,B^2)$ is a polynomial in B^2 of degree 2 and for a fixed B^2 it is a polynomial of degree 4 in K. In

general, for a P_N-L_M approximation there is a polynomial of degree $\frac{1}{2}M(N+1)$ in B^2 and of degree $M(N+1)$ in K.

The expansion of 2.36 gives

$$\begin{aligned} Q(K,B^2) = {} & 3K^4(w_{00}w_{11} - w_{01}^2) \\ & -3K^3V_o[2\Sigma_{tro}(w_{00}w_{11} - w_{01}^2) + w_{00}|F_{11}|] \\ & + K^2V_o^2[B^2(v_{11}w_{00} - 2v_{01}w_{01} + v_{00}w_{11}) \\ & \quad + 3\Sigma_{tro}^2(w_{00}w_{11} - w_{01}^2) + 6\Sigma_{tro}w_{00}|F_{11}|] \\ & - KV_o^3[\Sigma_{tro}B^2(v_{11}w_{00} - 2v_{01}w_{01} + v_{00}w_{11}) \\ & \quad + |F_{11}|(3\Sigma_{tro}^2w_{00} + B^2v_{00})] \\ & + B^2V_o^4[\frac{B^2}{3}(v_{00}v_{11} - v_{01}^2) + \Sigma_{tro}v_{00}|F_{11}|] = 0 \end{aligned} \tag{2.37}$$

First estimates of the roots of $Q(K,B^2)$ were obtained by plotting this function versus K at specified values of B^2. Some of these plots are indicated in Figure 2.1. These roots were then taken as first trial values in Newton Raphson method (33). Iterations were carried out on the IBM-360 computer until the desired accuracy was obtained. Values of the various cross sections used in the numerical calculation are given in the Appendix.

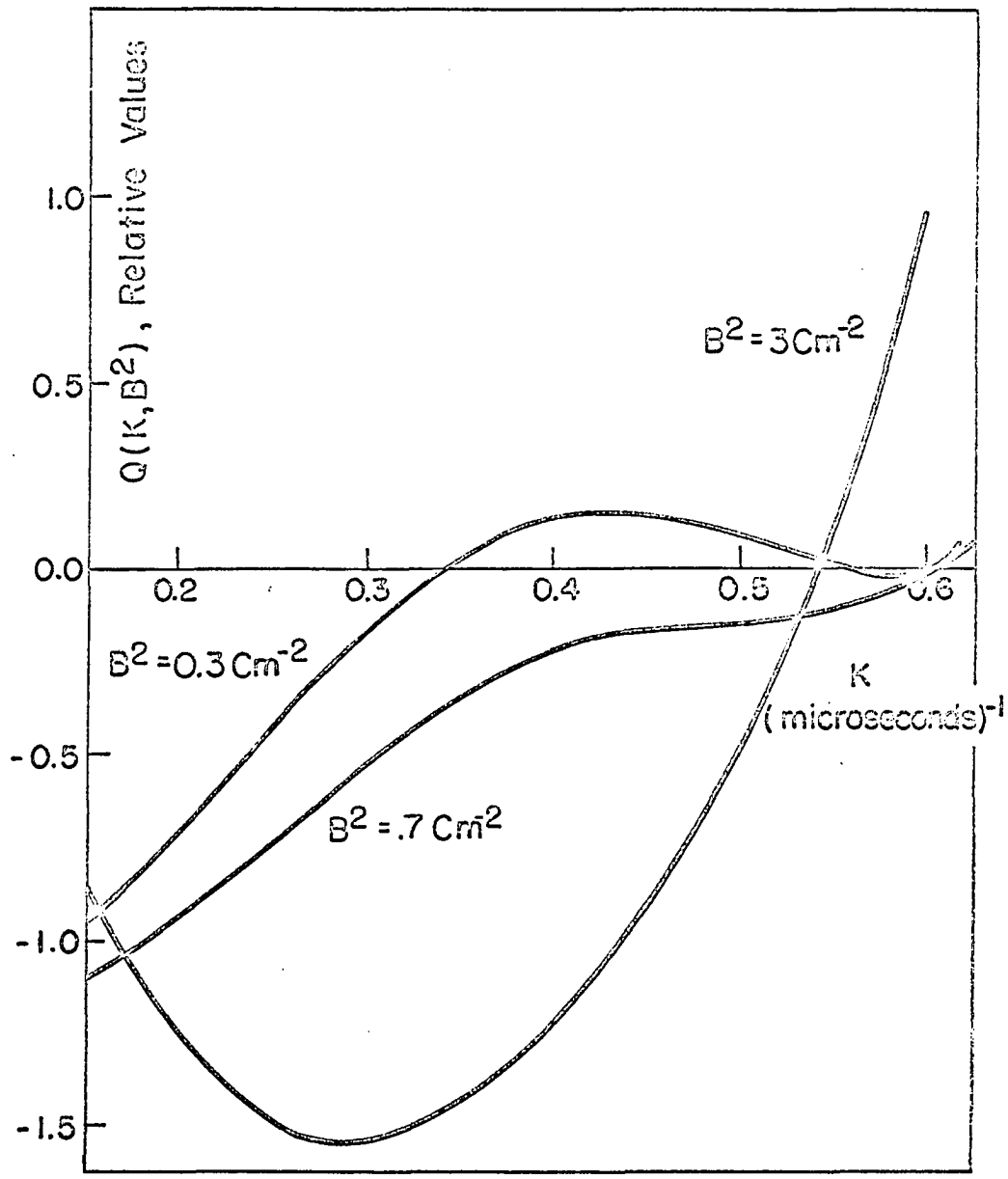

Figure 2.1. Roots of the polynomial, $Q(K,B^2)$, for various values of B^2 and $M_2 = 3.34\ cm^{-1}$

A study was made using the four scattering models listed in Table 2.4. The results are given in Table 2.5, 2.6, 2.7 and 2.8. The corresponding curves are shown in Figure 2.2, 2.3, 2.4 and 2.5 respectively. For the sake of comparison results obtained by the diffusion theory approximation are also listed in the respective tables. These tables show a number of features of interest:

a. The diffusion approximation gives only two eigenvalues compared to 4 in the P_1-L_1 approximation. This is because the latter approximation has the form of the telegrapher's equation (57) and differs from the diffusion equation by an additional term containing the second order time derivative.

b. The diffusion theory curves indicate that the decay constants increase indefinitely in direct proportion to B^2 and are always real. This behavior stems from the linear relationship between B^2 and K. For the P_1-L_1 approximation, on the other hand, there exist two limiting values of B^2, $B^2_{1,max.}$ and $B^2_{2,max.}$ such that:

   i. For $B^2 < B^2_{1,max.}$, all eigenvalues, K, are real.

   ii. For $B^2 > B^2_{2,max.}$, all eigenvalues are complex.

   iii. For $B^2_{1,max.} < B^2 < B^2_{2,max.}$, two real eigenvalues exist.

Table 2.5. The tabular entries give the decay constants in (microseconds)$^{-1}$ for $M_2 = 0.67$ cm^{-1}, the bucklings and theories indicated

B^2	P_1-L_1				Diff. Theory	
	K_0	K_1	K_2	K_3	K_0	K_1
0.0Cm^{-2}	.000000	.05342	.6216	.6286	.000000	.05342
.025	.000958	.05812	.62080	.62712	.000949	.05787
.05	.001898	.06067	.62000	.62500	.001878	.06014
.10	---	---	.6163	.62150	---	---
.20	.007218	.07698	.6022	.6214	.007089	.07414
.30	.01530	.08883	.5992	.6177	.010295	.08374
.40	.013920	.09923	.5762	.6152	---	---
.50	.016790	.11508	.56310	.6120	.016278	.10336
.70	.022757	.14560	.5309	.6078	.021883	.12337
.90	.028576	.18256	---	---	.027249	.14361
1.0	.032960	.20410	.4698	.6046	---	---
2.0	.060563	-**	-**	.5728	.054918	.25680
3.0	.092150	-**	-**	.5420	.079094	.36068
4.0	.127241	-**	-**	.5057	---	---
5.0	.173318	-**	-**	.4612	.126717	.56916
6.0	.240806	-**	-**	.394	.150387	.67354
7.0	-**	-**	-**	-**	---	---
- .50	-.024300	.01600	.676	.6377	-.025918	.01751
-1.50	-.09700	-.01900	.7629	.658	-.116506	-.01996
-2.0	-.132500	-.03100	.8011	.67	-.167261	-.03323
-2.5	---	-.04250	.8327	.6808	-.218704	-.04581
-3.0	---	-.05300	.8663	.691	-.270457	.05809

**The root has a complex value.

Table 2.6. The tabular entries give the decay constants in $(\text{microseconds})^{-1}$ for $M_2 = 3.34\text{cm}^{-1}$, the bucklings and theories indicated

B^2	P_1-L_1				Diff. Theory	
	K_0	K_1	K_2	K_3	K_0	K_1
0.0cm^{-2}	.000000	.27642	.62150	.63000	.000000	.27642
.025	.000967	.28052	---	---	.000958	.27866
.050	.001933	.28474	.61570	.62500	.001912	.28091
.100	---	---	.60670	.62330	---	---
.150	.005780	.30299	---	---	.005684	.28994
.200	.007686	.31314	.58650	.62050	.007545	.29449
.300	.011512	.33642	.56200	.61720	.011220	.30362
.400	---	---	.53050	.61450	---	---
.500	.019089	.42126	---	---	.018393	.32705
.700	.026609	-**	-**	.60680	.025350	.34071
.900	.034087	-**	-**	---	.032115	.35955
1.000	---	-**	-**	.59875	---	---
2.000	.075289	-**	-**	.56880	.066690	.46584
3.000	.114870	-**	-**	.53450	.095517	.56506
4.000	---	-**	-**	.49340	---	---
5.000	.219162	-**	-**	.43770	.149238	.76745
6.000	-**	-**	-**	.33000	.174970	.86977
7.000	-**	-**	-**	-**	---	---
-0.500	-.017400	.21180	.69810	.63840	-.020185	.23258
-1.500	-.061500	.12470	.80190	.66170	-.068173	.15251
-2.000	-.083600	---	.84430	.67290	-.097122	.11744
-2.500	-.106300	.06780	.88250	.68370	-.12985	.08614

**The root has a complex value.

Table 2.7. The tabular entries give the time eigenvalues, K, in $(\text{microseconds})^{-1}$ for $M_2 = 3.85\ \text{cm}^{-1}$, the bucklings and theories indicated

B^2	P_1-L_1				Diff. Theory	
	K_0	K_1	K_2	K_3	K_0	K_1
.0cm^{-2}	0.000000	.31394	.62250	.62730	.000000	.31394
.025	.000967	.32836	.61931	.62584	.000958	.32104
.050	.001934	.33321	.61500	.62350	.001913	.32328
.150	.005791	.35477	.59413	.62184	---	---
.200	.007715	.36729	.57670	.62001	.007563	.33684
.300	.011553	.39864	.54640	.61710	.011258	.34595
.500	.019200	-**	-**	.61200	.018492	.36433
.700	.026817	-**	-**	.60672	.025532	.38290
.900	.034418	-**	-**	.59985	.032396	.110164
2.000	.076627	-**	-**	.56812	.067665	.50723
3.000	.117461	-**	-**	.53350	.097155	.60580
5.000	.226681	-**	-**	.43211	.151995	.80706
6.00	-**	-**	-**	-**	.178175	.90893
- .500	-.019800	.25091	.70400	.63750	-.020044	.27481
-1.500	-.061900	.15550	.81210	.66200	-.066462	.19318
-2.000	-.081400	.12250	.85600	.67320	-.093730	.15642
-2.500	-.10300	.09810	.89460	.68400	-.124179	.12284
-3.000	-.125500	.07102	---	.69409	-.157929	.09257

**The root has a complex value.

Table 2.8. The tabular entries give the time eigenvalues, K, in $(\text{microseconds})^{-1}$ for $M_2 = 5.23\ \text{cm}^{-1}$, the bucklings and the theories indicated

B^2	P_1-L_1				Diff. Theory	
	K_0	K_1	K_2	K_3	K_0	K_1
0.0cm^{-2}	.000000	.43300	.62181	.63853	.000000	.43300
.025	.000968	.44066	.61923		.000959	.43529
.050	.001936	.44909	.60720	.62450	.001915	.43749
.150	.005809	.50411	.55512		.005712	.44650
.200	.007747	-**	-**	.62012	.007594	.45102
.300	.011625	-**	-**	.61730	.011326	.46009
.500	.019396	-**	-**	.61203	.018670	.47836
.700	.027194	-**	-**	.60610	.025861	.49678
.900	.035028	-**	-**	.59987	.032911	.51534
2.000	.079298	-**	-**	.56620	.069561	.61955
3.000	.123000	-**	-**	.53000	.100498	.71667
5.000	.246103	-**	-**	.41790	.157991	.91527
6.000	-**	-**	-**	-**	.285304	1.01601
- .500	-.019300	---	.72680	.63870	-.019810	.38879
-1.500	-.058200	.23415	.84550	.66310	-.063741	.30466
-2.000	-.078000	.19690	.89050	.67440	-.088352	.26525
-2.500	-.097600	.16500	---	.68530	-.115049	.22792
-3.000	-.122400	.13770	---	.69620	-.144030	.19288

**The root has a complex value.

Figure 2.2. Eigenvalue curves for $M_2 = 0.67\ cm^{-1}$ and the theories indicated

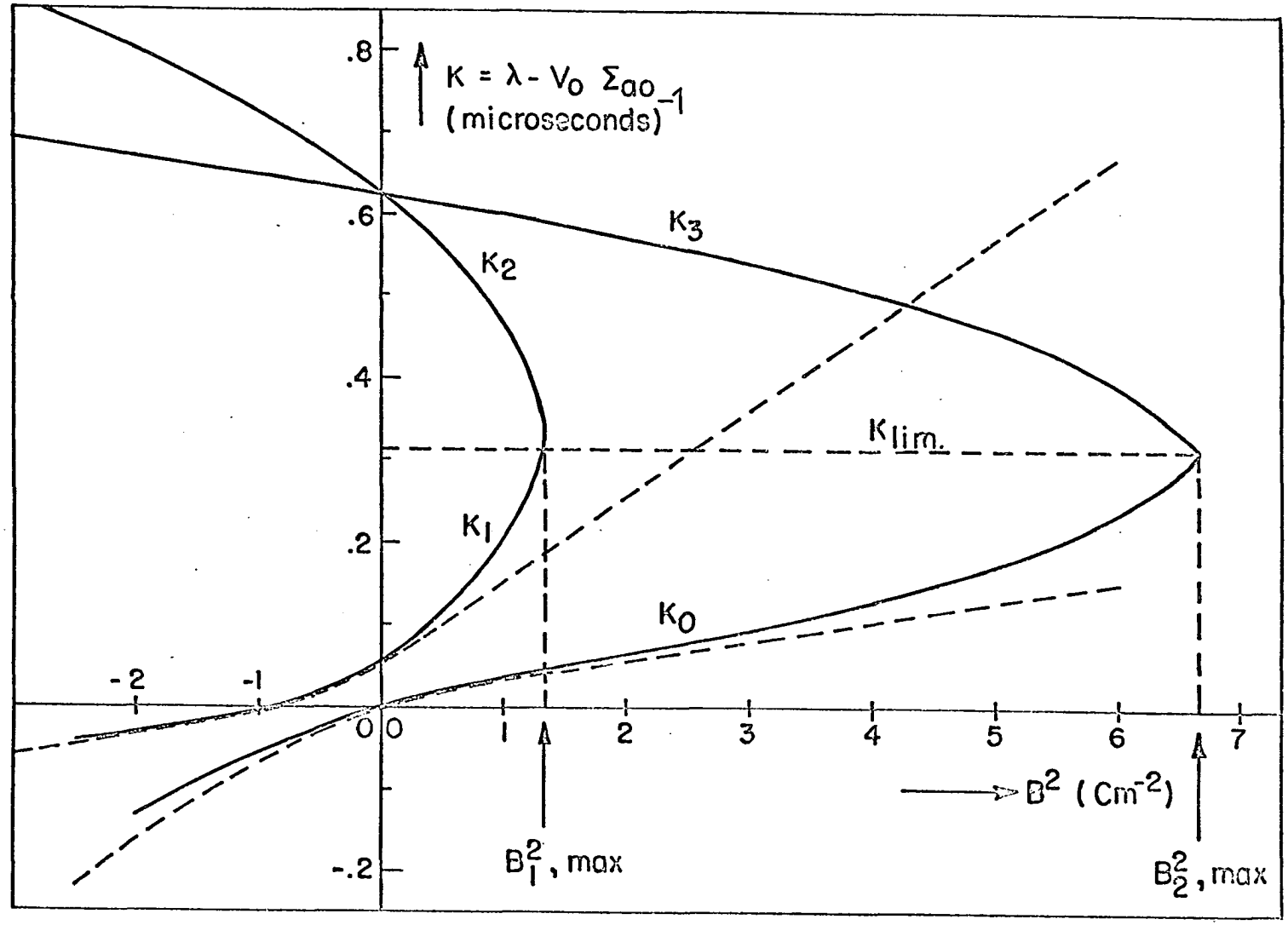

——— P_1-L_1 approximation ------ Diffusion approximation

Figure 2.3. Eigenvalue curves for $M_2 = 3.34\ cm^{-1}$ and the theories indicated

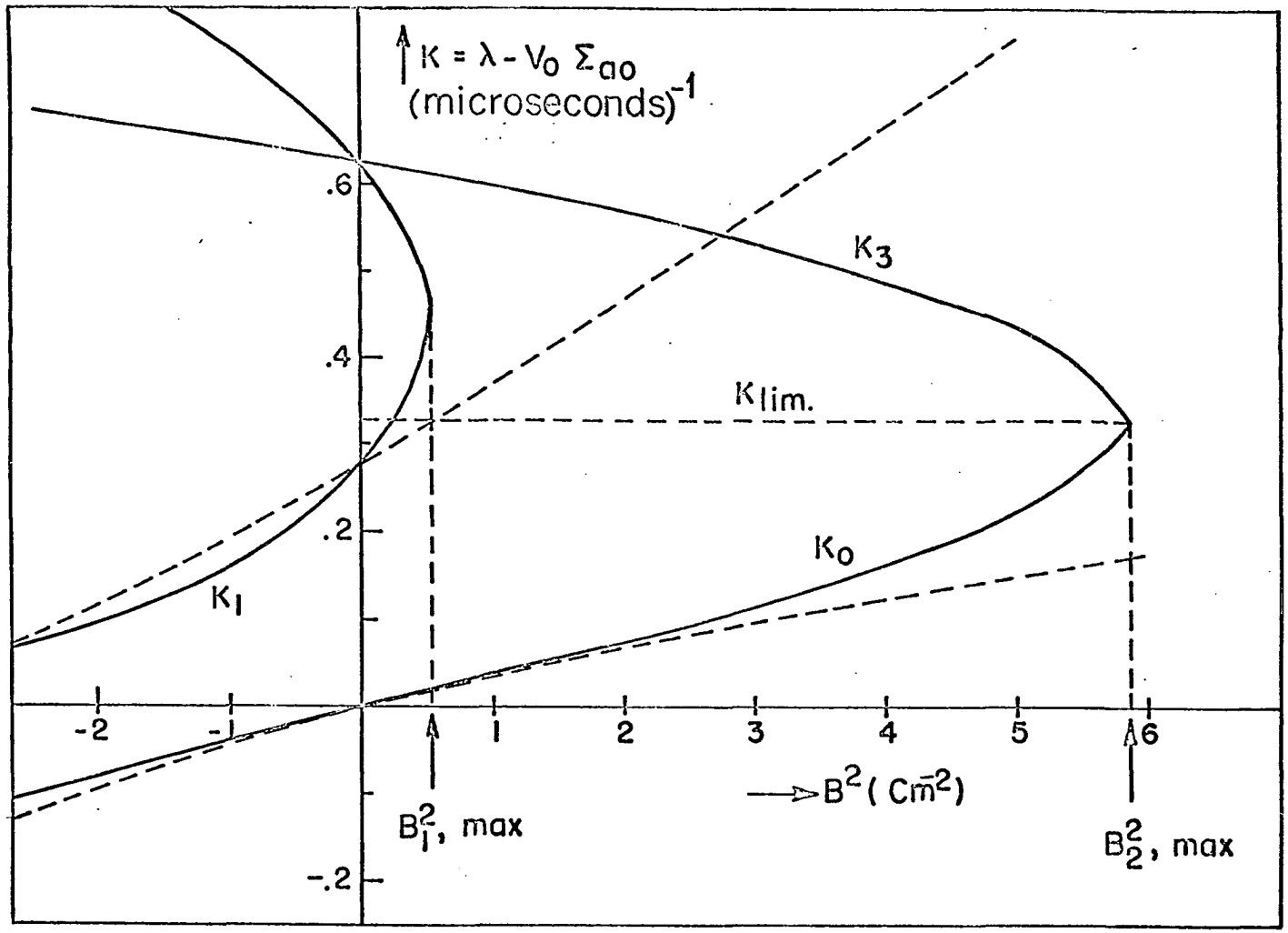

——— P_1-L_1 approximation ------ Diffusion approximation

Figure 2.4. Eigenvalue curves for $M_2 = 3.85\ cm^{-1}$ and the theories indicated

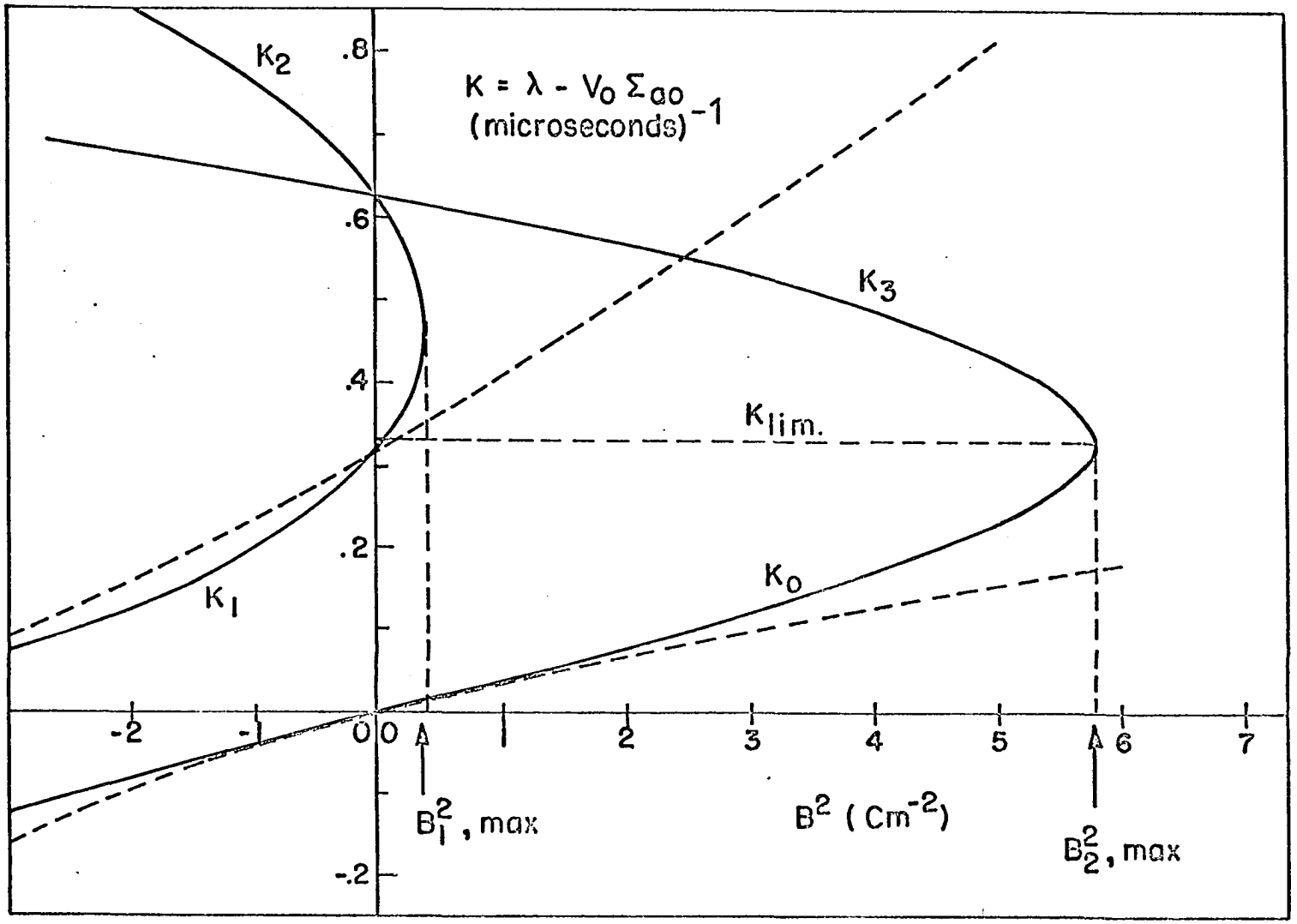

——— P_1-L_1 approximation ------ Diffusion approximation

Figure 2.5. Eigenvalue curves for $M_2 = 5.23\ cm^{-1}$ and the theories indicated

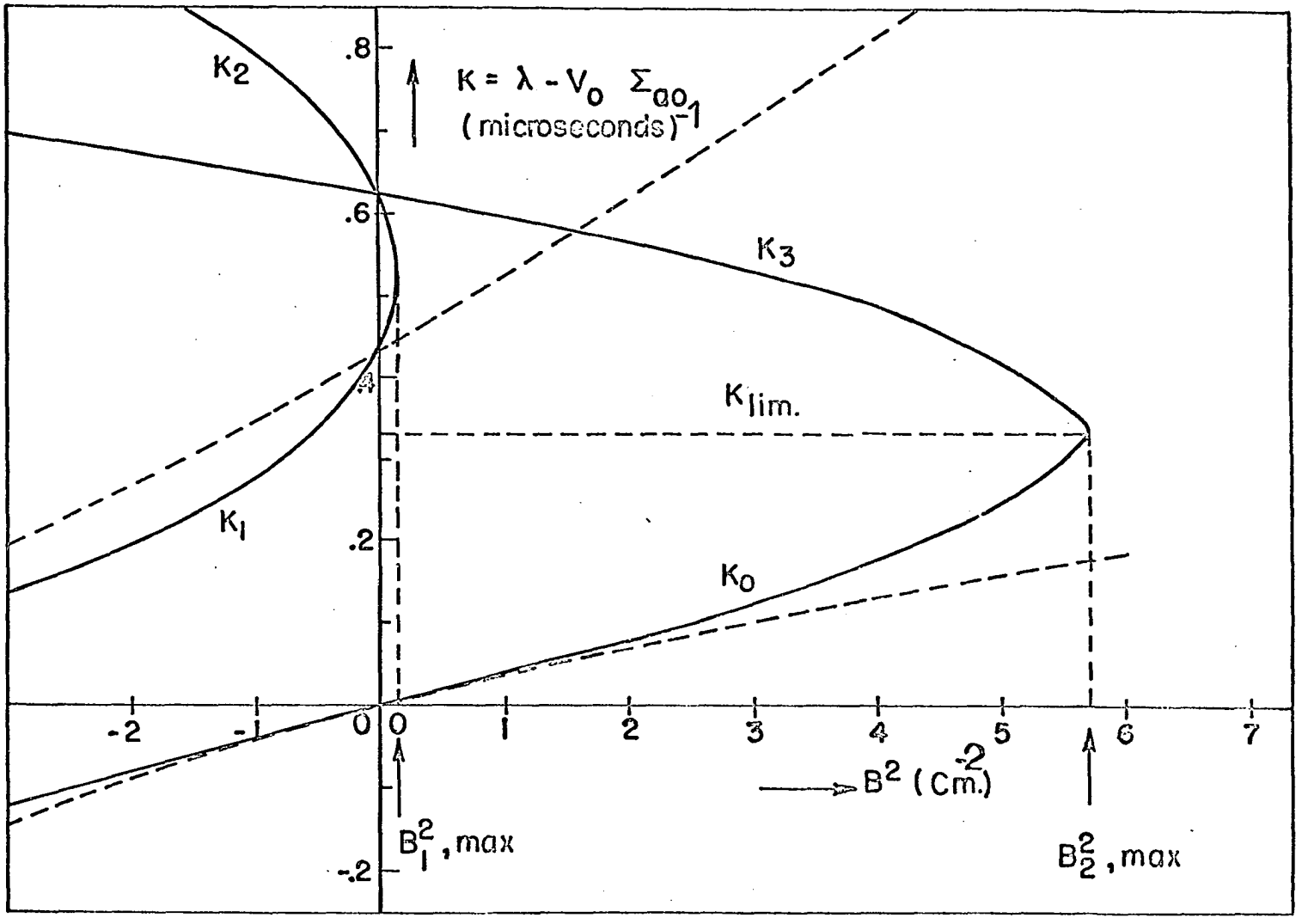

——— P_1-L_1 approximation ------ Diffusion approximation

These limiting values are listed in Table 2.9 as functions of M_2. It is clear from this table that, within the range of M_2's investigated, the limiting values are monotonic decreasing functions of M_2. In addition, the table shows that $B^2_{2,max.}$ is well above the experimental range of bucklings. Thus the usual expansion of the lowest eigenvalue in power series of B^2 is valid for the experimental ranges of B^2 reported in literature. On the other hand, $B^2_{1,max.}$ is within the range of pulsing experiments. For Nelkin's scattering kernel, for example, it has a value of 0.45 cm^{-2} and the expansion of the second lowest eigenvalue in power series of B^2 is doubtful.

c. The eigenvalue curve, which passes through $B^2 = K = 0$, has a negative curvature at this point for all the models in question. The amplitude of the curvature increases by decreasing M_2. For the Nelkin water, the curvature is in close agreement with the experimental results. Recently, Travelli and Calame (52) made a numerical investigation on thermal neutron space time eigenvalue spectrum of the multigroup P_N approximations for a modified form of Radkowsky kernel. Their results, in general, agree with the present findings. However, in a 4-group P_1 calculation, although the curve corresponding to the fundamental

Table 2.9. The limiting values of buckling and the corresponding decay constants for various water scattering kernels. Values of $\lambda_{lim.}$ obtained by other authors are also indicated

Kernel and references	M_2 (cm^{-1})	$B^2_{1,max}$ (cm^{-2})	$B^2_{2,max}$ (cm^{-2})	λ_{lim} ($10^{-4}sec^{-1}$)
Mass-18	0.67	1.37 ± .03	6.67 ± .05	31.700
Nelkin	3.34	0.45 ± .02	5.87 ± .05	33.300
Mass-1	3.85	0.37 ± .02	5.80 ± .07	33.500
Brown & St.John	5.23	0.15 ± .02	5.70 ± .07	33.800
Mass-1 (41)	--	---	---	33.650
GIN (41)[a]	--	---	---	31.512
Gorngold and Nichael (12)	--	---	---	30.000
Doppler-Corrected (45)	3.17	---	---	42.000

[a]Goldman improved Nelkin kernel.

eigenvalue correctly passes through the origin, its curvature is positive at that point, in disagreement with the experimental results. This leads to the conclusion that the continuous energy representation as given by two Laguerre polynomials predicts the results of pulsing experiments more accurately than a 4-group approximation.

With respect to the nature of the various eigenvalues in the P_1-L_1 approximation, one has the following argument: For the sake of simplicity let us identify them first by the sequence $K_0 < K_1 < K_2 < K_3$.

The (K_0,K_3) pair is identified separately from the (K_1,K_2) pair by virtue of the one-speed model. For this case equation 2.10.b reduces to the form

$$\frac{B^2}{3(\Sigma_{TR} - \frac{\lambda}{V})} - \frac{\lambda}{V} + \Sigma_a = 0$$

or

$$(\frac{\lambda}{V})^2 - \frac{\lambda}{V}(\Sigma_{TR} + \Sigma_a) + \Sigma_a\Sigma_{TR} + \frac{B^2}{3} = 0 \qquad (2.10.b')$$

For each value of B^2, this equation gives two roots,

$$K = \lambda - V\Sigma_a = \frac{V}{2}(\Sigma_{TR} - \Sigma_a)[1 \pm \sqrt{1 - \frac{4(3\Sigma_a\Sigma_{TR} + B^2)}{3(\Sigma_{TR} + \Sigma_a)^2}}], \qquad (2.10.b'')$$

which are identical to K_0 and K_3 except for some modifications due to the change in the energy spectrum. Equation 2.10.b'' emplies that K is real only if

$$B^2 \leq \frac{3}{4}(\Sigma_{TR} - \Sigma_a)^2 = \frac{3}{4}\Sigma_{tr}^2$$

This means that the basic physical phenomenon of traveling waves is not affected by the energy dependence as long as

the time behavior of the current is taken into consideration.

In case of no absorption and no leakage ($B^2 = 0$) the two eigenvalues of 2.10.b" become

$$K_0 = \lambda_0 = 0 , \qquad K_1 = \lambda_1 = V\Sigma_{tr} .$$

The eigenvalue zero corresponds to a mode which persists indefinitely; the corresponding eigenfunction has an arbitrary amplitude to match the initial flux but has no current component. The eigenvalue $V\Sigma_{tr}$ has an eigenfunction which has an arbitrary current amplitude to match the initial current. This second mode then is simply an angular transient which is due to the mismatch of the initial angular distribution of the persisting mode. The neutrons in the second mode do not leak out of the system nor are they absorbed since in this particular example $B^2 = \Sigma_a = 0$. In this case also the net current is zero according to equation 2.10.a. The time taken for the angular transient to rearrange itself [illegible] the persisting distribution is of the order of $(V\Sigma_{tr})^{-1}$.

As the leakage and absorption terms increase from zero, the net number of neutrons in the current transient becomes non-zero. This net number is just the number of neutrons that will actually leak from and be absorbed in the second mode. For large enough leakage or absorption the net number of neutrons in the transient can be considerable and the

influence of leakage is to make the properties of this transient more like that of the persisting mode.

On the other hand, the (K_0,K_1) pair can be identified from the (K_2,K_3) pair by the diffusion-theory approximation which gives a pair of eigenvalues close to the (K_0,K_1) pair at small values of B^2. Since in this case the time dependence of the neutron current is neglected and since in one-group diffusion approximation there is only one eigenvalue which is closely related to K_0 at small B^2, then K_1 is simply an eigenvalue of the energy transient. This transient is a distortion of the fundamental mode spectrum. It is essentially an eigenvalue of the scattering kernel. In conclusion the four eigenvalues are interpreted as follows:

K_0 = The fundamental eigenvalue.

K_1 = The eigenvalue of the energy transient.

K_2 = The eigenvalue of the angular transient which is a distortion to the second energy mode (with an eigenvalue K_1).

K_3 = The eigenvalue of the angular transient that distorts the fundamental mode.

The value of K at $B^2_{2,max.}$ is the limiting value, K_{lim}, for the fundamental eigenvalue K_0. The corresponding value of λ_{lim} is obtained by adding the constant term $V_o\Sigma_{ao}$. Values of λ_{lim} obtained by this method and as reported by

different authors are listed in Table 2.9. This table indicates that the limiting value is a function of the chemical binding of the water molecules and that it increases slowly with M_2.

Ohanian and Daitch (41) calculated λ_{lim} for the Mass-1 and the GIN (for the Goldman improved Nelkin) scattering kernels. Their calculations were based upon a numerical method employing a discrete representation of the energy variable. Their reported value for the Mass-1 kernel is in excellent agreement with the present value as shown in Table 2.9. One can also observe the good agreement between the value for the Mass-18 and that for the GIN kernel. The two values differ by less than 1%.

While all values reported in Table 2.9 agree with each other within 10%, the value reported by Purohit and Sjöstrand (45) is out of this range. From the foregoing this value for the Doppler-corrected kernel should lie in the range $33.0 \times 10^4 - 33.3 \times 10^4$ sec.$^{-1}$

C. Diffusion Parameters

In section B the discussion was mainly on the behavior of the time eigenvalues in the real (K,B^2) plane. In the light of the observations in that section, analytical expressions for various diffusion parameters of water will be developed here.

The first step in this direction is to write 2.37 in the form:

$$K^2 - KV_o\left[\frac{B^2(t_{11}w_{00} - 2t_{01}w_{01} + t_{00}w_{11}) + 3w_{00}|F_{11}|}{3(w_{00}w_{11} - w_{01}^2)}\right]$$

$$+ V_o^2\left[\frac{B^4(t_{00}t_{11} - t_{01}^2) + 3B^2t_{00}|F_{11}|}{9(w_{00}w_{11} - w_{01}^2)}\right] \qquad (2.38)$$

where t_{ik} is given by 2.27.

Equation 2.38 can be regarded as a transcendental quadratic equation with two roots given by

$$K_0 = \lambda_0 - V_o\Sigma_{ao}$$

$$= \tfrac{1}{2}[b_0 - (b_0^2 - 4c_0)^{1/2}] \qquad (2.39)$$

$$K_1 = \lambda_1 - V_o\Sigma_{ao}$$

$$= \tfrac{1}{2}[b_1 + (b_1^2 - 4c_1)^{1/2}] \qquad (2.40)$$

where

$$b_n = V_o\left[\frac{B^2(t_{11}^{(n)}w_{00} - 2t_{01}^{(n)}w_{01} + t_{00}^{(n)}w_{11}) + 3w_{00}|F_{11}|}{3(w_{00}w_{11} - w_{01}^2)}\right], \qquad (2.41)$$

$$c_n = V_o\left[\frac{B^4(t_{11}^{(n)}t_{00}^{(n)} - (t_{01}^{(n)})^2) + 3B^2t_{00}^{(n)}|F_{11}|}{9(w_{00}w_{11} - w_{01}^2)}\right], \qquad (2.42)$$

and

$$t_{ik}^{(n)} = V_o v_{ik}/(V_o \Sigma_{tro} - K_n) \quad ; \quad n = 0,1 \ . \tag{2.43}$$

From these equations valuable information can be obtained.

1. Diffusion cooling coefficient

The expansion of 2.39 in power series of B^2 is guaranteed only if $B^2 < B^2_{2,max.}$. If, in addition, B^2 is small the expansion assumes the simple form

$$K_0 = \lambda_0 - V_o \Sigma_{ao}$$

$$= D_T(B^2)B^2 - C_T(B^2)B^4 + OB^6 \tag{2.44}$$

where

$$D_T(B^2) = \frac{2}{3\sqrt{\pi}} V_o t_{00}^{(0)} \ , \tag{2.45}$$

$$C_T(B^2) = g\frac{D_T^2(B)}{V_o M_2} \ , \tag{2.46}$$

$$g = \frac{\sqrt{\pi}}{4}\left[1 + \frac{8}{\sqrt{2}} \frac{v_{01}}{v_{00}} \left(\sqrt{2}\frac{v_{01}}{v_{00}} - 1\right)\right] \tag{2.47}$$

The numerical factor, g, is a function of the energy dependence of the transport mean free path and the number of the Laguerre polynomials used in the series expansion of the flux. Values of the factor g are given in Table 2.10 for the several approximations used.

Table 2.10. Comparison of several expressions for the numerical factor g

Values of g under several approximations	Nelkin (38)	Purohit (43)	Perez et al. (42)	P_1-L_1
Energy dependent transport mean free path	1.772	---	1.772	1.776
Constant transport mean free path	0.443	0.443	0.443	0.443

The coefficient, C_T, of B^4 is the transport analog of the diffusion cooling coefficient C_D, obtained from the diffusion theory. C_T, however, differs from C_D in its dependence on B^2. To suppress the B^2-dependence, one should write

$$D_T(B^2)B^2 = D_o B_T^2 \tag{2.48}$$

$$C_T(B^2)B^4 = CB_T^4 \tag{2.49}$$

where

D_o = The diffusion coefficient

$$= V_o v_{00}/3w_{00}\Sigma_{tro}, \tag{2.50}$$

C = The diffusion cooling coefficient

$$= gD_o^2/V_o M_2 \tag{2.51}$$

and B_T^2 is given, to the order of B^6, by

$$B_T^2 = B^2/[1 - D_o B^2(1 - gD_o B^2/V_o M_2)/V_o \Sigma_{tro}] \qquad (2.52)$$

This expression shows that B_T^2 is a function of both the geometric and the scattering properties of the moderator. The ratio B_T^2/B^2 is plotted versus B^2, for $M_2 = 3.34$ cm^{-1}, in Figure 2.6. The curve shows that, for the values of B^2 considered, B_T^2 differs from B^2 by no more than 4%. Hence one can consider B_T^2 as a transport buckling with a non-diffusive correction for B^2. Furthermore, the values of B_T^2/B^2 reported in Table 2.11 show that the ratio is not sensitive to M_2 for small values of B^2.

The substitution of 2.48 and 2.49 into 2.44 gives

$$K_o = \lambda_o - V_o \Sigma_{ao}$$

$$= D_o B_T^2 - CB_T^4 + OB_T^6 \qquad (2.53)$$

Both D_o and C are independent of B^2.

Expression 2.51 for C was first derived by Nelkin (38) using the Rayleigh-Ritz variational principle, based upon the neutron temperature concept. Using the same concept, Mani (35) modified it to take into account the variation of the transport mean free path with energy. Singwi (48) developed a general theory of the diffusion cooling based upon the expansion of the asymptotic energy distribution by a sum of the associated Laguerre polynomials of order one. Häfele and Dresner (26) have also given a similar theory for the calcu-

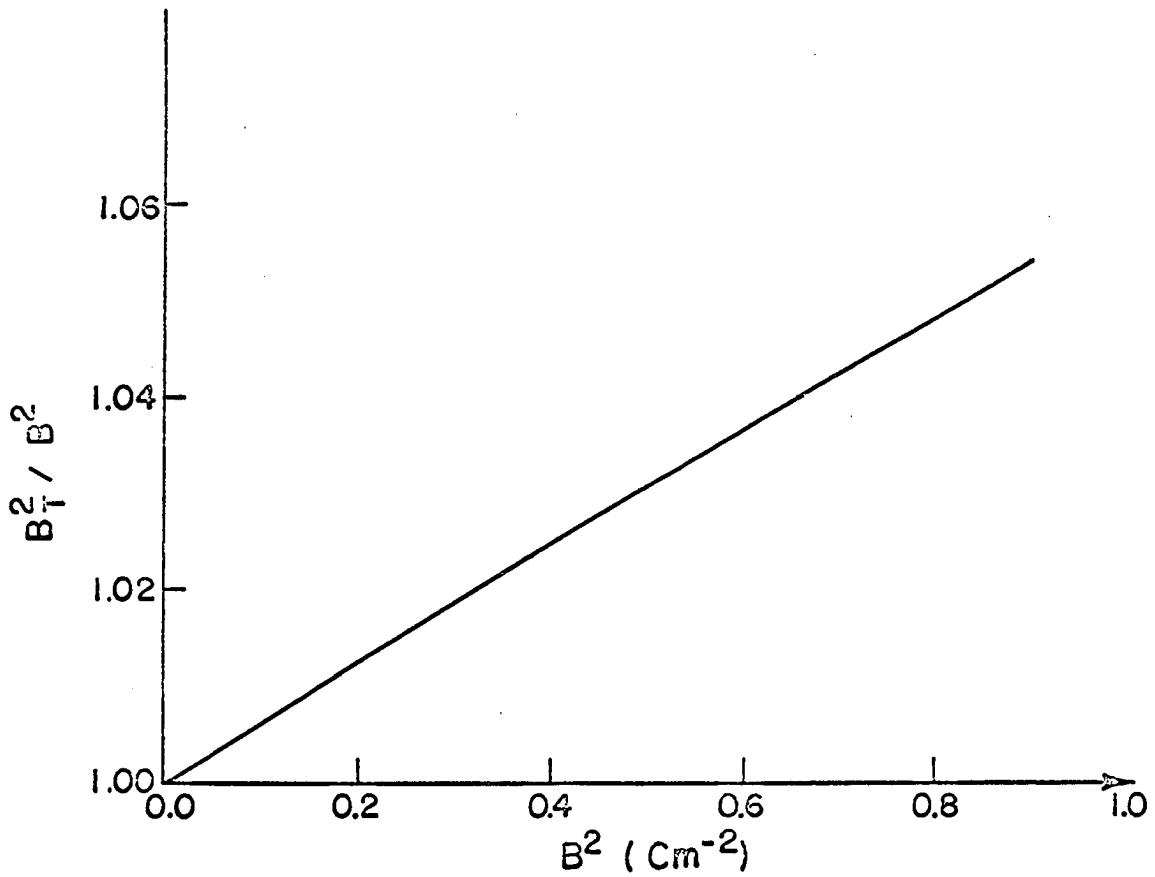

Figure 2.6. A plot of the ratio B_T^2/B^2 versus B^2 for M_2 = 3.34 cm^{-1}

Table 2.11. The ratios of B_T^2/B^2 for various values of B^2 and two values of M_2

$B^2(cm^{-2})$	B_T^2/B^2	
	$M_2 = 3.34\ cm^{-1}$	$M_2 = 3.85\ cm^{-1}$
0.000	1.0000	1.0000
0.025	1.0016	1.0016
0.050	1.0031	1.0031
0.150	1.0093	1.0093
0.200	1.0124	1.0124
0.300	1.0184	1.0184
0.500	1.0303	1.0305
0.700	1.0427	1.0431

lation of the diffusion cooling coefficient in a monoatomic heavy gas, using the same expansion. Kazarnovsky et al. (30) also used the Laguerre polynomials in their study of neutron thermalization problems. All of these studies were undertaken for the finite medium under the diffusion approximation. Nelkin (39) studied the decay of a thermalized neutron pulse in an infinite plane geometry using the transport theory in the Fourier space. The Fourier variable, B, in Nelkin's formalism has been left ill-defined. The appli-

cation of this method to a moderator with finite size and energy dependent transport mean free path is not unique (59).

Expression 2.50 and 2.51 were derived using neither the neutron temperature concept nor the Fourier transform technique. By the application of the proper boundary conditions, it will be shown later that the variable B in this thesis has a definite physical meaning.

Table 2.12 shows a comparison between values of C and D_o, obtained by the suppression of the B^2-dependence and those reported by other authors. It is clear that there is an agreement between the present values for the Nelkin's water and the P_3 values obtained by Gelbard and Davis for the Radkowsky kernel.

As a further check on the validity of the above expansion, λ_0 was calculated from 2.53 and 2.39 with an iterative technique. The results are listed in table 2.13 for $M_2 = 3.34\ cm^{-1}$. The table indicates that, within the limits of accuracy set for the computer, both values agree quite satisfactorily.

2. Thermalization time constant

The thermalization time constant is defined as the time constant with which the neutrons attain an asymptotic energy distribution by colliding with the atoms of a moderator. In case of an infinite and non-absorbing medium equation 2.39

Table 2.12. Values of the diffusion cooling coefficient, C, and diffusion coefficient, D_o, for various methods

Method and references	Kernel	C $cm^4.sec.^{-1}$	D_o $cm^2.sec.^{-1}$	Range of bucklings cm^{-2}
P_1-L_1	H gas	3139	38692	---
"	Mass-18	18038	38692	---
"	Nelkin	3618	38692	---
"	Brown & St. John	2311	38692	---
P_3 (24)	Radkowsky	3614	38380	---
Calame (7)	Nelkin	2931	36810	---
Scott et al. (46)	---	---	38500±800	.006-.018
Antonov et al. (1)	---	4000±1000	35000±1000	.09 -.93
Lopez and Beyster (34)	---	4852±800	36700±370	.0 -1.00

Table 2.13. Values of the fundamental decay constant, λ_0, as obtained from the correct form 2.39 and the expansion form 2.53, for M_2 = 3.34 cm^{-1} [a].

B^2	$\lambda_0(sec.^{-1})$		
(cm^{-2})	Correct value	Expansion value	($\lambda_0$corr - λ_0 expans.)
0.000	4876	4876	0.00
0.025	5843±5	5843	0.00
0.050	6809±5	6809	0.00
0.150	10656±5	10651	5.00±5
0.200	12572±5	12563	9.00±5
0.300	16388±5	16359	29.00±5
0.500	23965±5	23850	115.00±5
0.700	31485±5	31170	315.00±5

[a]Nelkin scattering model.

and 2.40 reduce respectively to

$$K_0 = \lambda_0 = 0 \ , \tag{2.54}$$

$$K_1 = \lambda_1 = -V_o w_{00} F_{11} / (w_{00} w_{11} - w_{01}^2)$$

$$= 2V_o M_2 / 3\sqrt{\pi} \tag{2.55}$$

In this case there is an asymptotic energy distribution. The decay of this distribution is governed by λ_0 equals to zero. If the atoms of the moderator have a Maxwellian velocity distribution, then the asymptotic distribution is also the Maxwellian distribution which is established with a thermalization time constant equals to the reciprocal of λ_1. In the case of a finite medium, the zeros eigenvalues associated with the higher spatial modes also play an important role in the establishment of the final asymptotic energy distribution. If the amplitudes of higher modes are very small compared with the fundamental spatial mode, then the first eigenvalue, λ_1, would give the thermalization time constant in the finite medium. The discussion, here, is limited to the time constant with which the Maxwellian distribution is established.

The thermalization time constant is given by the reciprocal of λ_1

$$t_{th} = \frac{3\sqrt{\pi}}{2V_o M_2} f_t \tag{2.56}$$

a result which is identical with that derived from the diffusion theory (43). f_t is a correction factor due to higher order polynomials than L_1^1. Its value is 1.15 (45).

Various models have been considered in calculating t_{th} according to equation 2.56. The results are presented in Table 2.14. Two cases were treated. In case I the transport mean free path is energy dependent; while in case II it is taken as a constant. As could be seen from this table, t_{th} for the constant λ_{th} is about 4 times as large as that for the energy dependent case for all the models used. Thus a comparison between these results and the experimental values of t_{th} would indicate the energy behavior of the transport mean free path. Fortunately, Möller and Sjöstrand (37) have measured t_{th} in light water by obtaining information on the change of the neutron spectrum with time from the reaction rate with spectrum indicators dissolved in the system. They reported a value of 4.1 ± 0.4 usec. This agrees with the value of 4.16 usec obtained for $M_2 = 3.34\ cm^{-1}$ in the energy dependent case. One concludes, therefore, that the transport cross section for light water behaves more or less like 1/V.

De Jurene (17) took into account the spectral changes caused by diffusion-cooling and reported a value of 2.77 ± 0.65 usec. Although this result disagrees with the experimental value reported by Möller, yet it is in accord with the theoretical value for $M_2 = 5.23\ cm^{-1}$ (Brown and St.John

Table 2.14. Thermalization time constant for light water in the P_1-L_1 approximation for various scattering models

Kernel	M_2 (cm^{-1})	t_{th} (microseconds)	
		Case I ($\lambda_{tr} \alpha \sqrt{E}$)	Case II (λ_{tr} = const.)
Nelkin	3.34	4.16	16.69
Mass-1	3.85	3.61	14.48
Mass-18	0.67	13.85	83.17
Brown & St.John	5.23	2.66	10.66

scattering model).

Wood (60) represented water with the effective width kernel of Egelstaff (22). He calculated t_{th} for water as a function of the reciprocal of the effective width parameter, d, of the scattering law. His results are listed in Table 2.15 which shows that the value of t_{th} at d = 0.27 is in agreement with the P_1-L_1 value for the Nelkin's model.

The thermalization time constant can also be expressed in terms of the cooling coefficient by eliminating M_2 between 2.51 and 2.55. The result is

$$t_{th} = \frac{6C}{D_o^2}\left[1 + \frac{8}{\sqrt{2}}\frac{v_{01}}{v_{00}}\left(\sqrt{2}\,\frac{v_{01}}{v_{00}} - 1\right)\right]^{-1} f_t \quad , (\lambda_{tr} \alpha \sqrt{E})$$

$$= \frac{6C}{D_o^2} f_t \quad , (\lambda_{tr} = \text{const.}), \tag{2.57}$$

Table 2.15. Thermalization time constant for light water by other authors

Reference	Kernel	t_{th} (microseconds)
Möller & Sjöstrand (37)	---	4.10 ± .4 (water)
DeJurene (17)	---	2.77 ± .65
Wood (60)	Effective width	4.50 (d[a] = .21)
"	" "	4.13 (d = .27)
"	" "	3.71 (d = .50)
"	Mass-1	3.60
"	Mass-1.88	4.89
"	Mass-2	5.05

[a]d is the reciprocal of the effective width parameter of Egelstaff Kernel (22).

in agreement with the expression obtained by Purohit (43).

D. Space and Energy Dependent Eigenfunctions

The existence of a unique buckling depends on the validity of the first fundamental theorem of reactor theory *vis*. space and energy are separable:

$$\phi(\underline{r},E) = X(\underline{r})Y(E) \qquad (2.58)$$

This is true in a homogeneous infinite medium. It requires, however, some justification in finite systems. What is done is to seek an "asymptotic" region inside the medium far from the boundaries in which the first fundamental theorem

is valid. Experiments (29) have been performed to test this assumption. Those by Inönu at Oak Ridge are particularly interesting. Inönu measured the thermal and epithermal fluxes and showed that only if data within 3-3.5 inches of the boundary of a large critical aqueous U-235 solution were included was the extrapolation distance independent of energy i.e. equation 2.58 applies. This example is an extreme example; in non-multiplying medium the effect will be less.

On physical grounds the exact solution can be written in the form

$$\phi(\underline{r},E) = \phi_{as}(\underline{r},E) + \phi_{trans.}(\underline{r},E)$$

$$= X(\underline{r})Y(E) + \phi_{trans.}(\underline{r},E) \qquad (2.59)$$

The asymptotic part establishes a unique extrapolation distance, $d(B^2)$, for a given buckling and energy. Figure 2.7 shows how this extrapolation distance is related to the asymptotic flux. The distance S is the width of the zone in which the term $\phi_{trans.}(\underline{r},E)$ is important.

In this section analytical expressions for ϕ_{as} and $\phi_{trans.}$ are established. In a latter section an expression for $d(B^2)$ will be found.

As has been mentioned before, the polynomial $C(K,B^2)$ given by equation 2.37 is of degree 2 in B^2. For $K = K_0$ (the lowest eigenvalue), the equation for B^2 becomes

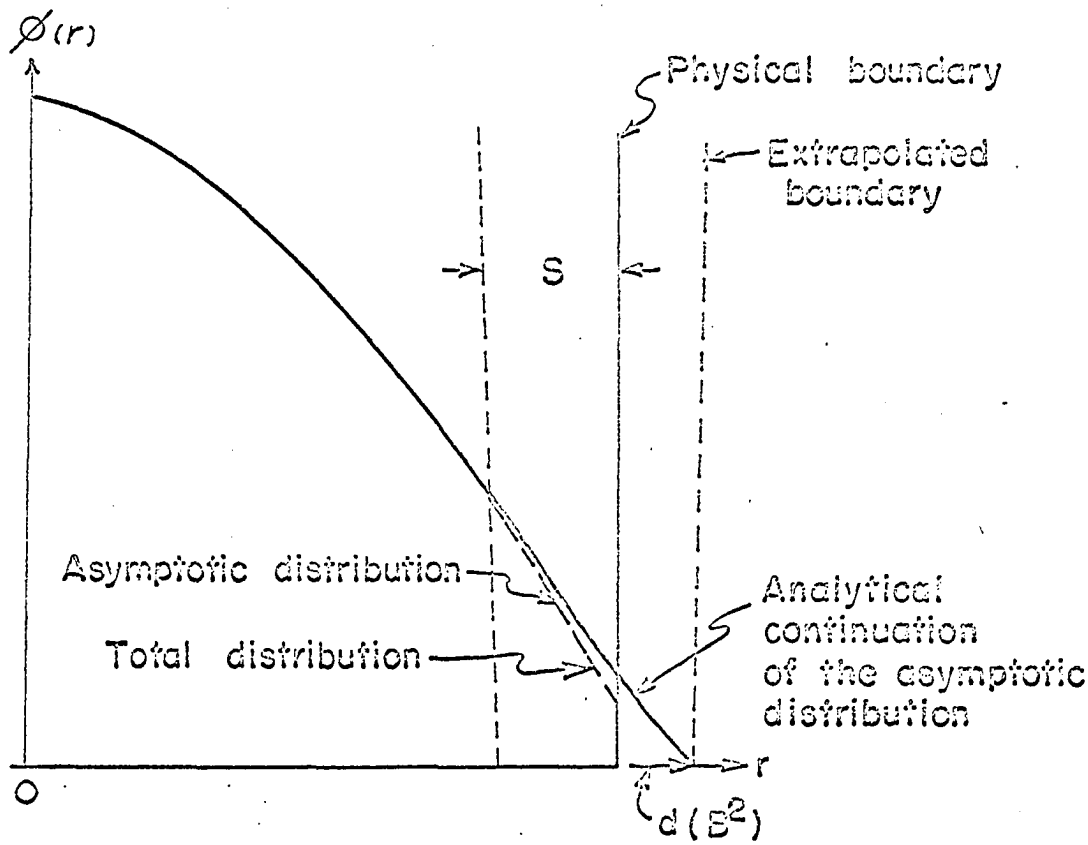

Figure 2.7. The relation between the extrapolation distance, $d(B^2)$, and the asymptotic flux distribution. The width, S, of the transient zone is indicated

$$(t_{00}^{(0)}t_{11}^{(0)} - t_{10}^{(0)2})B^4 + [\frac{3t_{00}^{(0)}M_2}{4} - \frac{3K_0}{V_o}(t_{11}^{(0)}w_{00} - 2t_{01}^{(0)}w_{01}$$

$$+ t_{00}^{(0)}w_{00})]B^2 + \frac{9K_0^2}{V_o^2}(w_{00}w_{11} - w_{01}^2) - \frac{9K_0w_{00}M_2}{4V_o} = 0 \qquad (2.60)$$

where $t_{ik}^{(0)}$ is given by 2.43.

For $K_0 \leq K_{lim.}$ all the coefficients in 2.60 are real. In addition, in case of light water, the term $(t_{00}^{(0)}t_{11}^{(0)} - t_{01}^{(0)2})$ is a positive quantity. The last coefficient is negative only if

$$K_0 < \frac{V_o w_{00} M_2}{4(w_{00}w_{11} - w_{01}^2)} \qquad (2.61)$$

Thus it is easily established, by requiring that the coefficient of B^2 is positive, that for

$$K_0 < \frac{V_o M_2}{4(v_{00}w_{11} + v_{11}w_{00} - 2v_{01}w_{01})} \qquad (2.62)$$

$$\approx 1.88 \times 10^4 M_2$$

there exist two values of B^2

$$B^2 = B_0^2 \quad , \quad B^2 = -U^2 \qquad (2.63)$$

where both B_0^2 and U^2 are positive quantities. The interpretation of B_0^2 as the geometric buckling, B_g^2, of the system depends on the application of the boundary condition at the vacuum-

matter interface. The commonly used outer face boundary conditions are the Marshak and the zero extrapolated flux boundary condition. The first boundary condition will be used in this thesis. Taking B_0^2 as B_g^2, one can write the scalar flux in the form

$$\phi_0(r,E) = F_0(B,E)j_0(Br)$$
$$F_0(B_g,E)j_0(B_g r) + F_0(U,E)j_0(iUr) \qquad (2.64)$$

where

$$F_0(B_g,E) = A_{B_g} E e^{-E}[F_0^0(B_g) + \frac{1}{\sqrt{2}}(2 - E)F_0^1(B_g)] , \qquad (2.65)$$

$$F_0(U,E) = A_U E e^{-E}[F_0^0(U) + \frac{1}{\sqrt{2}}(2 - E)F_0^1(U)] \qquad (2.66)$$

Recalling equation 2.59, one can associate the first term of 2.64 with $X(\underline{r})Y(E)$ and the second term with $\phi(\underline{r},E)_{trans}$.

1. The relaxation length

The physical meaning of U^{-1} is understood by writing 2.64 in the form

$$\phi_0(r,E) = A_{B_g} E e^{-E}\left\{[F_0{}^0(b_g) + \frac{1}{\sqrt{2}}(2 - E)F_0{}^1(B_g)]j_0(B_g r)\right.$$
$$\left. + \frac{A_U}{A_{B_g}}[F_0{}^0(U) + \frac{1}{\sqrt{2}}(2 - E)F_0{}^1(U)]j_0(iUr)\right\} \qquad (2.67)$$

The ratio A_U/A_{B_g} is determined by applying the Marshak's boundary condition at the vacuum interface. It is found that

$$\frac{A_U}{A_{B_g}} j_0(iUr) \approx \text{const} \times \frac{e^{-U(R-r)}}{r} \tag{2.68}$$

Thus for distances $> U^{-1}$ this term decays rapidly and U^{-1} is interpreted as a relaxation length which is a measure of the transient zone near the boundary. U^{-1} is given by

$$U = \left|\sqrt{U^2}\right| ,$$

$$U^2 = 1{\cdot}4027 \times 10^{-11} K_0 (V_o \Sigma_{tro} - K_0)\left(\frac{7{\cdot}315 \times 10^4 M_2}{K_0} - 2{\cdot}9465\right)$$

$$\times \left[1 + \left(1 + \frac{1{\cdot}3349 \times 10^6 (M_{2/4} K_0 - 3{\cdot}0208 \times 10^{-6})}{(2{\cdot}926 \times 10^5 M_{2/4} K_0 - 2{\cdot}9465)^2}\right)^{1/2}\right] \tag{2.69}$$

For the Nelkin's water, calculations indicate that U^{-1} = 0.483 cm in the limit as $B_g^2 \to 0$. The results suggest that deviation from the asymptotic solution begins to become large at points of the order of 0.5 cm from the boundary. Table 2.16 shows the variation of U^{-1} with buckling. The observed increase of the relaxation length with B_g^2 is expected on the basis that the energy spectrum deviates more from the Maxwellian distribution for small systems. U^{-1} is very sensitive to the value of M_2 and the effect of chemical binding on the space-energy separability can be studies through this parameter. From Table 2.16 it can be seen that the smaller the value of M_2 the less accurate is the space-energy

Table 2.16. The variation of the relaxation length for water with buckling and M_2[a]

B_g^2 (cm^{-2})	U^{-1}(cm)			
	$M_2 = 0.67 cm^{-1}$	$M_2 = 3.34 cm^{-1}$	$M_2 = 3.85 cm^{-1}$	$M_2 = 5.23 cm^{-1}$
0.000	1.07000	0.48300	0.44300	0.38200
0.025	1.10244	0.48557	0.45187	0.38732
0.050	1.12898	0.48818	0.45403	0.38876
0.150	1.24405	0.49889	0.46284	0.39462
0.200	1.30713	0.50439	0.46736	0.39762
0.300	1.44415	0.51571	0.47663	0.40374
0.500	1.73918	0.53967	0.49617	0.41656
0.700	-**	0.56552	0.51714	0.43017
0.900	-**	0.59339	0.53964	0.44466

[a]The values of M_2 correspond to the scattering kernels listed in Table 2.4.

**A complex value.

separability, i.e., the smaller is the asymptotic region. For $M_2 = .67\ cm^{-1}$ there is no unique buckling above a value of $0.5\ cm^{-2}$ where the inequality 2.62 is invalidated.

2. The asymptotic diffusion-cooled neutron spectrum

The spectrum of the asymptotic distribution is given by

$$F_0(B_g,E) = A_{B_g} E e^{-E}[F_0^0(B_g) + \frac{1}{\sqrt{2}}(2 - E)F_0^1(B_g)] \quad (2.70)$$

where $F_0^0(B_g)$ is an arbitrary constant that can be taken as unity since it originates in the set of two homogeneous equations given by 2.32. The quantity $F_0^1(B_g)$ has the form

$$F_0^1(B_g) = \frac{B_g^2 t_{00}^{(0)}/3 - w_{01}K_0/V_o}{B_g^2 t_{11}^{(0)}/3 - w_{11}K_0/V_o + M_{2/4}} \qquad (2.71)$$

The latter expression is obtained from 2.32 and is considered as a measure of the deviation from the Maxwellian distribution. Figure 2.8 shows a plot of $F_0^1(B_g)$ versus B_g^2. It is clear from this Figure that $F_0^1(B_g)$ is zero only for an infinite medium where the energy distribution follows the Maxwellian distribution.

Examples of the diffusion-cooled spectra for the Nelkin's scattering model are shown in Figure 2.9. The corresponding data are listed in Table 2.17. In Figure 2.9, the shifting of the peak of the curve toward lower energy values with increasing B_g^2 is evident, and the change of the shape of the curve is indicated. The Maxwellian distribution is seen to represent the limiting value of $F_0(B_g'E)$ as $B_g^2 \to 0$. The magnitude of the cooling effect is indicated by the shifting of the peak value of the curve from one unit of KT for $B_g^2 = 0$ to .87 units of KT for $B_g^2 = .9$ cm^{-2}.

Recently, Clendenen (9) made similar calculations for light water treated with the Nelkin model. He used a new iterative method applied to a P_{11} approximation although

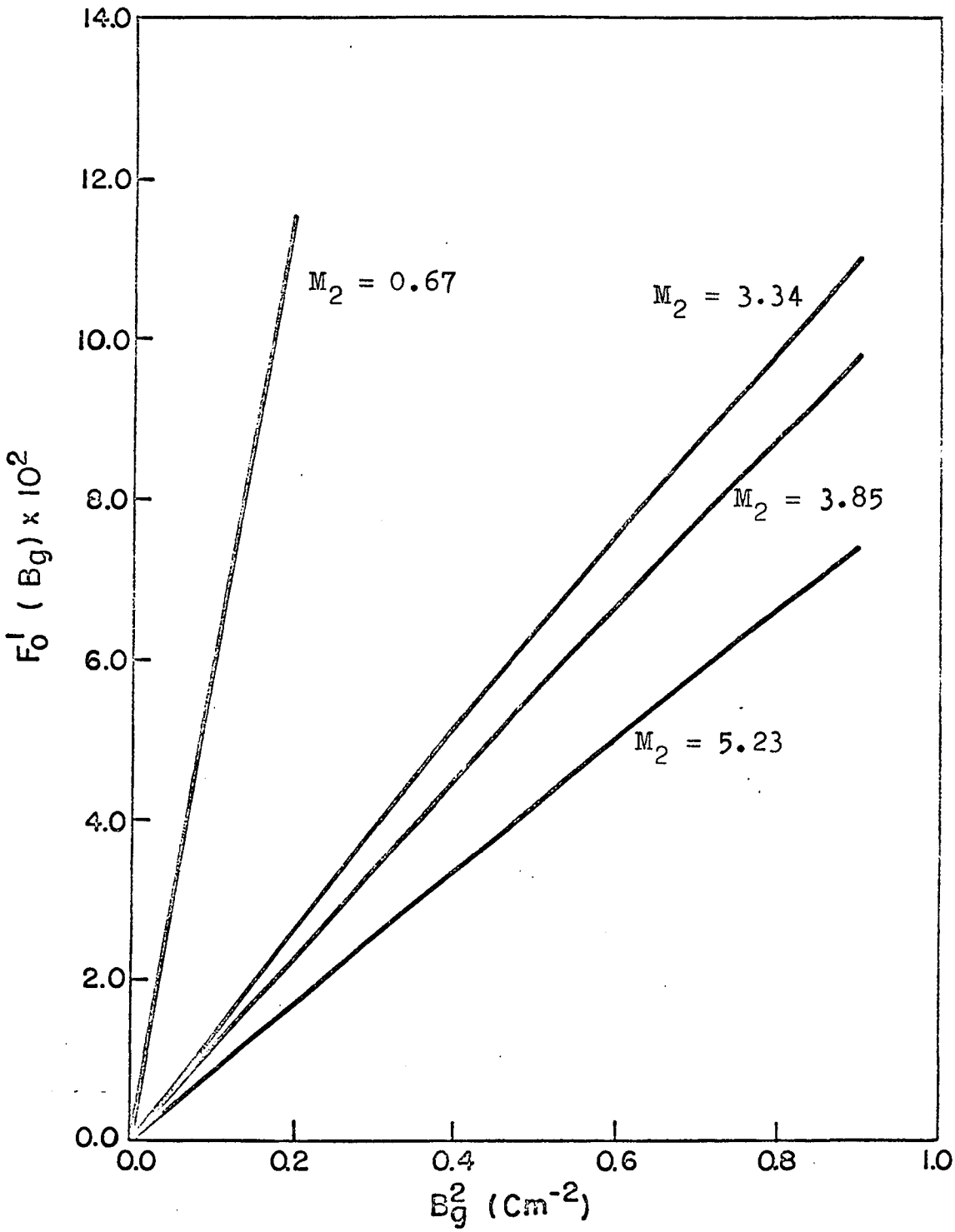

Figure 2.8. Buckling dependence of $F_0^1(B_g)$ for various values of M_2

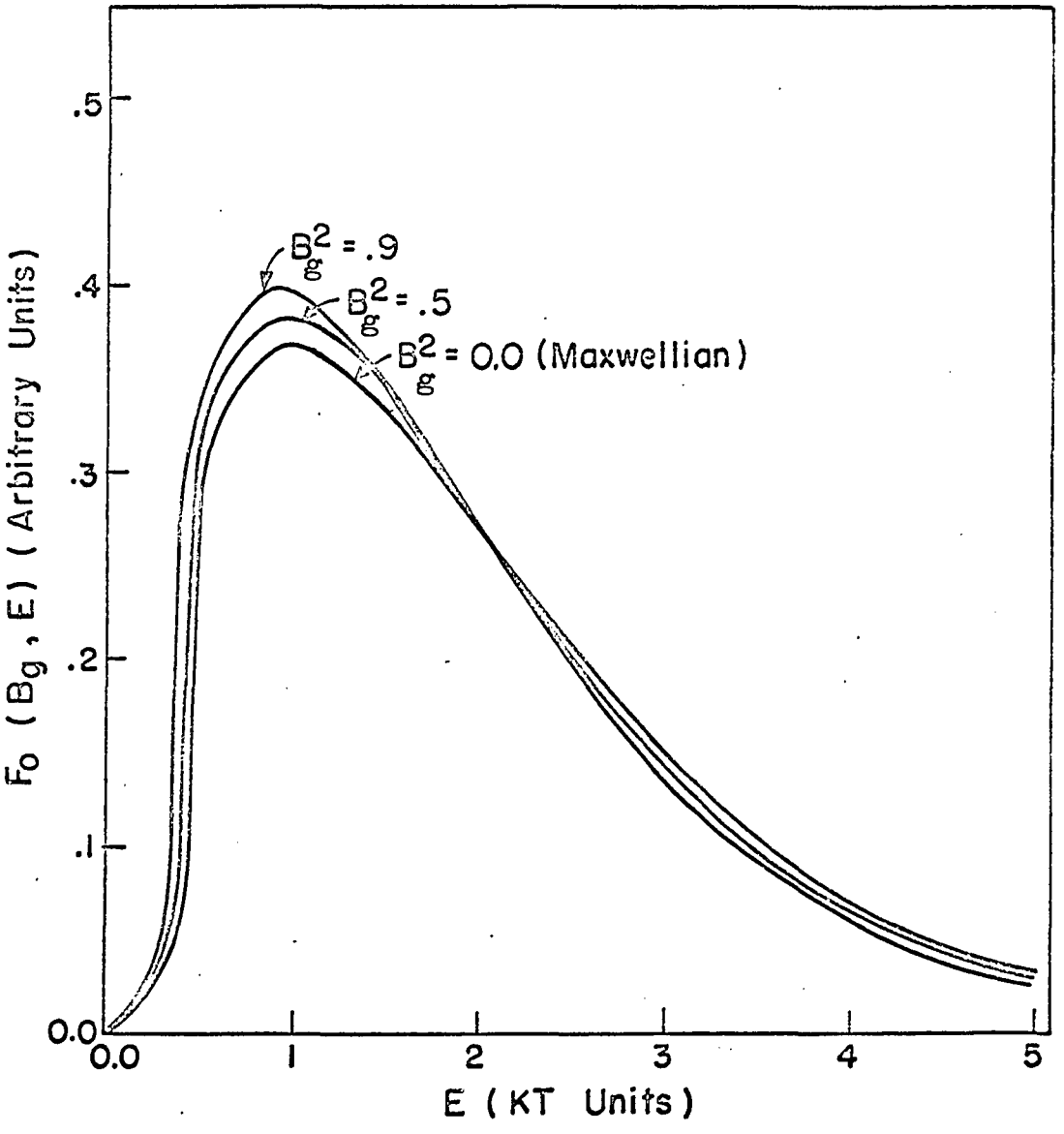

Figure 2.9. Diffusion-cooled neutron spectra for Nelkin model of water moderator at room temperature. Variation with buckling B_g^2 (cm^{-2}) is shown

Table 2.17. Normalized values of diffusion-cooled neutron spectra for Nelkin model of water moderator at room temperature. Variation with buckling B_g^2 is indicated

Energy, E	$F_0(B_g,E)$		
in units of KT	$B_g^2 = 0.0 cm^{-2}$	$B_g^2 = 0.5\ cm^{-2}$	$B_g^2 = 0.9\ cm^{-2}$
0.000	0.0000	0.0000	0.0000
0.025	0.0245	0.0266	0.0280
0.500	0.3033	0.3235	0.3385
0.750	0.3543	0.3740	0.3885
1.000	0.3679	0.3842	0.3963
1.500	0.3347	0.3421	0.3476
2.000	0.2707	0.2707	0.2707
0.500	0.2052	0.2006	0.1973
3.000	0.1493	0.1427	0.1378
3.500	0.1057	0.0987	0.0930
4.000	0.0732	0.0667	0.0619
4.500	0.0500	0.0445	0.0403
5.000	0.0337	0.0292	0.0259

his results generally agree with the present findings, the method does not directly give the limiting value of $F_0(B_g,E)$ as $B_g^2 \to 0$. Besides, this method is only suited to high-order approximations to the transport equation.

3. The energy spectrum of the transient component

This spectrum is given by

$$F_0(U,E) = A_U E e^{-E}\left[1 + \frac{1}{\sqrt{2}}(2 - E)F_0^1(U)\right] \tag{2.72}$$

where

$$F_0^1(U) = \frac{U^2 t_{00}^{(0)}/3 + w_{00}K_0/V_o}{U^2 t_{01}^{(0)}/3 + w_{01}K_0/V_o} \tag{2.73}$$

$F_0^1(U)$ is plotted, for various scattering kernels, in Figure 2.10. It starts from a non-zero value for an infinite medium and increases steadily with decreasing the size of the system. The implication of these results is that the energy spectrum of the transient distribution is always a non-Maxwellian distribution and that its magnitude becomes significant for small systems. Examples of this spectrum, for the Nelkin's water are shown in Figure 2.11. The corresponding data are listed in Table 2.18. Each of these curves is shown to have a minimum and a maximum the location of which depends on the value of B_g^2, i.e., on the cooling effect.

Having discussed the energy spectra of the asymptotic and the transient components of the scalar flux, it is of practical importance to discuss this distribution as a function of the position r. The flux $\phi_0(\underline{r},E)$ as given by 2.63 is plotted in Figure 2.12 versus the ratio r/R at $B_g^2 = 0.5$ cm^{-2} and two different values of energy. For the sake of

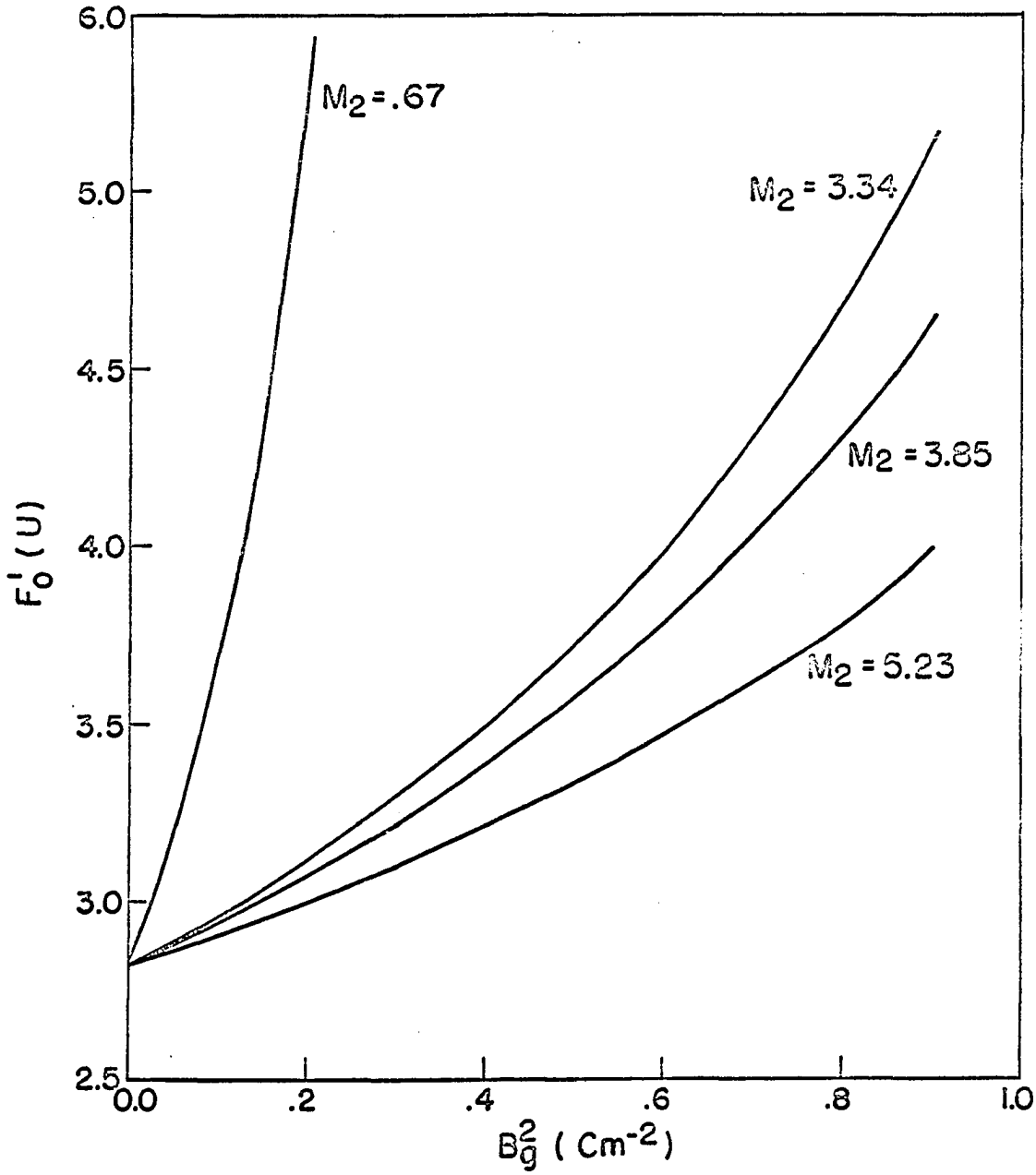

Figure 2.10. Buckling dependence of $F_0^1(U)$ for various values of M_2

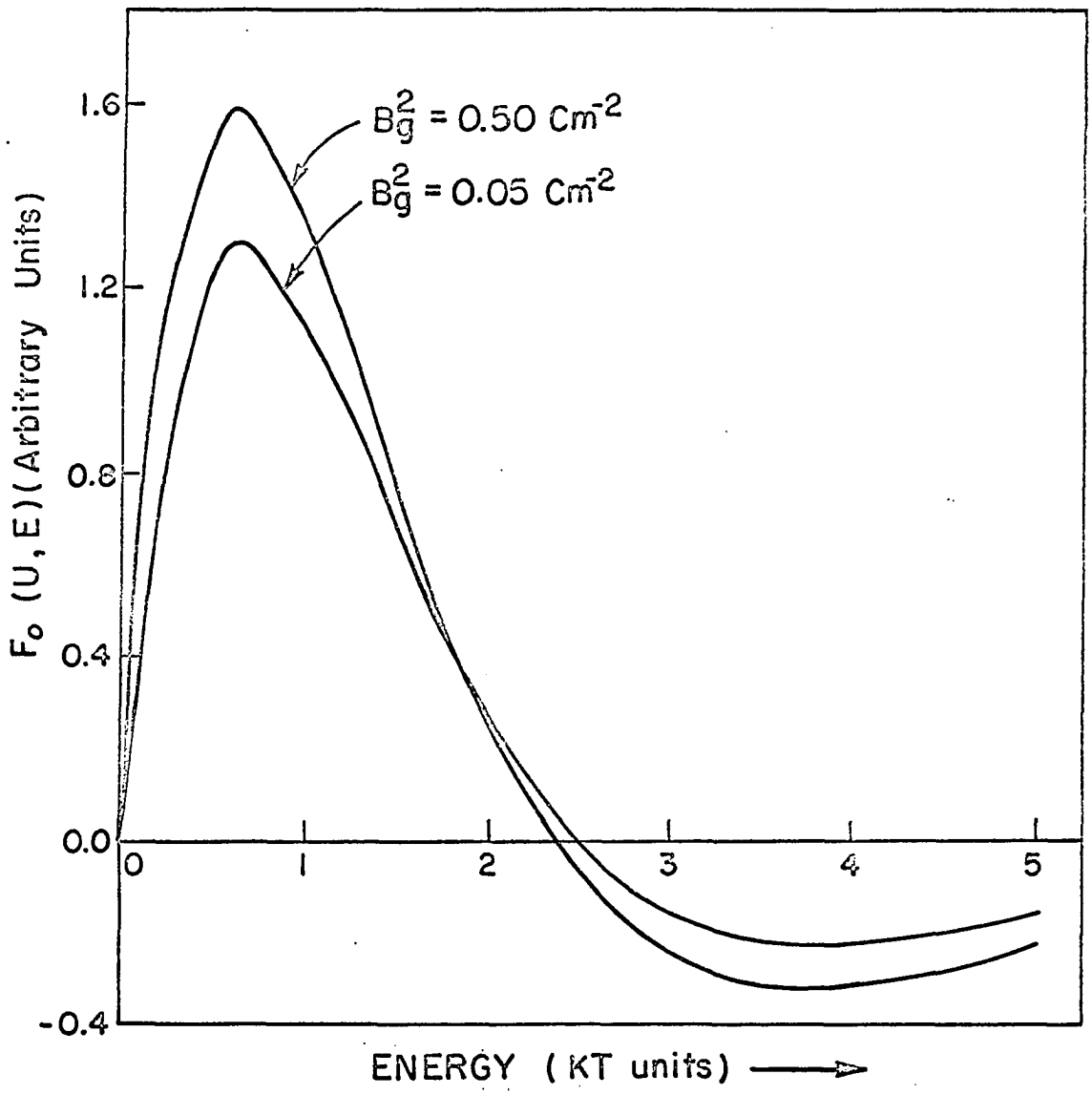

Figure 2.11. Transient energy spectra for Nelkin's water at room temperature. Variation with buckling $B_g^2(cm^{-2})$ is shown

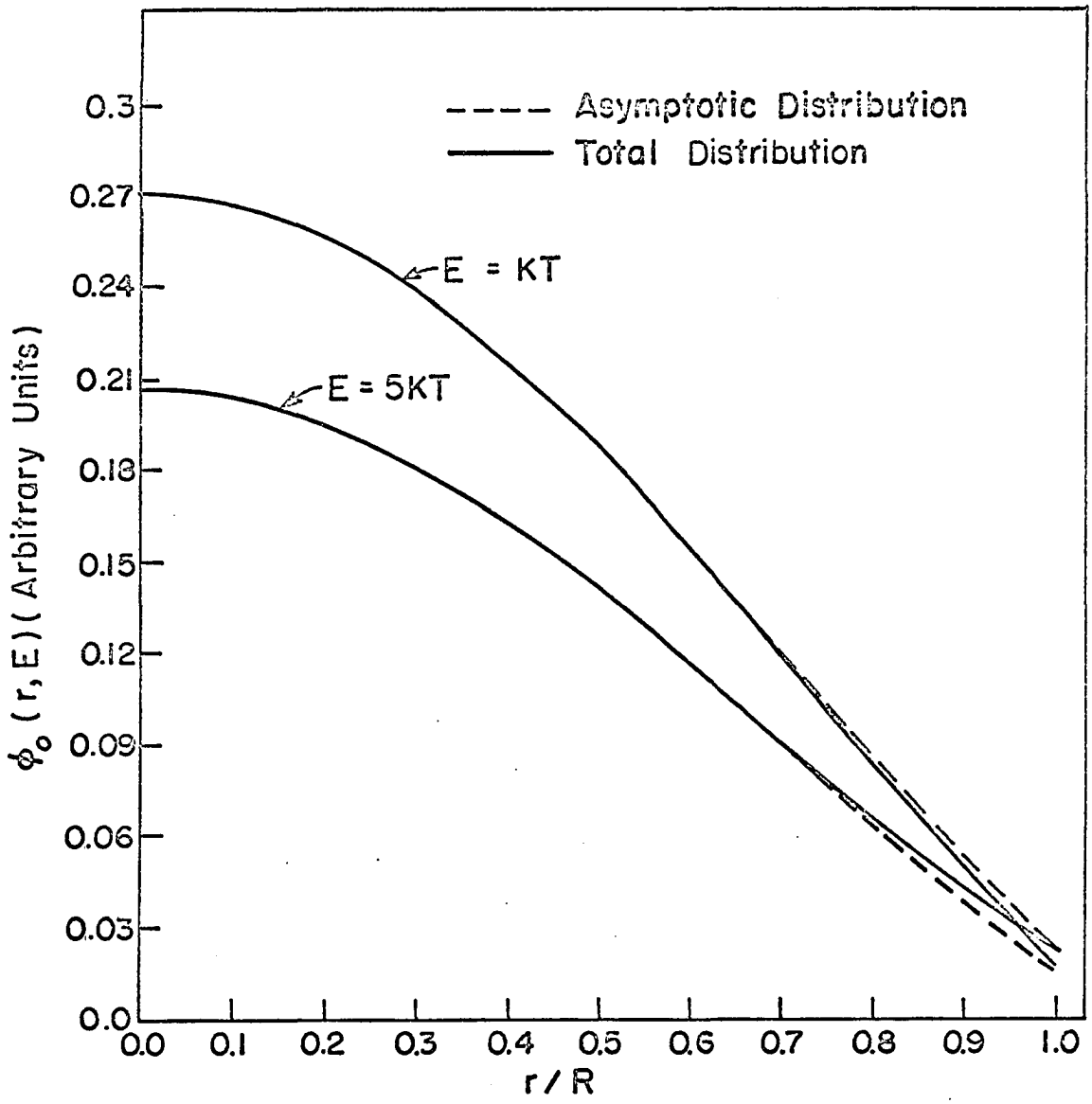

Figure 2.12. Flux distribution as a function of space points at $B_g^2 = 0.5\ cm^{-2}$

Table 2.18. Transient energy spectra at room temperature for the Nelkin's water. Variation with buckling $B_g^2(cm^{-2})$ is indicated

Energy, E, (KTUnits)	$F_0(U,E)$ (Arbitrary Units)	
	$B_g^2 = 0.05\ cm^{-2}$	$B_g^2 = 0.5\ cm^{-2}$
0.000	0.0000	0.0000
0.025	0.1235	0.1534
0.500	1.2342	1.5170
0.750	1.2605	1.5360
1.000	1.1207	1.3490
1.500	0.6772	0.7810
2.000	0.2707	0.2707
2.500	-0.0048	-0.0625
3.000	-0.1562	-0.2490
3.500	-0.2187	-0.3152
4.000	-0.2264	-0.3143
4.500	-0.2058	-0.2835
5.000	-0.1732	-0.2360

comparison, the asymptotic flux distribution is also plotted in the same Figure from which one can observe the following:

1. For points far from the physical boundary by amounts of the order of U^{-1}, the total flux, independent of energy, has the same value as the asymptotic distribution.
2. Close to the boundary the two fluxes differ from each other. The difference depends on the energy.

At low energies (close to KT), the asymptotic flux has a higher value; while at high energies (in the order of 5KT) the asymptotic flux has a lesser magnitude than the total flux.

Thus the effect of the transient flux near the boundary is a function of energy. At high energy the effect is subtractive and the predicted extrapolation length, according to the "total" flux distribution, is greater than that for the asymptotic distribution. On the other hand, at low energies the effect is additive giving rise to an extrapolation distance lower than the asymptotic value. In practice, however, the flux distribution is measured by a boron trifluride detector over a range of energy. The net transient effect in this range is found to be additive. This point will be made more clear in the next section in the discussion of the effective average energy.

In support of the above observations, are the results of Walker (56) who illustrated the effect of the flux distortion on the extrapolated endpoint of a 4-in cubic container filled with water. His results indicated that the extrapolation distance increases steadily by including more points closer to the boundaries.

E. Spectrum-Averaged Parameters

Having obtained $\Phi_0(r,E)$, one is in a position to calculate various parameters averaged over the space-dependent

neutron spectrum. Two of these of interest in the thermalization problem are

1. Effective average energy.
2. Effective buckling.

1. Effective average energy

The effective average energy is defined (59) by

$$\bar{E}_{eff}(r,B_g^2) = \frac{\int_0^\infty E\phi_0(r,E)dE}{\int_0^\infty \phi_0(r,E)dE} \tag{2.74}$$

This leads to

$$\bar{E}_{eff}(r,B_g^2) = 2\left[1 - \frac{1}{\sqrt{2}} \frac{F_0^1(B_g)j_0(B_g r) + \frac{A_U}{A_{B_g}} F_0^1(U)j_0(iUr)}{j_0(B_g r) + \frac{A_U}{A_{B_g}} j_0(iUr)}\right] \tag{2.75}$$

where

$$\frac{A_U}{A_{B_g}} = -\frac{F_0^1(B_g)j_0(B_gR) + \frac{2}{3}(t_{01}^{(0)} + t_{11}^{(0)}F_0^1(B_g)\, j_1(B_gR)}{F_0^1(U)j_0(iUR) - \frac{2i}{3}(t_{01}^{(0)} + t_{11}^{(0)}F_0^1(U))\, Uj_1(iUR)} \tag{2.76}$$

and

$j_1(x)$ = First order spherical Bessel function

$$= \frac{\sin x}{x^2} - \frac{\cos x}{x}$$

$\bar{E}_{eff}(r,B_g^2)$ is a measure of the way in which the neutron

energy spectrum changes with position and how accurately space and energy can be made separable. Two special cases are of interest: $\bar{E}_{eff}(0,B_g^2)$ and $\bar{E}_{eff}(R,B_g^2)$. These are respectively given by

$$\bar{E}_{eff}(0,B_g^2) = 2\left[1 - \frac{1}{\sqrt{2}} \frac{F_0^1(B_g) + (UA_U/B_gA_{B_g})F_0^1(U)}{1 + (UA_U/B_gA_{B_g})}\right] \qquad (2.77)$$

$$\bar{E}_{eff}(R,B_g^2) = 2\left[1 - \frac{1}{\sqrt{2}} \frac{F_0^1(B_g) + YF_0^1(U)}{1 + Y}\right] \qquad (2.78)$$

where

$$Y = - \frac{F_0^1(B_g) + \frac{2}{3}[t_{01}^{(0)} + t_{11}^{(0)}F_0^1(B_g)](B_g\coth B_gR - 1/R)}{F_0^1(U) + \frac{2}{3}[t_{01}^{(0)} + t_{11}^{(0)}F_0^1(U)](U\coth UR - 1/R)}$$

For an infinite medium

$$\bar{E}_{eff}(R\to\infty\ ,\ B_g^2\to 0) = 2KT \quad , \qquad (2.79)$$

the same as that one obtained by assuming space and energy to be rigorously separable. This average is for the Maxwellian distribution. For a finite medium, however, there is a preferential leakage that depends strongly on the behavior of the transport mean free path with energy (59). For light water, λ_{tr} is proportional to the square root of energy and the preferential leak is in favor of the high

energy neutrons, a matter that results in a diffusion cooling phenomenon. For most of the crystalline moderators, like beryllium, the reverse is true (59) and one has a diffusion heating.

The effective average energy for light water is plotted as a function of position in Figure 2.13. The plot (for $M_2 = 3.34\ cm^{-1}$) shows the constancy of the average energy with position up to a distance from the boundary in the order of U^{-1}. Close to the outer boundary, there is a marked increase in $\bar{E}_{eff}$. A physical explanation of these results can be given in the light of certain experiments. According to Zinn (61) the temperature of neutrons emitted from a paraffin surface was 390°K whereas their temperature inside the medium was 300°K .

In conclusion, for a precise calculation of the neutron spectrum in a finite system it is necessary to take into account the changes in neutron density and spectrum in the vicinity of the boundary of the medium, which are caused by escape, and also the transfer of neutrons from a group with one energy to a group with another as a sequence of the energy exchange in the medium.

2. Effective buckling

The asymptotic region can be displayed quite easily by the expression (24)

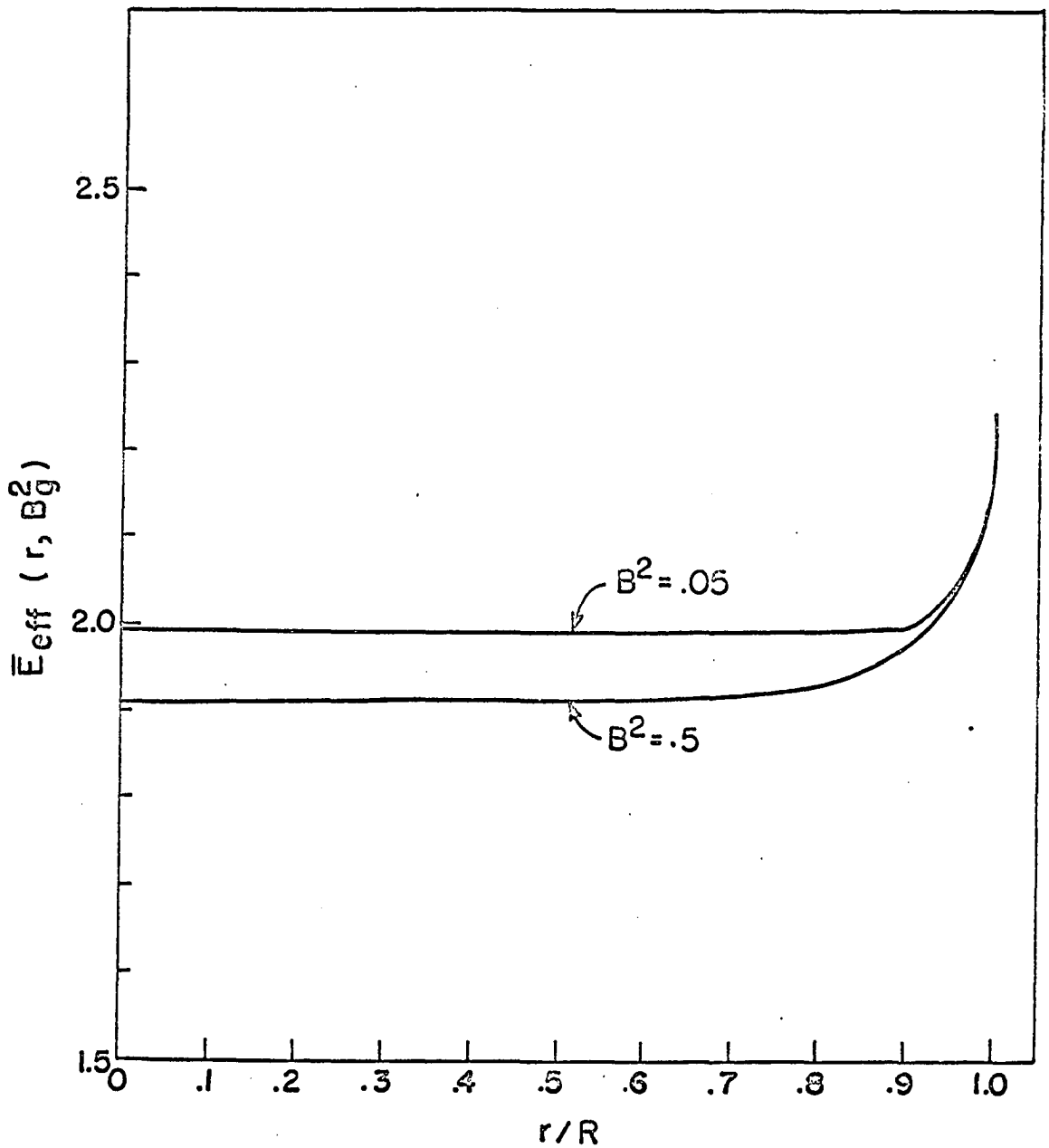

Figure 2.13. Variation of the effective average energy with position for M_2 = 3.34 cm^{-1}. Water is taken as 1/V scatterer

$$B^2_{eff} = - \frac{\Delta \int_0^\infty \phi_0(r,E)dE}{\int_0^\infty \phi_0(r,E)dE}$$

$$= B_g^2 \frac{\sin B_g r - \frac{U}{B_g} \sinh Ur}{\sin B_g r + \frac{B_g}{U} \sinh Ur} \qquad (2.80)$$

disregarding the second term of 2.80, i.e., taking into account the asymptotic flux, then $B_g^2 = B^2_{eff}$. Thus the space variation of B^2_{eff} and its departure from B_g^2 indicate the departure from the asymptotic region. B^2_{eff} and $-\Delta\phi_0(r,E)/\phi_0(r,E)$ for a sphere of water are plotted in Figure 2.14. Here $B_g^2 = 0.5\ cm^{-2}$. The effective buckling behaves in a fashion similar to the effective average energy defined above. However, the relative variation of B^2_{eff} is much greater than that of the average energy. The Figure also indicates that B^2_{eff} corresponds to $-\Delta\phi_0(r,E)/\phi_0(r,E)$ at $E = 2KT$.

F. The Buckling Dependence of the Extrapolation Distance

To obtain the extrapolation distance in case of the existence of an asymptotic region the boundary conditions must be applied. For the vacuum-matter interface the Marshak's boundary condition can be used. In the P_1 approximation it has the form:

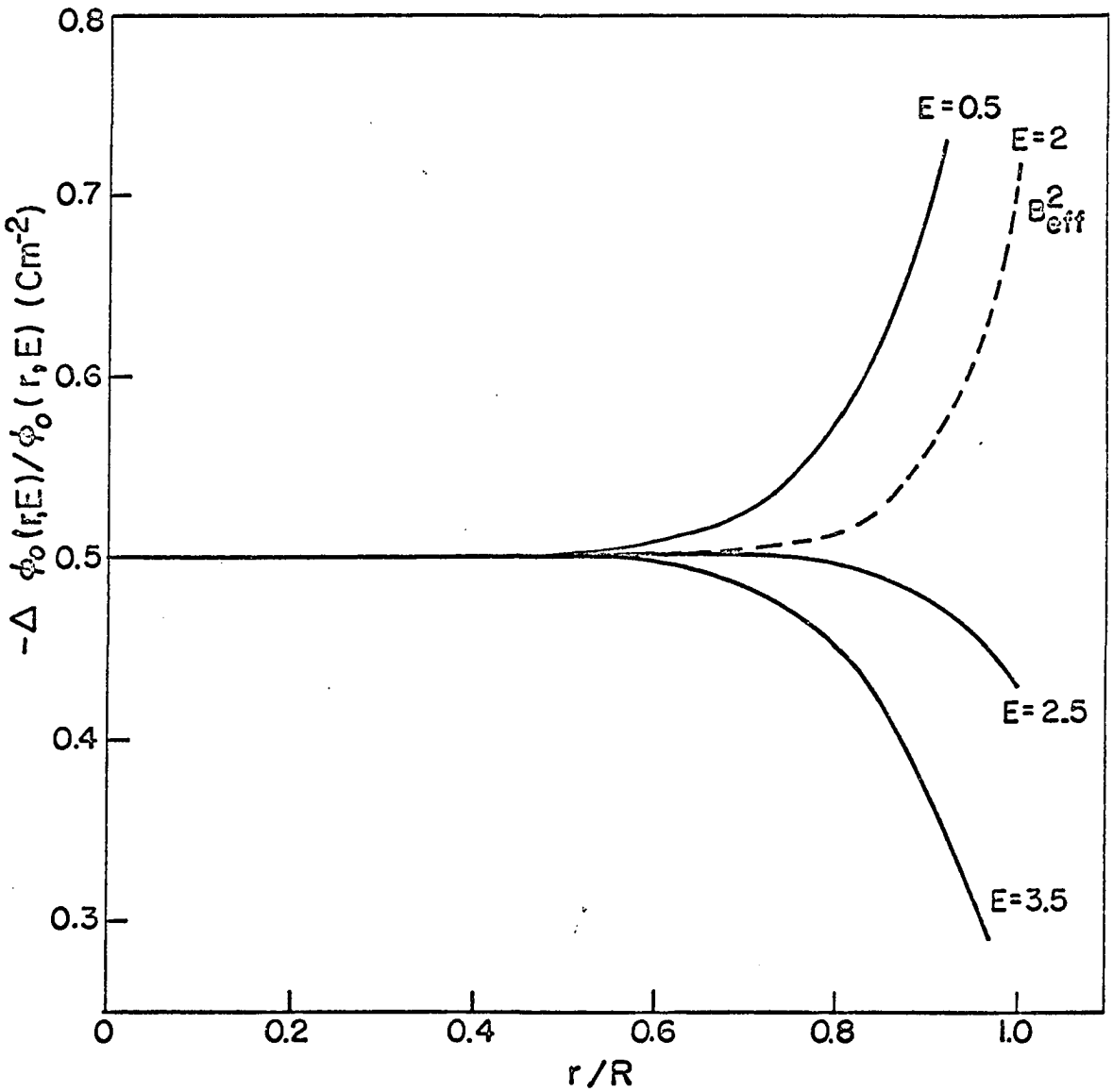

Figure 2.14. Variation of the effective buckling and $-\Delta\phi_0(r,E)/\phi_0(r,E)$ with position for M_2 = 3.34 cm^{-1}. Water is taken as 1/V scatterer

$$\phi_0(R,E) - 2\phi_1(R,E) = 0 \tag{2.81}$$

and in the L_1 approximation:

$$\phi_0^0(R) - 2\phi_1^0(R) = 0 \tag{2.82.a}$$

$$\phi_0^1(R) - 2\phi_1^1(R) = 0 \tag{2.82.b}$$

From equation 2.6, 2.16, 2.33 and 2.63

$$\phi_0^0 = A_{B_g} j_0(B_g R) + A_U j_0(iUR) \tag{2.83}$$

$$\phi_0^1 = A_{B_g} F_0^1(B_g) j_0(B_g R) + A_U F_0^1(U) j_0(iUR) \tag{2.84}$$

$$\phi_1^0(R) = \frac{A_{B_g} B_g}{3}[t_{00}^{(0)} + t_{01}^{(0)} F_0^1(B_g)] j_1(B_g R) + i\frac{A_U U}{3}[t_{00}^{(0)} + t_{01}^{(0)} F_0^1(U)] j_1(iUR) \tag{2.85}$$

$$\phi_1^1(R) = \frac{A_{B_g} B_g}{3}[t_{01}^{(0)} + t_{11}^{(0)} F_0^1(B_g)] j_1(B_g R) + \frac{iA_U U}{3}[t_{01}^{(0)} + t_{11}^{(0)} F_0^1(U)] j_1(iUR) \tag{2.86}$$

By the substitution of these equations into 2.82, the following characteristic equation can be obtained.

$$\begin{vmatrix} j_0(B_gR) - \frac{2B_a}{3}(t_{00}^{(0)} + t_{01}^{(0)}F_0^1(B_g))j_1(B_gR) & \\ \frac{B_a}{U}j_0(iUR) - \frac{2iB_a}{3}(t_{00}^{(0)} + t_{01}^{(0)}F_0^1(U))j_1(iUR) & \\ j_0(B_gR) - \frac{2}{3}B_g(t_{01}^{(0)} + t_{11}^{(0)}F_0^1(B_g))j_1(B_gR) & \\ \frac{B_a}{U}j_0(iUR) - \frac{2i}{3}B_g(t_{01}^{(0)} + t_{11}^{(0)}F_0^1(U))j_1(iUR) & \end{vmatrix} = 0 \qquad (2.87)$$

The conventional definition of the geometric buckling for a sphere with a radius R is

$$B_g^2 = (\frac{\pi}{R + d})^2$$

This definition can only be retained if $d = d(B_g^2)$. The substitution of

$$j_0(B_gR)/n_0(B_gR) = \tan B_g d \qquad (2.88)$$

into 2.87 yields

$$d(B_g) = \frac{1}{B_g}\left[\tan^{-1}\left(\frac{\frac{2}{3}B_g^2(t_{00}^{(0)} + t_{01}^{(0)}F_0^1(B_g)) \times \left(1 - \frac{t_{01}^{(0)} + t_{11}^{(0)}F_0^1(B_g)}{t_{00}^{(0)} + t_{01}^{(0)}F_0^1(B_g)} \times \frac{a}{h}\right)}{1 - \frac{2}{3R}(t_{00}^{(0)} + t_{01}^{(0)}F_0^1(B_g)) - (F_0^1(B_g) - \frac{2}{3R}(t_{01}^{(0)} + t_{11}^{(0)}F_0^1(B_g)))\frac{a}{h}}\right)\right] \qquad (2.89)$$

where

$$g = R - \frac{2}{3}[t_{00}^{(0)} + t_{01}^{(0)}F_0^1(U)][1 - URcothUR] , \qquad (2.90)$$

$$h = RF_0^1(U) - \frac{2}{3}[t_{01}^{(0)} + t_{11}^{(0)}F_0^1(U)][1 - URcothUR] \qquad (2.91)$$

The physical meaning of the factor $(t_{00}^{(0)} - t_{01}^{(0)}F_0^1(B_g))$ is made clear by observing that

$$\lambda_{tr}(E) = 1/[\Sigma_{TR}(E) - \frac{\lambda_0}{V_0}]$$

and

$$\frac{\int_0^\infty F_0(B_g,E)\lambda_{tr}(E)dE}{\int_0^\infty F_0(B_g,E)dE} = t_{00}^{(0)} + t_{01}^{(0)}F_0^1(B_g) = \langle \lambda_{tr}(E) \rangle_{F_0} \qquad (2.92)$$

Thus this factor is the effective transport mean free path averaged over the asymptotic distribution. It gives the buckling dependence of the extrapolation distance resulting from the diffusion cooling.

Equation 2.89 is a transcendental equation since it emplicitly contains $d(B_g)$ in the right hand side. The extrapolation distance for a given buckling was obtained through an iterative technique carried out on the IBM-360 computer. The results, for various scattering kernels, are listed in Table 2.19 and plotted in Figure 2.15. Gelbard and Davis

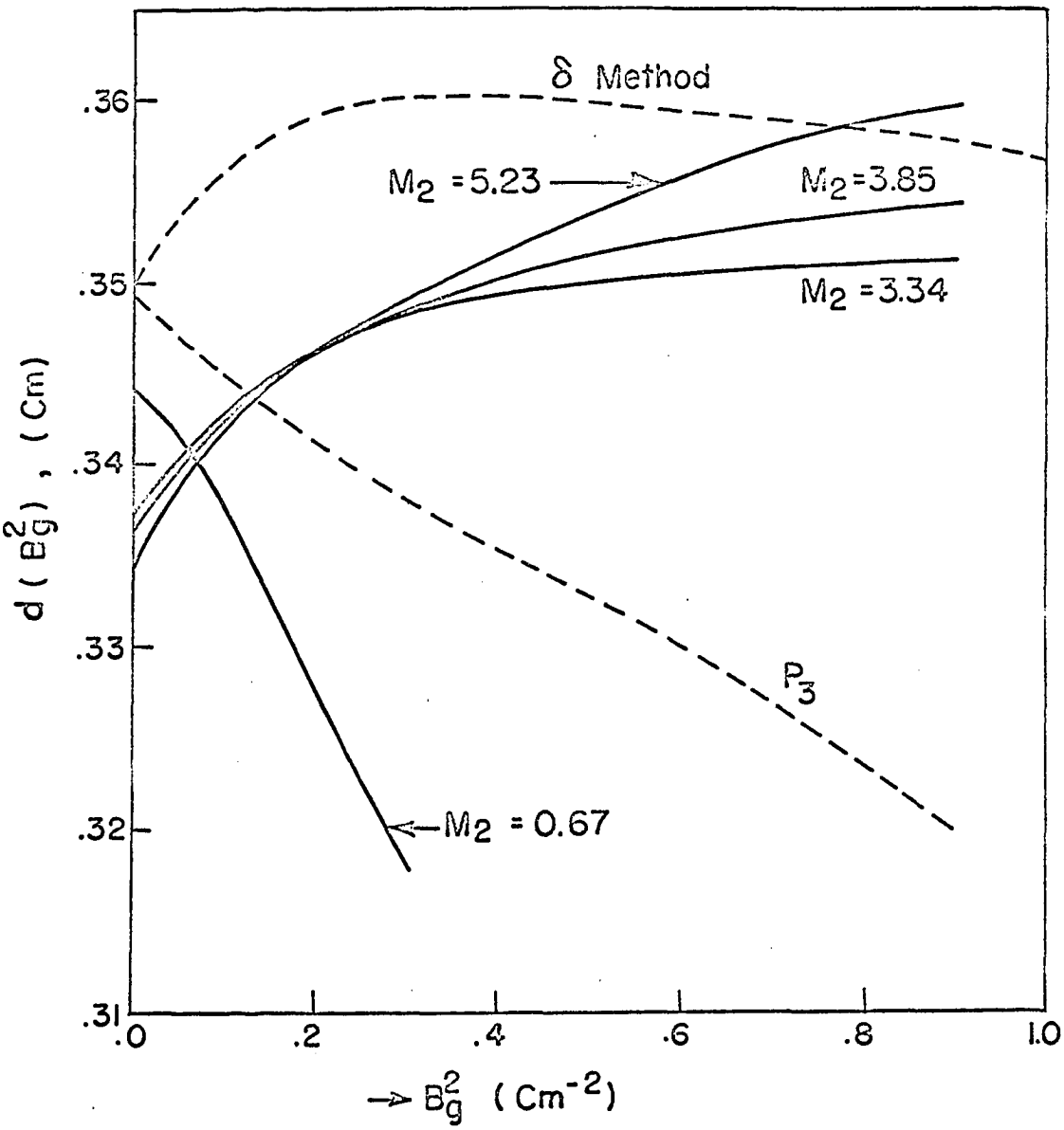

——— Calculated using 2.89
------ Gelbard and Davis (24)

Figure 2.15. The buckling dependence of the extrapolation distance in spherical geometry. The variation with M_2 is indicated

Table 2.19. The buckling dependence of the extrapolation distance in spherical geometry for different values of M_2

B_g^2 (cm^{-2})	Extrapolation distance, $d(B_g^2)$ cm			
	M_2 = 0.67 cm^{-1}	M_2 = 3.34 cm^{-1}	M_2 = 3.85 cm^{-1}	M_2 = 5.23 cm^{-1}
0.000	0.3432	0.3369	0.3362	0.3347
0.025	0.3430	0.3389	0.3383	0.3369
0.050	0.3416	0.3409	0.3404	0.3392
0.150	0.3326	0.3451	0.2451	0.3446
0.200	0.3276	0.3464	0.3466	0.3465
0.300	0.3182	0.3482	0.3488	0.3495
0.500	-**	0.3502	0.3517	0.3541
0.700	-**	0.3511	0.3536	0.3576
0.900	-**	0.3514	0.3548	0.3605

**The theory does not hold at this value of B_g^2.

(24) have also calculated the extrapolation distance for the P_3 and the diffusion approximation. The dotted curves show their results. For the P_3 calculations, the authors employed the Radkowsky kernel and the Marshak's boundary condition. The diffusion theory curve was obtained by the delta method that consists of defining a linear extrapolation distance

$$-\frac{1}{\delta} = \frac{d}{dr}\left(\frac{\sin B_g r}{r}\right)\Bigg|_{r=R} \Big/ \left(\frac{\sin B_g r}{r}\right)\Bigg|_{r=R} \qquad (2.93)$$

and an augumentation length ($d(B_g)$ in this section). By

plotting δ versus B_g^2 and starting with a trial value equals to $d(0)$, $d(B_g)$ can be obtained by iterating between 2.93 and

$$B_g^2 = \left[\frac{\pi}{R + d(B_g)}\right]^2$$

From Figure 2.15 it is clear that, while the P_1-L_1 curves have the general shape of the delta-curve, they markedly disagree with the P_3 curve. It can be concluded, therefore, that the P_1-L_1 approximation in spherical geometry with the Marshak's boundary condition over-estimates the buckling dependence of the extrapolation distance.

Gelbard (23) remarked that in a P_N approximation of any order the eigenvalue of a spherical reactor is exactly equal to the eigenvalue of an "equivalent" slab reactor. An "equivalent" slab reactor is a slab reactor of half thickness R, having the same composition as the sphere. The flux in the "equivalent" reactor is constrained to be antisymmetric about its midplane. Thus the main mode of a bare sphere having a diameter 2R is equal to the second mode of a bare slab, of the same composition, with thickness 2R. In another paper by Gelbard and Davis (24) it has been pointed out that the extrapolation distances for a sphere and the corresponding equivalent slab are exactly the same in the P_3 approximation.

To test the validity of Gelbard's observations in case of the P_1-L_1 approximation, the equivalent slab calculations

were carried out using (53):

$$d(B_g) = \frac{1}{B_g}\left[\tan^{-1}\left(\frac{2}{3}B_g\left(t_{00}^{(0)} + t_{01}^{(0)}F_0^1(B_g)\right)\right.\right.$$

$$\left.\left. \times \frac{1 - \left(\dfrac{t_{01}^{(0)} + t_{11}^{(0)}F_0^1(B_g)}{t_{00}^{(0)} + t_{01}^{(0)}F_0^1(B_g)}\right)\frac{g}{h}}{1 - F_0^1(B_g)\frac{g}{h}}\right)\right] \qquad (2.94)$$

with g and h assuming the new forms:

$$g = 1 + \frac{2}{3}\left[t_{00}^{(0)} + t_{01}^{(0)}F_0^1(U)\right]U\tanh UR \qquad (2.95)$$

$$h = F_0^1(U) + \frac{2}{3}\left[t_{01}^{(0)} + t_{11}^{(0)}F_0^1(U)\right]U\tanh UR \qquad (2.96)$$

It should be noted that R in 2.94 is the half thickness of the "equivalent" slab and B_g^2 is its second lowest eigenvalue. Furthermore this equation can be obtained from 2.89 by deleting all terms explicitly containing R and replacing coth(UR) by tanh(UR). Thus the extrapolation distance of the equivalent slab is a limiting case of the corresponding bare sphere.

The extrapolation distances for the equivalent slab are listed in Table 2.20 and plotted in Figure 2.16 from which one can observe the marked improvement in the behavior of the extrapolation distance as a function of buckling. In this case the curve for the Nelkin's water agrees qualitatively with the P_3 curve. The difference in the magnitude is partly because of the error involving the P_1 approximation and

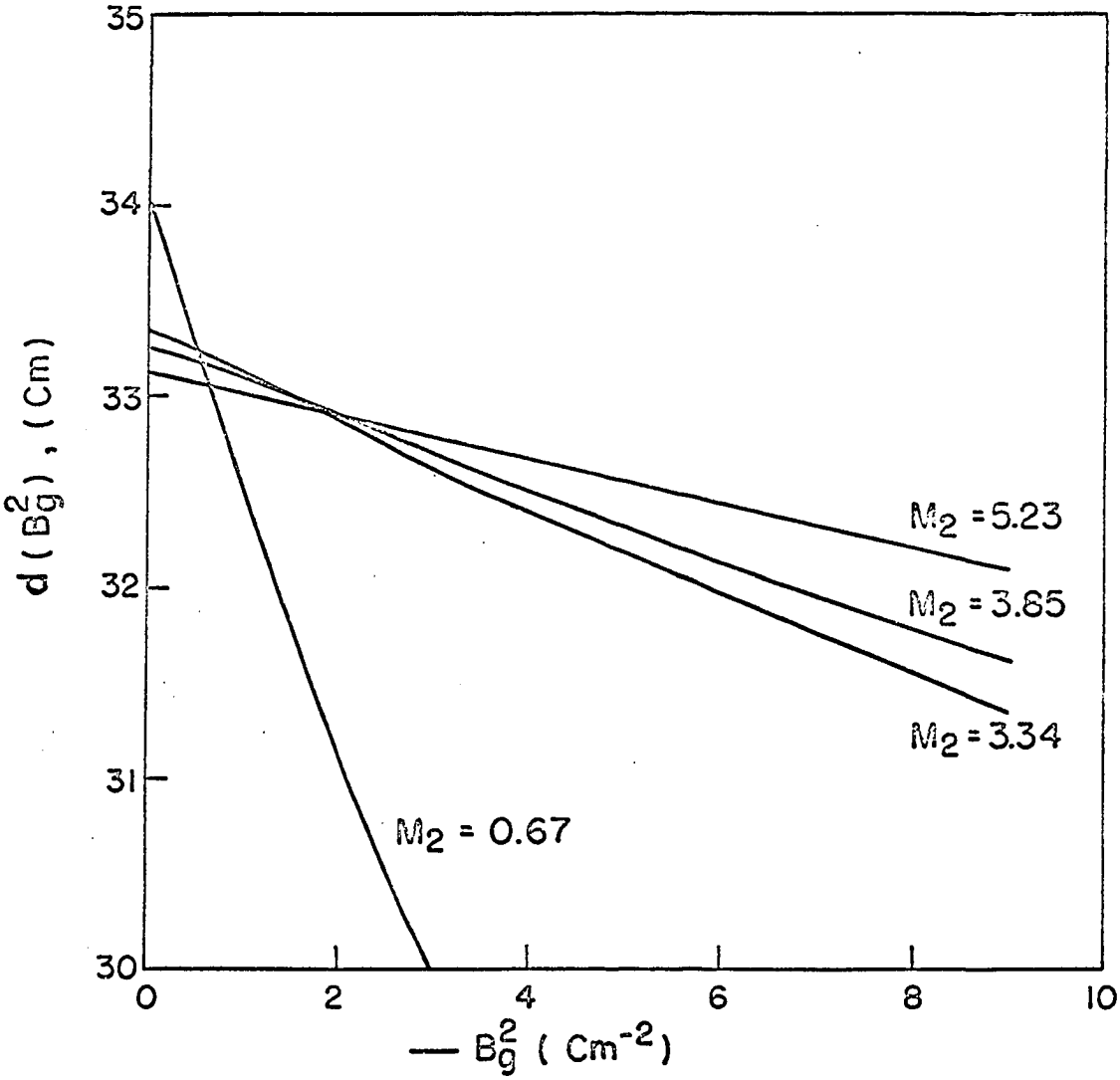

Figure 2.16. The buckling dependence of the extrapolation distance in "equivalent" slab geometries. The variation with M_2 is indicated

Table 2.20. The buckling dependence of the extrapolation distance in "equivalent" slab geometry for different values of M_2

B_g^2	Extrapolation distance, $d(B_g^2)$ cm			
(cm^{-2})	M_2 = 0.67 cm^{-1}	M_2 = 3.34 cm^{-1}	M_2 = 3.85 cm^{-1}	M_2 = 5.23 cm^{-1}
0.000	0.3405	0.3349	0.3313	0.3328
0.025	0.3366	0.3329	0.3310	0.3323
0.050	0.3327	0.3323	0.3307	0.3319
0.150	0.3180	0.3299	0.3295	0.3299
0.200	0.3113	0.3287	0.3289	0.3289
0.300	0.2994	0.3264	0.3277	0.3270
0.500	-**	0.3219	0.3254	0.3233
0.700	-**	0.3176	0.3232	0.3197
0.900	-**	0.3136	0.3211	0.3164

**The theory does not hold at this value of B_g^2.

partly because of the error in the L_1 approximation; besides, the two kernels are different.

From the foregoing, it can be concluded that in order for the P_1-L_1 approximation in spherical geometry to be useful in the analysis of pulse experiments the extrapolation distance of an equivalent slab should be used. This is because the Marshak's boundary condition is more suited to a slab than to a spherical geometry.

III. EQUIPMENT

The main components of the apparatus used in the experimental work are

A. Neutron generator.

B. Pulsing system.

C. 400-channel analyser.

D. Timer system.

E. Neutron detection system.

F. Spherical containers.

G. Shielding facility and detector mount.

The experimental arrangement of these components was as indicated by the schematic diagram shown in Figure 3.1. The individual components are described below. The generator control and pulsing console, 400-channel analyser, timer system and monitor detector are shown in Figure 3.2.

A. Neutron Generator

Fast neutrons were produced by the reaction of an accelerated positive ion beam (deutrons or protons) on a tritium target according to the following reaction:

$$D^2 + T^3 \rightarrow n^1 + He^4 + 17.6 \text{ Mev.}$$

The ion beam was produced by the Texas Nuclear Corporation Model 9400 Neutron Generator whose operation depends on the production, extraction and acceleration of ions. The major

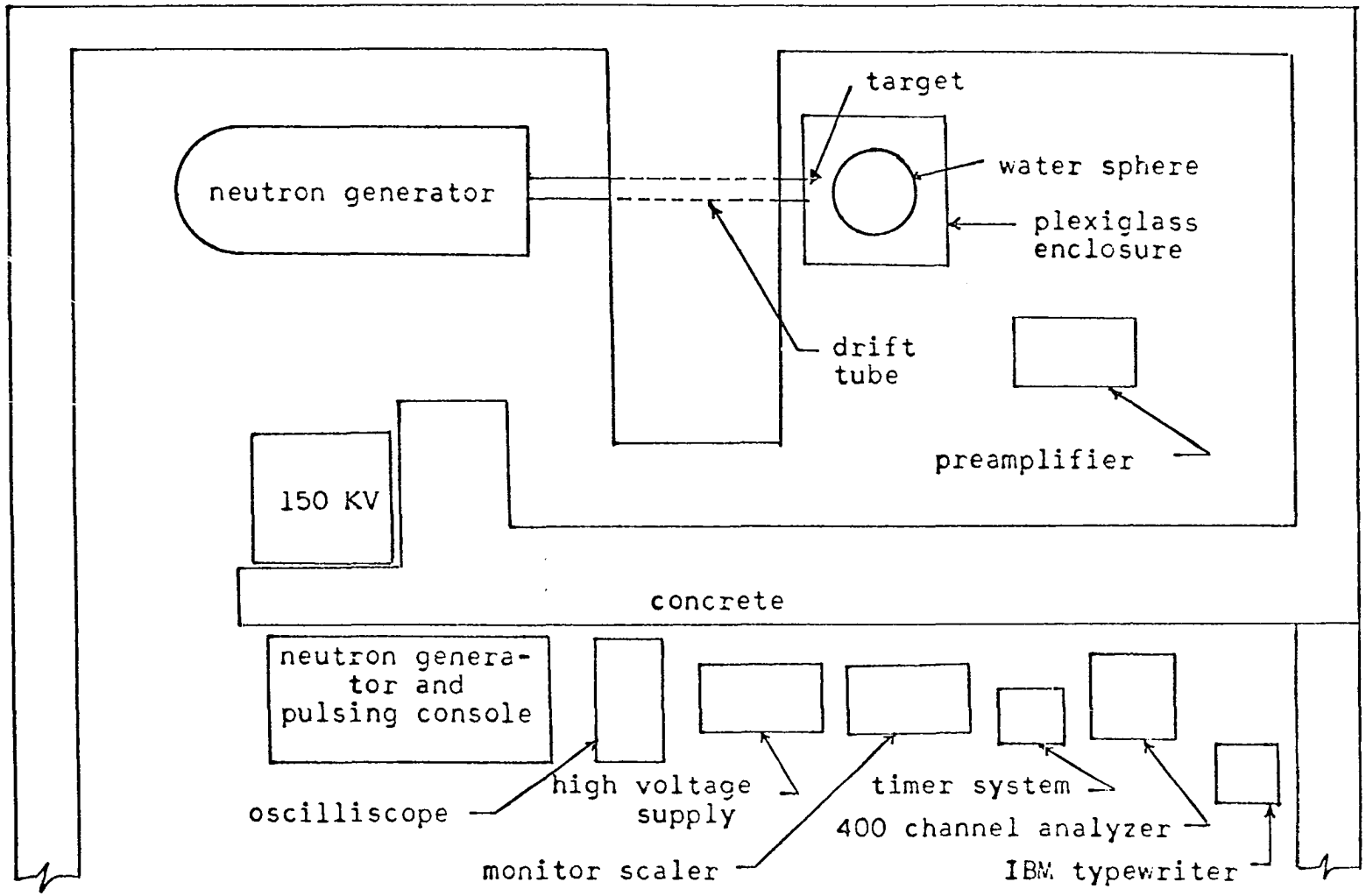

Figure 3.1. Arrangement of experimental equipment

Figure 3.2. Neutron generator and pulsing console, monitor scaler timer system, 400-channel analyzer, and accessory equipment

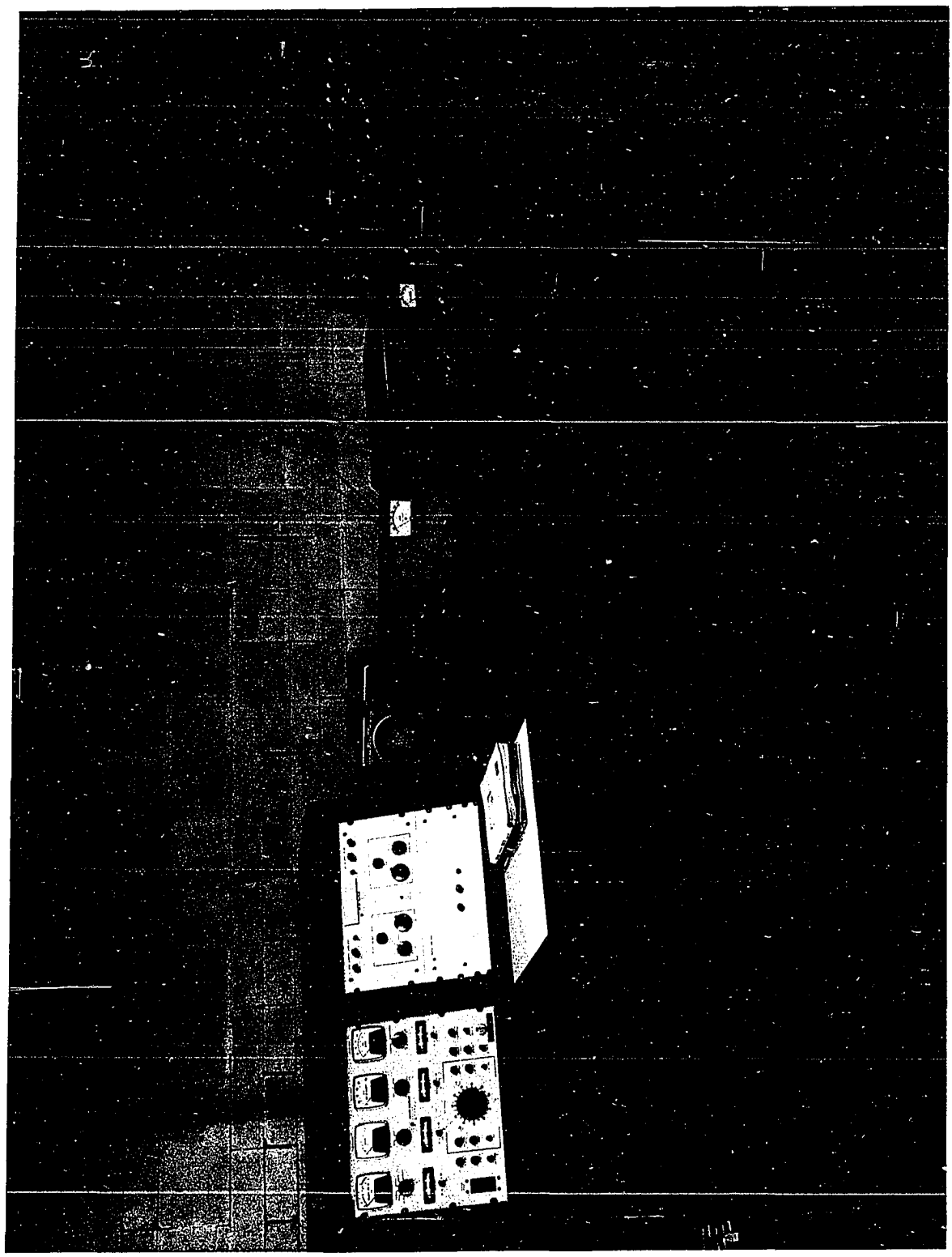

components of this generator are shown pictorially in Figure 3.3 and schematically in 3.4. Positive ions are produced in a radio-frequency type ion source and are extracted by applying a potential across the ion source bottle. The ions are focused by a gap lens situated directly after the exit canal of the ion source base. The ions leave the gap lens and enter the field of the accelerating tube where they are accelerated through a potential of 150 Kv. After leaving the accelerating tube, the ions drift through a potential free region (drift tube) until they strike the target. A vacuum is maintained through the entire system to minimize scattering of the ion beam.

The ion source used in the generator is a radio frequency type which is capable of producing an ion beam current in excess of one milliampere. The current is composed approximately of 90% singly ionized atomic ions and 10% molecular ions. Hydrogen (or deuterium) gas is allowed to flow into the pyrex ion bottle by means of a palladium leak. The gas from the leak enters through a hole in the ion source base. An r-f field (approximately 60 Mc/sec.) applied to the two excitor rings causes intense ionization of the hydrogen gas. The positive ions in the discharge are forced towards the exit canal by applying a positive potential across the bottle. A magnetic field whose lines of force are in the direction of the long axis of the bottle

Figure 3.3. Neutron generator

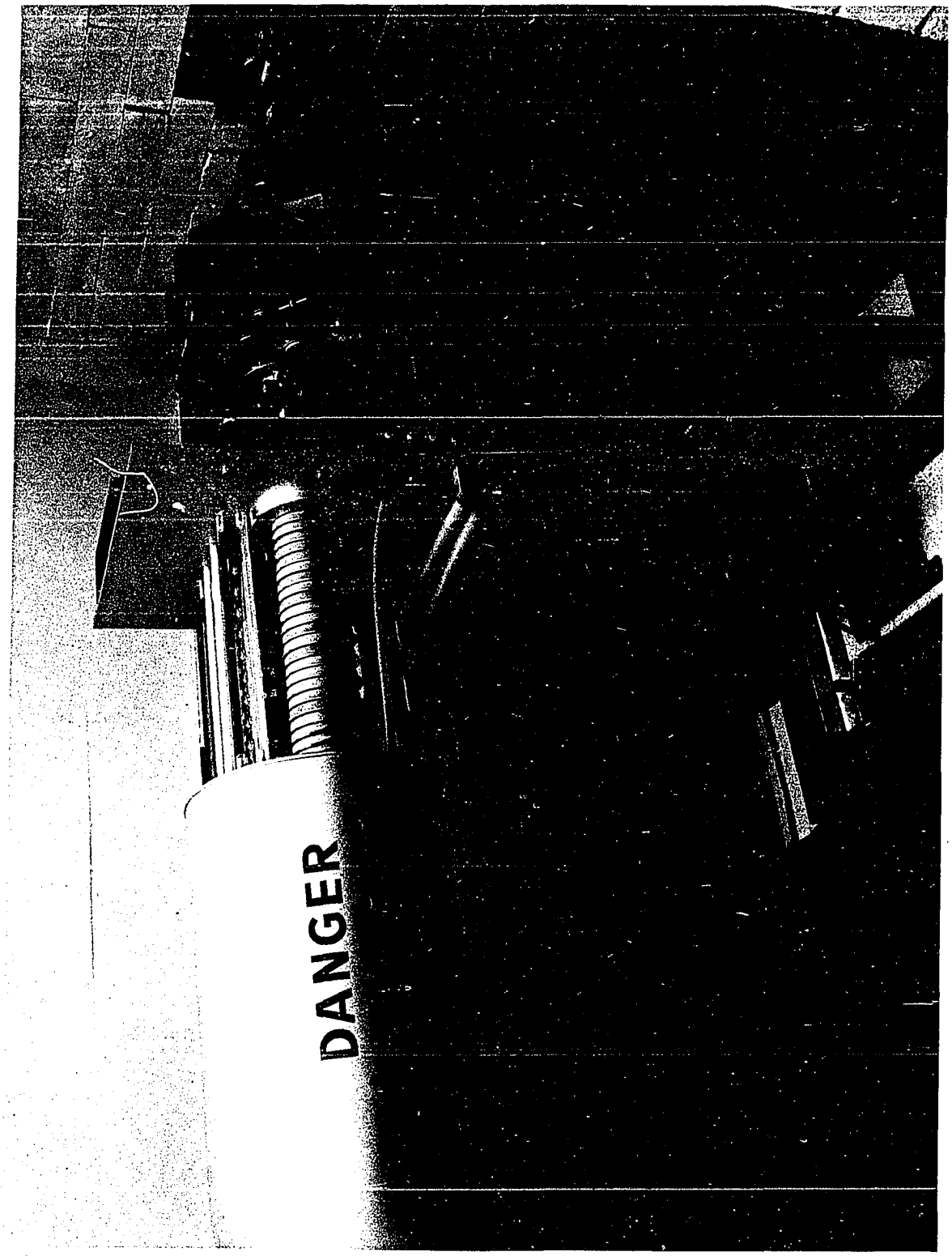
DANGER

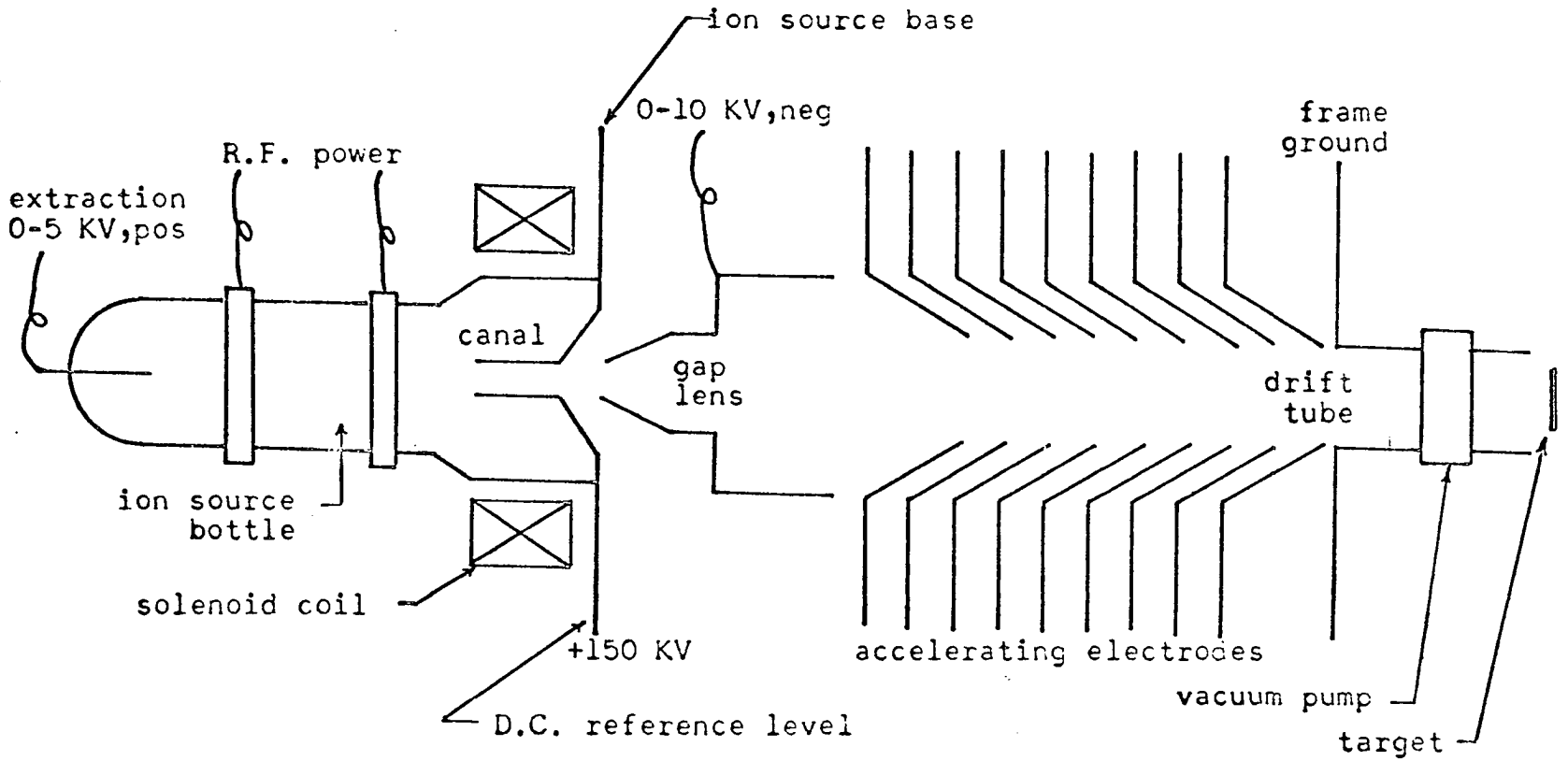

Figure 3.4. Major components of neutron generator

is produced by a solenoid coil and serves in restricting the electron paths to the center portion of the bottle and causes them to spiral. The spiraling motion increases the ionization probability in the region of the exit canal.

The target used with the 9400 consists of tritium absorbed onto a thin layer of titanium approximately 2 to 3 mg/cm^2 thick. The layer has been evaporated onto a 0.01 inch thick copper disc. The active area of the disc is 1.0 inch in diameter.

B. Pulsing System

The Texas Neutron Generator is equipped with a dual pulsing system which essentially eliminates any residual beam between pulses. This system is composed of pre-acceleration and post-acceleration systems operating simultaneously. The post and pre-acceleration systems are similar in the electrostatic deflection of the beam. After leaving the ion source, the beam is deflected by the pre-acceleration system. The post-acceleration system deflects the beam in the drift-tube section after it has been accelerated.

By using the dual pulsing system, an ion beam current is supplies to the target with the following specifications:

1. Pulse repetition rates over the continuous range from 10-10^5pps, or continuous beam operation.

2. Pulses 1 μ sec. to 10^4 μ sec. duration; duty cycle not to exceed 90 percent.
3. Pulse rise and decay times of approximately 0.5 u sec.
4. Peak pulse currents variable from 0 to 1 ma.
5. Residual beam between pulses approximately 0.0006 percent of the peak pulse current.

The above specifications were obtained from the Texas Nuclear Corporation instruction manual for pulsing systems (50).

C. 400-Channel Analyzer

The neutron flux as a function of time was recorded by the RIDL Model 34-12B transistorized 400-channel analyzer made by the Radiation Instrument Development Laboratory. The time analyzer was designed with a channel selector to provide 50, 100, 200 or 400 total channels with any desired duration. In its time mode it operates as though it were a large number of single channel analyzers. Each address channel becomes the equivalent of one single channel analyzer, with gross counting of input pulses through a controlled time period in each of the sequentially assigned channels. At the end of the time interval, the address is advanced to the next sequential channel. This operating cycle is advanced through the analyzer with a repetition rate determined by the product of the channel width and the total number of channels selected.

This means that the total time between pulses is constant, with any error in time divided by the number of channels that have been selected. The minimum cycle time for this operation is 10 μ sec. per channel.

There is provision for the temporary storage of one count during address advance, thus providing an effective zero dead time when the probability of two or more pulses within the 10 μ sec. time interval is small.

D. Timer System

For the operation of the channel analyzer in its time mode, an accessory time base control was used. This system is a Radiation Instrument Development Laboratory Model 88-901 Timer System. It consists of a set of two single size modular units installed in a Designer Series Model 29-1 instrument case and power supply. These units are a Model 54-6 Time Base Generator and a Model 52-9 Time Mode System Controller.

The Model 54-6 Time Base Generator furnishes pulses to the analyzer to provide channel advance. The timing provided for a channel width is adjustable from 12.5 u sec. to 800 μ sec. The analyzer dead time is held to a constant 12.5 μ sec. for the shorter channel widths. A normal automatic cycle consists of a period of dwell time, the same period of dwell in the second channel, a channel advance, etc. This is repeated until the number of channels selected as a subgroup

in the analyzer has been used; then the analyzer signals completion of one sequence and the Model 54-6 may stop automatically or it may repeat the sequence, depending on settings of its controls.

The Model 52-9 provides an optional automatic programming control for Model 34-12 and Model 54-6 combination. It permits the analyzer, operating in the time mode, to be recycled through a preset number of store cycles and then to be transferred to a read cycle for automatic readout or printout.

E. Neutron Detection System

The components of this system are two BF_3 proportional counters, a preamplifier, a linear amplifier and a Radiation Instrument Development Laboratory scaler.

The first detector serves as a transverse detector inside the sphere. This detector is a Miniature Model Mn i, produced by the N. Wood Counter Laboratories. It is one-fourth inch in diameter and one inch long. Its active length is about 2.2 cm. The filling gas is BF_3 with 96 percent enrichment in B^{10}. The gas pressure is only known to lie between 20 and 60 centimeters of mercury. For protection against water, the detector was sealed inside a long lucite light pipe to be held by a clamp mounted on a vertically graduated aluminum holder.

The second BF_3 neutron detector was used as a monitor for normalization purposes. The detector is about one-half inch in diameter and four inches long. The active length is about one inch. The detector was placed at a fixed position inside the shielded tank and coupled to a Radiation Instrument Development Laboratory scaler.

At intervals during the series of measurements, the detector and the time analyser were checked by a Chi-square test for randomness and reproducibility.

F. Spherical Containers

The spherical geometry was made possible by placing water inside round bottom pyrex flasks. Each flask was chosen to have the narrowest possible neck so that it would approximate a sphere when filled up to the neck with distilled water. The degree of sphericity of each flask was checked by comparing its average radius, as determined by volumetric methods, with the radius along the neck axis measured from the center to the water level. The two values were found to agree up to the first decimal.

The flasks used have the following average radii:

Flask number	Average radius
1	17.025 ± 0.005 cm.
2	14.412 ± 0.005 cm.
3	10.830 ± 0.004 cm.
4	8.968 ± 0.003 cm.

5	7.735 ± 0.003 cm.
6	6.348 ± 0.004 cm.
7	4.863 ± 0.001 cm.
8	4.196 ± 0.0005 cm.
9	3.553 ± 0.0003 cm.

The spheres were held in position by placing them on cork rings lined with 20 mils cadmium to minimize scattering by the cork material.

G. Shielding Facility and Detector Mount

Figure 3.5 is a photograph of the rectangular tank enclosure used to prevent room-return neutrons from entering the water system. The tank is supported by a wooden frame 17.5 x 17.5 x 19.0 inch and lined from inside to the outside with a 40-mil cadmium sheet followed by a paraffin layer 1.25 inch thick, 20-mil cadmium layer then an outermost layer of 2-inch thick plexiglass. An opening just large enough for the target assembly was left in the middle of the side facing the drift tube. The top of the assembly was covered by similar layers which could be removed to insert the sphere and allow the positioning of the traverse detector at a given source-sphere distance.

The detector holder consists of an aluminum sliding bridge, a graduated vertical stand and a plastic sliding clamp for holding the detector. The bridge slides on alu-

Figure 3.5. Shielding facility and detector mount

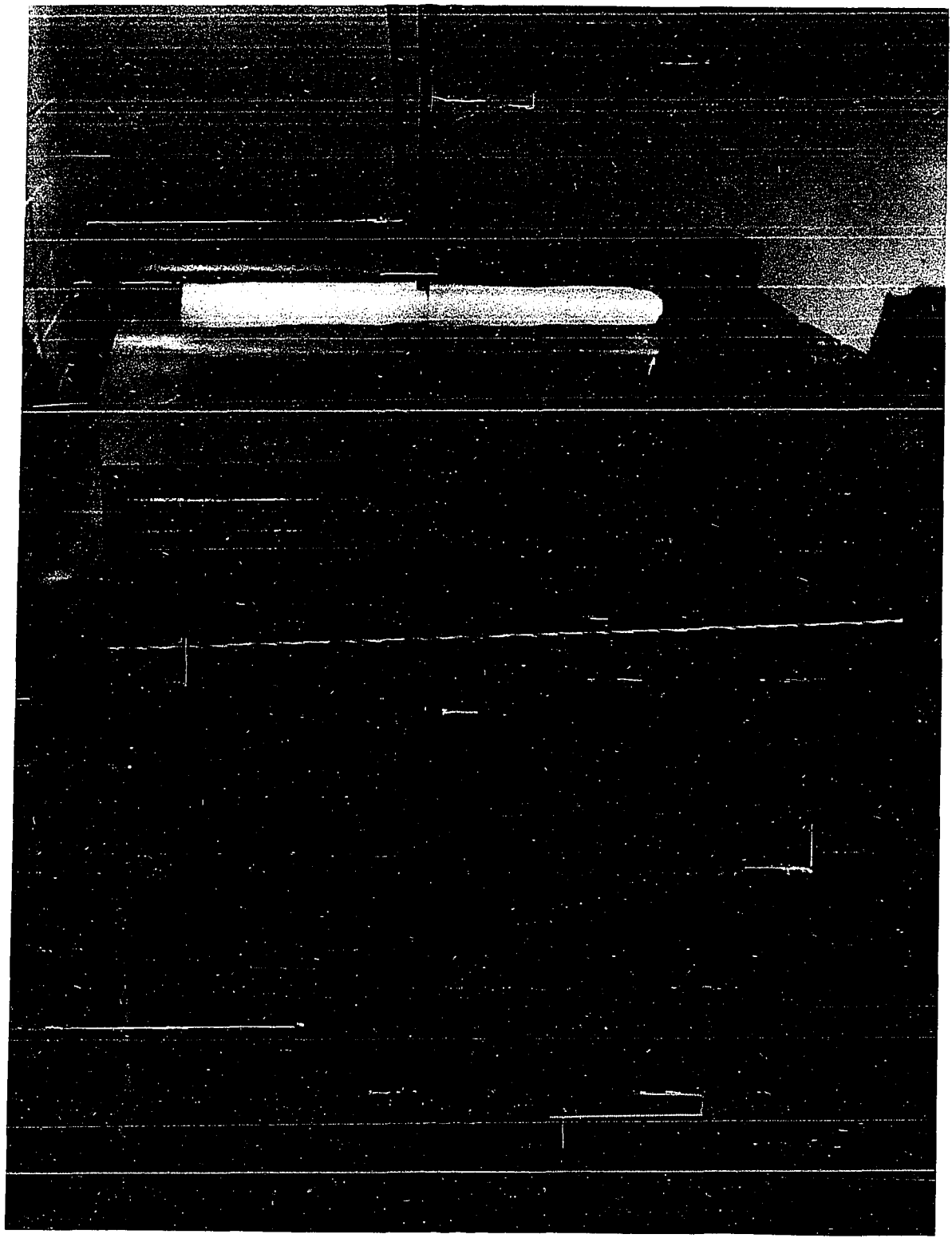

minum rails in a direction parallel to the axis of the drift tube. The vertical stand is positioned at the middle of the sliding bridge and supports the detector clamp that can be moved in a vertical direction. Thus the motion of the detector is restricted to an axial and vertical direction with respect to the source.

IV. EXPERIMENTAL PROCEDURE

To measure the flux distribution in a sphere along its Z-direction (the neck axis) it was necessary to locate the effective center of the detector. This was done by sliding the detector into a cadmium sleeve with a transverse slit 0.2 cm wide. The position of the slit on the detector was recorded and the detector was then placed inside a paraffin block in a neutron field from Po-Be source. The count rate at the given slit position was taken and the procedure was repeated until the whole length of the detector was surveyed. The differential curve obtained by this method and corrected for the background is shown in Figure 4.1 together with the corresponding integral curve. This integral curve represents the total count rate as a function of the Cd-uncovered length of the detector.

The differential curve is seen to exhibit an asymmetric Gaussian distribution. The position at the maximum of this distribution corresponds to the effective center of the detector; while the full width at half-maximum was considered as the effective length of the detector.

The average radius of each sphere was determined according to the following procedure. The sphere was cleaned with chromic-sulphuric acid mixture and rinsed with distilled water, alcohol, and then ether. After evaporating

Figure 4.1. Determination of the effective center of the BF_3 detector

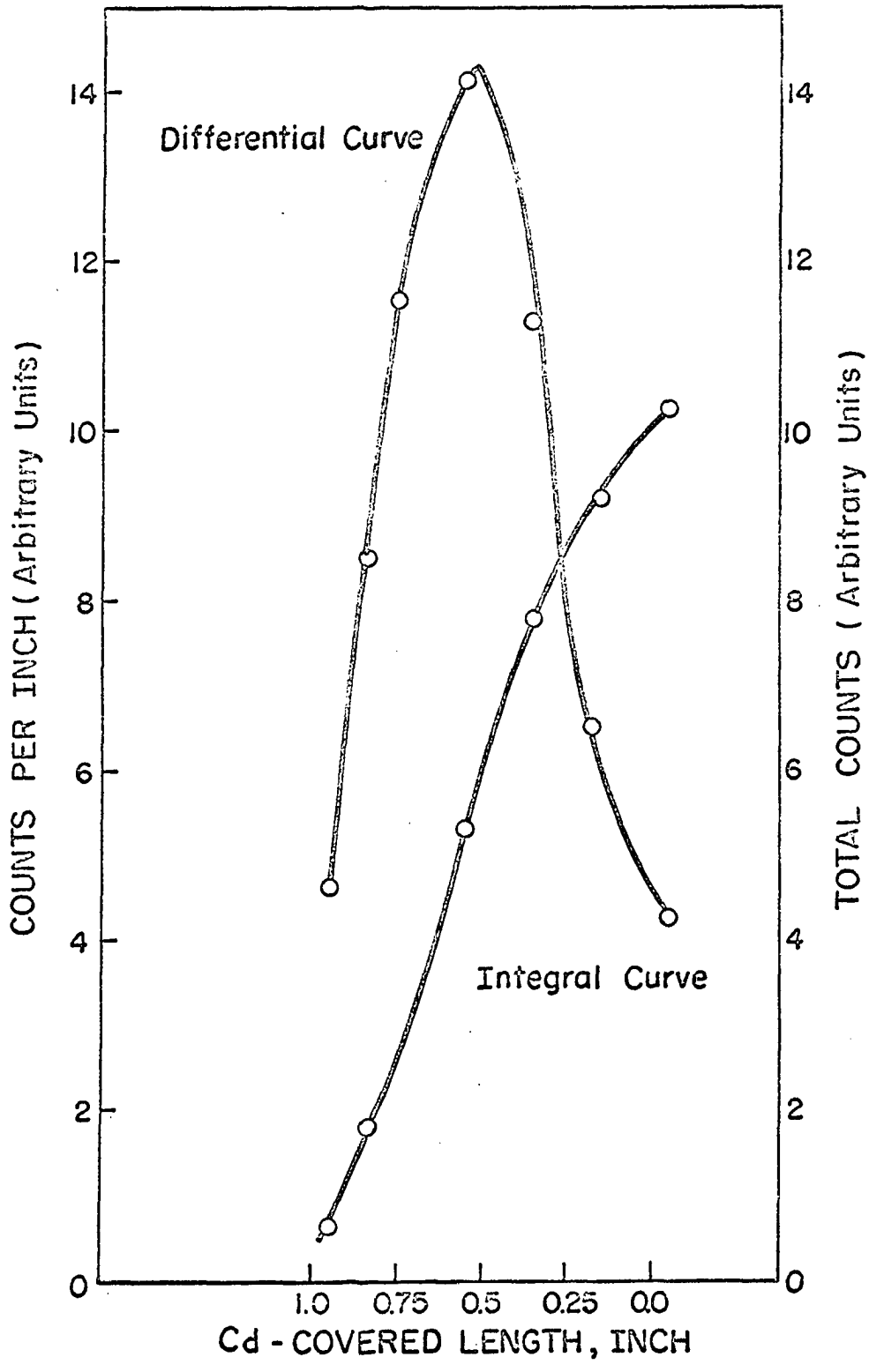
Differential Curve
Integral Curve
COUNTS PER INCH (Arbitrary Units)
TOTAL COUNTS (Arbitrary Units)
Cd - COVERED LENGTH, INCH
0
2
4
6
8
10
12
14
1.0
0.75
0.5
0.25
0.0

the ether in a dry air current and allowing the sphere to reach equilibrium at room temperature, water was added quantitatively to a level at which the tangent of the meniscus coincides with the spherical continuation at the neck. The transferal of water was carried out using volumetric flasks and burettes standardized at 20°C. With the volume of water in the sphere known, the average radius could be calculated.

Each sphere containing light water was symmetrically bombarded at the equatorial plane by pulses of fast neutrons (see Figure 4.2). These neutrons were produced by the D-T reaction as described earlier in chapter III. The ion beam was constantly maintained at 600 microamps. Pulsing was carried out at a rate of 50 pulses per second, with a neutron pulse width of 100 microsecond.

The counts from the detector were recorded and stored in the 400-channel analyzer. One hundred channels were used each having a 25-microsecond channel width and a dead time of 12.5 microseconds. The monitor detector counts were recorded on the monitor scaler that served as a basis to normalize each run to a constant pulsed source exposure.

Measurements were taken at a detector position until the monitor registered a preassigned total counts. This ranged from 50,000 counts for the largest sphere to 120,000 counts for the smallest one. The monitor and the 400-channel

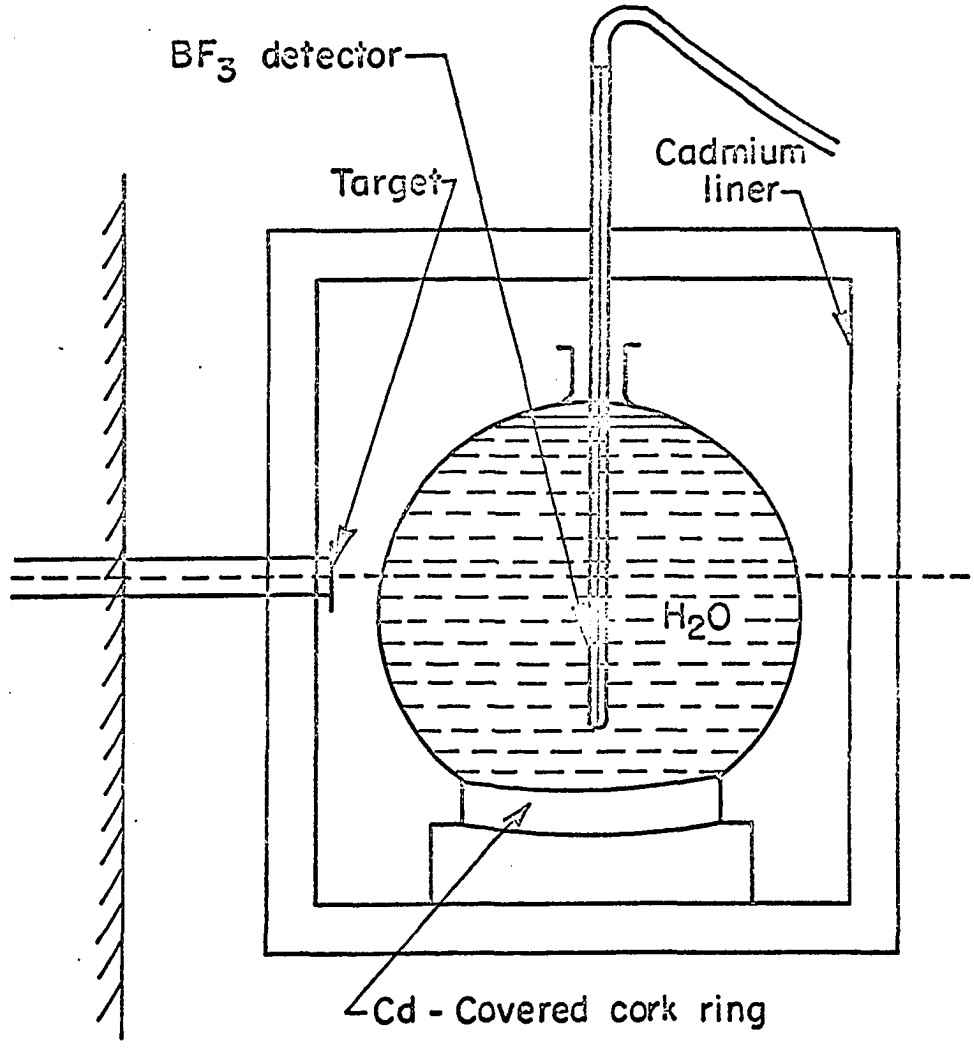

Figure 4.2. Experimental arrangement of neutron source, the spherical container and BF_3 detector

analyzer were then switched to the off position at the same time. The data stored in the 400-channel were automatically printed out by means of an accessory IBM typewriter. The detector was moved vertically to a new position and the procedure repeated until the accessible part of the z-axis was surveyed. The data were then corrected for the dead time and background.

V. ANALYSIS OF DATA, RESULTS AND DISCUSSION

A. Parameters of Pulsed Neutron Experiments

1. Determination of the decay constants for large spheres

Consider M space points along the z-axis (see Figure 5.1). Then at time t_k (which corresponds to the midpoint of the kth time channel), one has M measurements of the neutron flux

$$\phi(r_m,t_k) = \sum_{i=0}^{\infty} A_i(t_k) j_0(B_i,r_m) \qquad (5.1)$$

where

$$B_i^2 = \left[\frac{(i+1)\pi}{R + d(B_g)}\right]^2 \quad , i = 0,1,2,\ldots,$$

$B_0^2 = B_g^2$ = The geometric buckling.

Using only N terms in 5.1, one has M equations of conditions and N + 1 unknown coefficients to determine

$$\phi(r_1,t_k) = A_0(t_k)j_0(B_0,r_1) + A_1(t_k)j_0(B_1,r_1) + \ldots.$$
$$+ A_N(t_k)j_0(B_N,r_1)$$
$$\vdots$$
$$\phi(r_M,t_k) = A_0(t_k)j_0(B_0,r_M) + A_1(t_k)j_0(B_1,r_M) + \ldots.$$
$$+ A_N(t_k)j_0(B_N,r_M) \qquad (5.2)$$

or, using matrix notation,

Figure 5.1. Flux maping along the z-axis of a sphere with R_z = 14.46 cm and an average radius of 14.412 cm

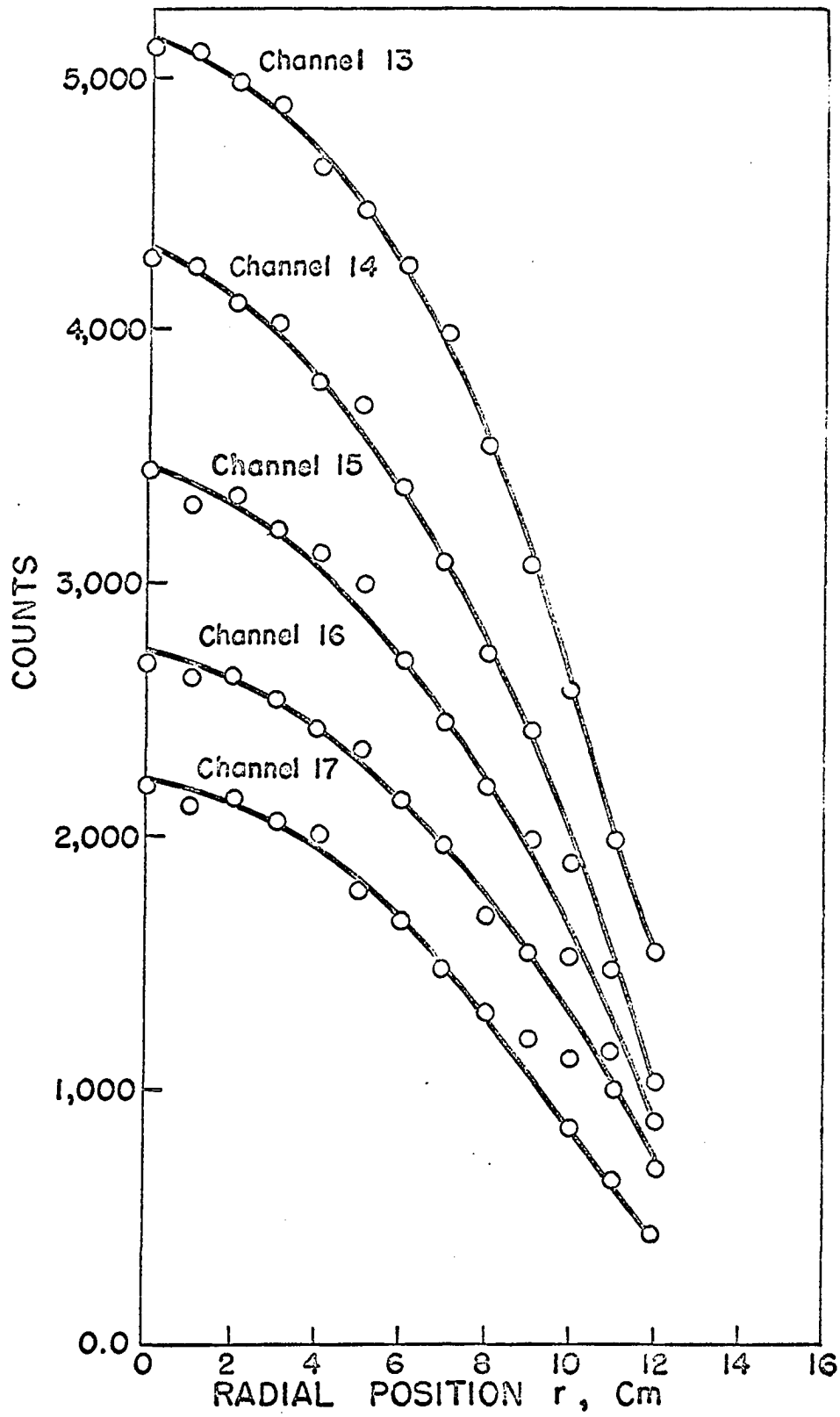
Channel 13
Channel 14
Channel 15
Channel 16
Channel 17
5,000
4,000
3,000
2,000
1,000
0.0
COUNTS
0
2
4
6
8
10
12
14
16
RADIAL POSITION r, Cm

$$\underline{X}(t_k) = W\,\underline{A}(t_k) \tag{5.3}$$

where $\underline{X}$ is a M-dimensional column vector, $\underline{A}$ is an $(N+1)$-dimensional column vector and W is an $Mx(N+1)$ matrix. By pre-multiplication of both sides of 5.3 by $(W^TW)^{-1}W^T$, one gets

$$\underline{A}(t_k) = (W^TW)^{-1}W^T\underline{X}(t_k) \tag{5.4}$$

The harmonic amplitudes of the four largest spheres were obtained from 5.4 by the method of least squares (32). Examples of these amplitudes are shown in Figure 5.2 and 5.3. For amplitudes higher than A_2, oscillations with time were observed. They were found to be independent of the truncation order of 5.2. The occurrence of these oscillations became significant for small spheres. The data in Table 5.1 illustrates this phenomenon for a sphere with an average radius of 8.968 cm. From this table one observes the fundamental amplitude decreasing with time in an exponential way free from any oscillation. The oscillations appear with the first harmonic amplitude and increase with increasing order of the harmonic.

There are two possible explanations for this unique feature of the spherical geometry. The first is the fact that the zeroth-order spherical Bessel functions have amplitudes that behave like 1/r and the count rate per unit length of a detector in a sphere is not symmetrically dis-

Figure 5.2. Relative decay of the fundamental mode and the higher harmonics along the z-axis of a sphere with R_{av} = 17.025 cm, R_z = 16.42 cm

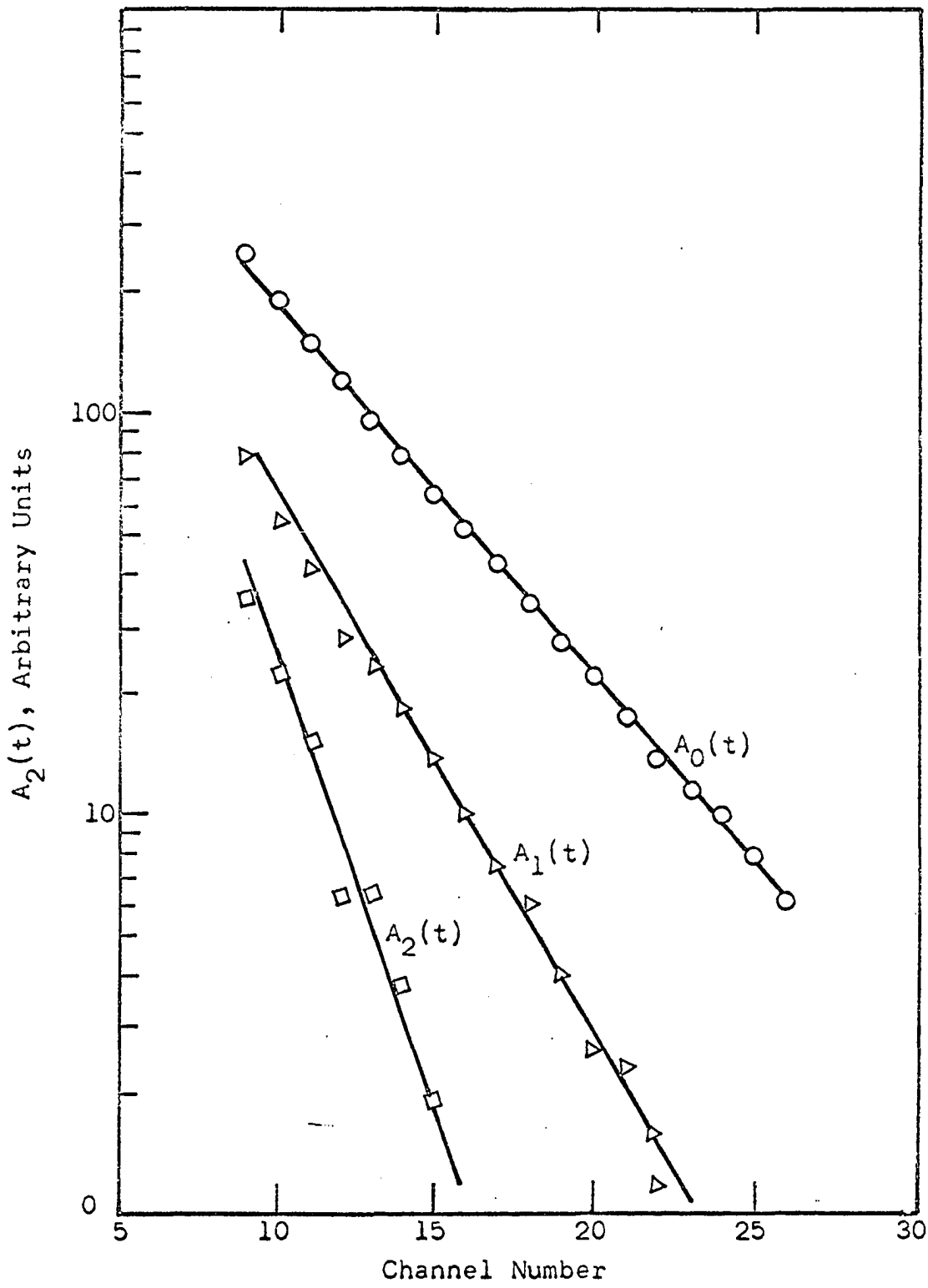
$A_2(t)$, Arbitrary Units
100
10
0
5
10
15
20
25
30
Channel Number
$A_0(t)$
$A_1(t)$
$A_2(t)$

Figure 5.3. Relative decay of the fundamental and the higher harmonics along the z-axis of a sphere with R_{av} = 14.42 cm

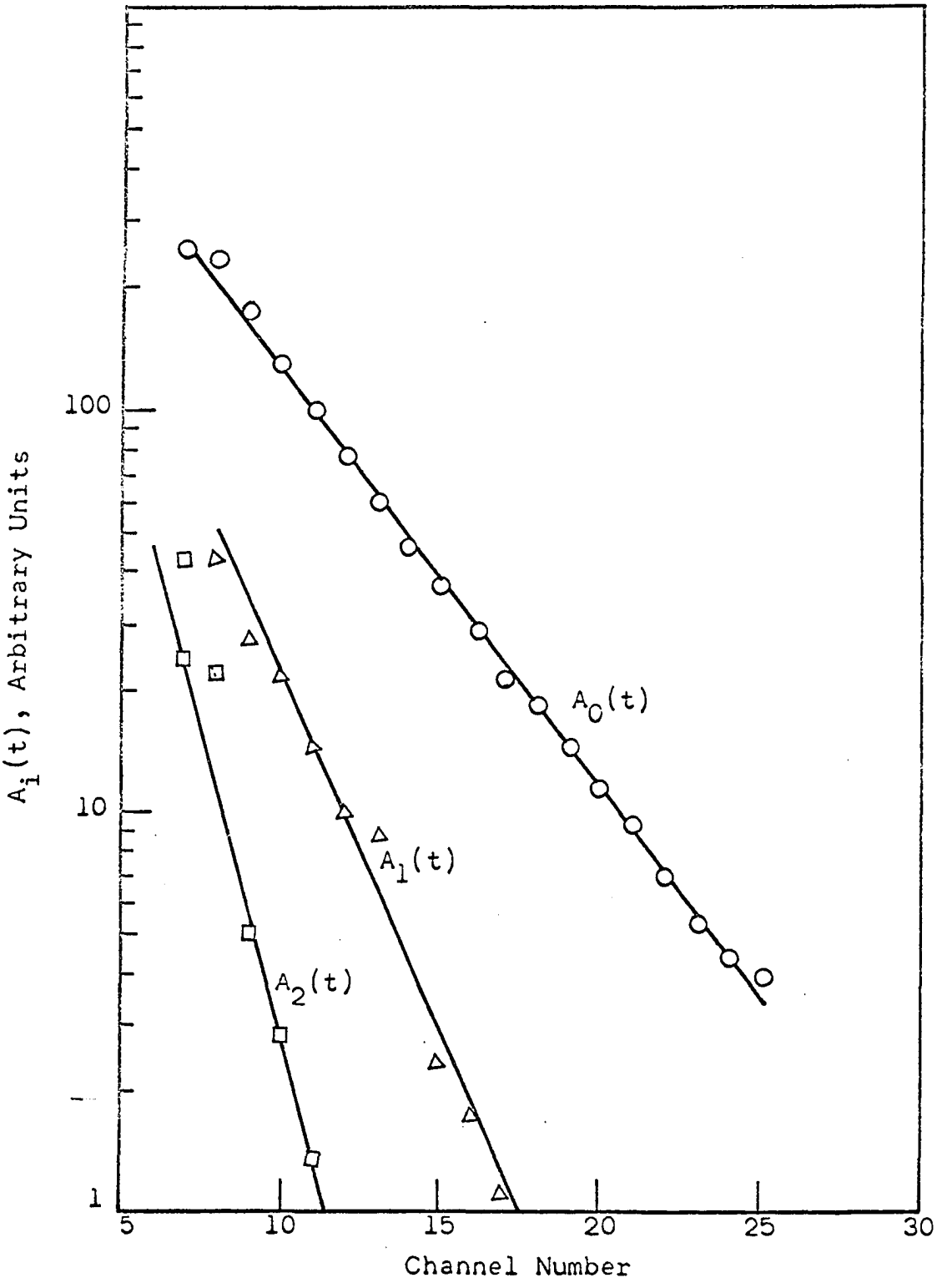
100
10
1
5
10
15
20
25
30
$A_i(t)$, Arbitrary Units
Channel Number
$A_0(t)$
$A_1(t)$
$A_2(t)$

Table 5.1. Oscillatory behavior of higher harmonics for a sphere with an average radius of 8.968 cm

Channel number	$A_0(t)$	$A_1(t)$	$A_2(t)$	$A_3(t)$	$A_4(t)$
4	67622.69	-6493.60	1638.28	-112.21	-181.51
5	46423.29	-2718.35	396.64	85.40	-25.68
6	32480.63	-1653.73	513.06	40.33	-91.37
7	22510.83	-801.09	449.31	-139.06	58.84
8	15956.35	-290.89	288.42	-82.03	-45.41
9	11216.57	-82.61	104.78	-5.16	25.82
10	8119.30	-78.24	84.74	-23.30	-4.29
11	5736.41	-96.42	205.52	-95.96	5.28
12	4204.54	-5.86	43.13	-37.42	25.49
13	3033.79	-84.15	48.65	-12.21	1.09
14	2166.71	-24.69	21.98	-7.92	3.46
15	1538.44	-15.48	-2.81	9.98	-3.33
16	1133.28	-25.16	25.31	-9.82	-1.04
17	764.18	-23.82	31.06	-8.03	4.31

tributed about the effective center of the detector. As a result, the detector does not behave like a point detector and would be, in a sphere, more sensitive to any variation with time than it would be in any other geometry. For the sake of illustration consider a sphere with an extrapolated radius R_{ext} and a slab with a extrapolated thickness H_{ext}. Consider two similar detectors placed in positions as shown in Figure 5.4. For detector number 2 there is a zero net contribution from the two equal shaded areas on both sides

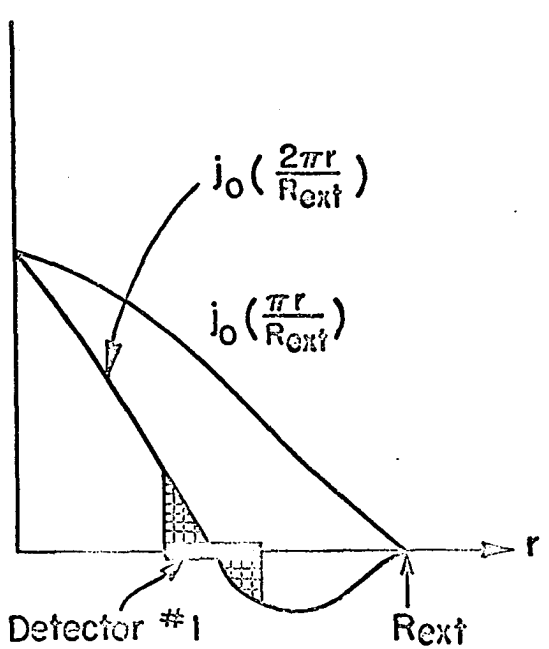

Figure 5.4.a. First and second harmonic in a sphere

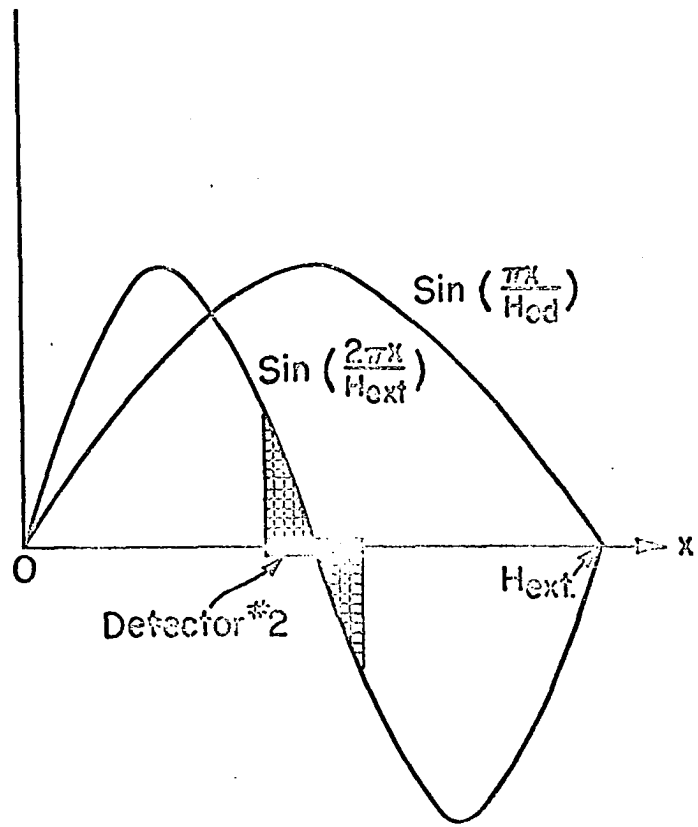

Figure 5.4.b. First and second harmonic in a slab

of its effective center. On the other hand, the net contribution to detector number 1 is non-zero since the two areas are not equal. This implies, therefore, that detector number 2 at that position behaves like a point detector; while number 1 retains the response of its effective length.

The other possible explanation is the inefficiency of the expansion form given by 5.2. However, it will be found later that the method of this section gives fundamental decay constants compatible with both theoretical and experimental results obtained by other authors.

In either case, it should not be taken for granted that these oscillations are inherent in the character of the higher amplitudes and, accordingly, that they describe the traveling wave phenomenon discussed before. Rather, there is a belief that if the expansion 5.2 is proper, these oscillations are mere contaminations, the degree of which depends on the order of the amplitude and the size of the sphere. In support of this idea is the fact that it is possible to isolate a portion of the oscillating harmonic amplitude that decays exponentially with decay constant characteristic of the given harmonic.

The data for the harmonic amplitudes, or selected portions thereof, were then analyzed by means of the "Cornell Method" (10) assuming that, for the kth channel of width Δt:

$$A_i(t_k) = A \exp[-\lambda_i k(\Delta t)] \qquad (5.5)$$

where A is a constant and λ_i is the presumed decay constant of the ith harmonic. The method is summarized in that, for n channels such that n/3 = b is an integer, λ_i is given by

$$\lambda_i = -\frac{1}{b\Delta t} \ln \frac{\sum_{k=b+1}^{2b} |A_i(t_k)| - \sum_{k=2b+1}^{3b} |A_i(t_k)|}{\sum_{k=1}^{b} |A_i(t_k)| - \sum_{k=b+1}^{2b} |A_i(t_k)|} \qquad (2.6)$$

The variance of the fundamental decay constant was calculated by separately analyzing successive portions of the n-channel data utilizing four overlapping series of (n-3) channels each (1-(n-3), 2-(n-2) and 4-n) or seven overlapping series of (n-6) channels each (1-(n-6), ..., 7-n). This procedure takes into account the random distribution of the original counts about their best fit.

In several cases there were uncertainties in the radial buckling along the z-axis as a result of the uncertainty in the water level at the neck of the sphere. In these cases more than one run was made with varying water level. The points of each run were treated separately using the above procedure.

Values of λ_0 for the four largest spheres are listed in Table 5.2 together with both the average and the corresponding radial bucklings along the z-axis. It should be noted that the values of the fundamental decay constants are for the z-direction unless it is otherwise stated. In calculating the

Table 5.2. Fundamental decay constants for the largest spheres. The space points used in the analysis are indicated

R_{av}[a] (cm)	$B^2_{g,av}$[a] (cm^{-2})	R_z[b]	$B^2_{g,z}$[b]	λ_0 ($sec.^{-1}$)	
				5 space points	11 space points
17.025 ± 0.005	0.03270	16.420 ± 0.008	0.0351	---	5706 (for B^2_{av}) 5910 (for B^2_z)
14.412 ± 0.005	0.04508	14.460 ± 0.006	0.04500	6452±207	6465±200
14.412 ± 0.005	0.04508	14.400 ± 0.05	0.04504	6457±215	6462±203
10.830 ± 0.004	0.07900	10.790 ± 0.05	0.07960	7825±157	---
10.830	0.07900	10.900 ± 0.05	0.07810	7798±165	
8.968 ± 0.003	0.1137	8.97 ± 0.03	0.1137	9069±240	---

[a] R_{av} and $B^2_{g,av}$ are the average radius and the average buckling respectively.

[b] R_z is the radius measured along the z-axis and $B^2_{g,z}$ is the corresponding buckling.

the buckling, the P_3 extrapolation distances (24) were used.

The decay constants for the higher harmonics are given in Table 5.3. For the sake of comparison, the theoretical values were calculated from

$$\lambda_i = \lambda_0 + [(i + 1)^2-1]D_o B^2_{g,z} - [(i + 1)^4-1]CB^4_{g,z} \quad (5.7)$$

where $B^2_{g,z}$ is the radial buckling along the z-axis, D_o = 38692 cm^2 $sec.^{-1}$, $V_o\Sigma_{ao}$ = 4876 $sec.^{-1}$ and C = 3618 cm^4 $sec.^{-1}$. These values are the P_1-L_1 values for the Nelkin's water (see Table 2.12). The results are also listed in Table 5.3 from which it is clear that both the theoretical and experimental results agree with each other within 9%.

2. Determination of the decay constants for small spheres

The method used here to separate the fundamental mode decay from the higher modes is based on the determination of the optimum source distance and the waiting time. The source distance is here defined as the distance between the target and the facing point on the surface of the sphere (see Figure 4.2). The ratio of this distance to the average radius of the given sphere will be referred to as the "normalized" source distance, s. Figure 5.5 is a plot of the ratio of the first and the second mode amplitude to the fundamental as a function of this distance. The plot is for a sphere with an average radius of 10.83 cm at the 8^{th} time channel.

Table 5.3. Decay constants of higher harmonics along the z-axis of the corresponding sphere

$B^2_{g,z}$ (cm^{-2})	λ_1 ($sec.^{-1}$)			λ_2 ($sec.^{-1}$)		
	Measured	Calculated	$\frac{\Delta\lambda_1}{(\text{measured})}$ %	Measured	Calculated	$\frac{\Delta\lambda_2}{(\text{measured})}$ %
0.0351	9425	10249	8.9	15324	16749	9.3
0.0450	11120	11723	5.4	18660	19951	6.9
0.0796	16020	16833	5.1	28500	30747	7.9
0.1137	20936	21739	3.8	37813	40753	7.8

According to this Figure, s is about 0.4, i.e., double the value reported for rectangular geometry (34). Data for other channels essentially gave similar results.

The waiting time is defined as that time required for a particular mode in a given sphere to decay to 1 percent of the fundamental amplitude. Use has been made of the data of the previous section to plot the waiting time t_w versus sphere average radius R_{av} in Figure 5.6. The curves were then interpolated to lower values of t_w. The Figure shows that for radii less than 6 cm the waiting time is practically zero. Since the first mode can be eliminated to an appreciable extent by placing the detector at half of the extrapolated radius, the waiting time would be mainly determined by the second mode amplitude.

The data obtained by the waiting time method were then fitted to the logarithmic difference of the counts in two

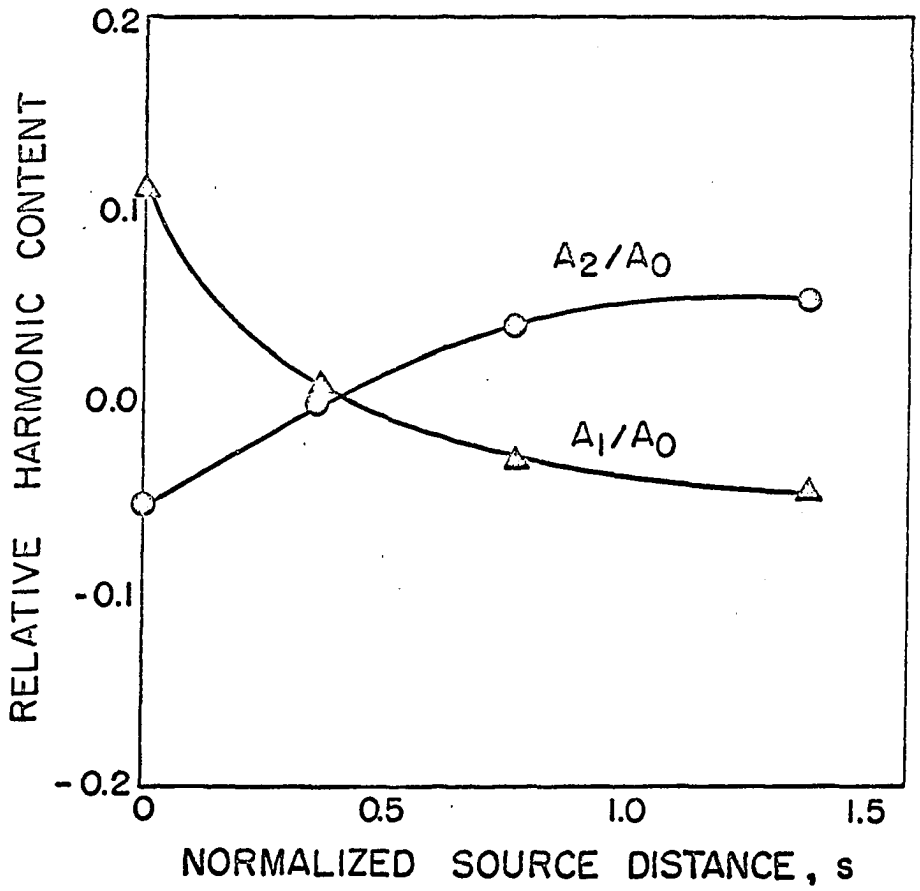

Figure 5.5. Relative harmonic content at the 8^{th} time channel as a function of normalized source distance, s

Figure 5.6. Experimental minimum waiting time versus average radius, R_{av}

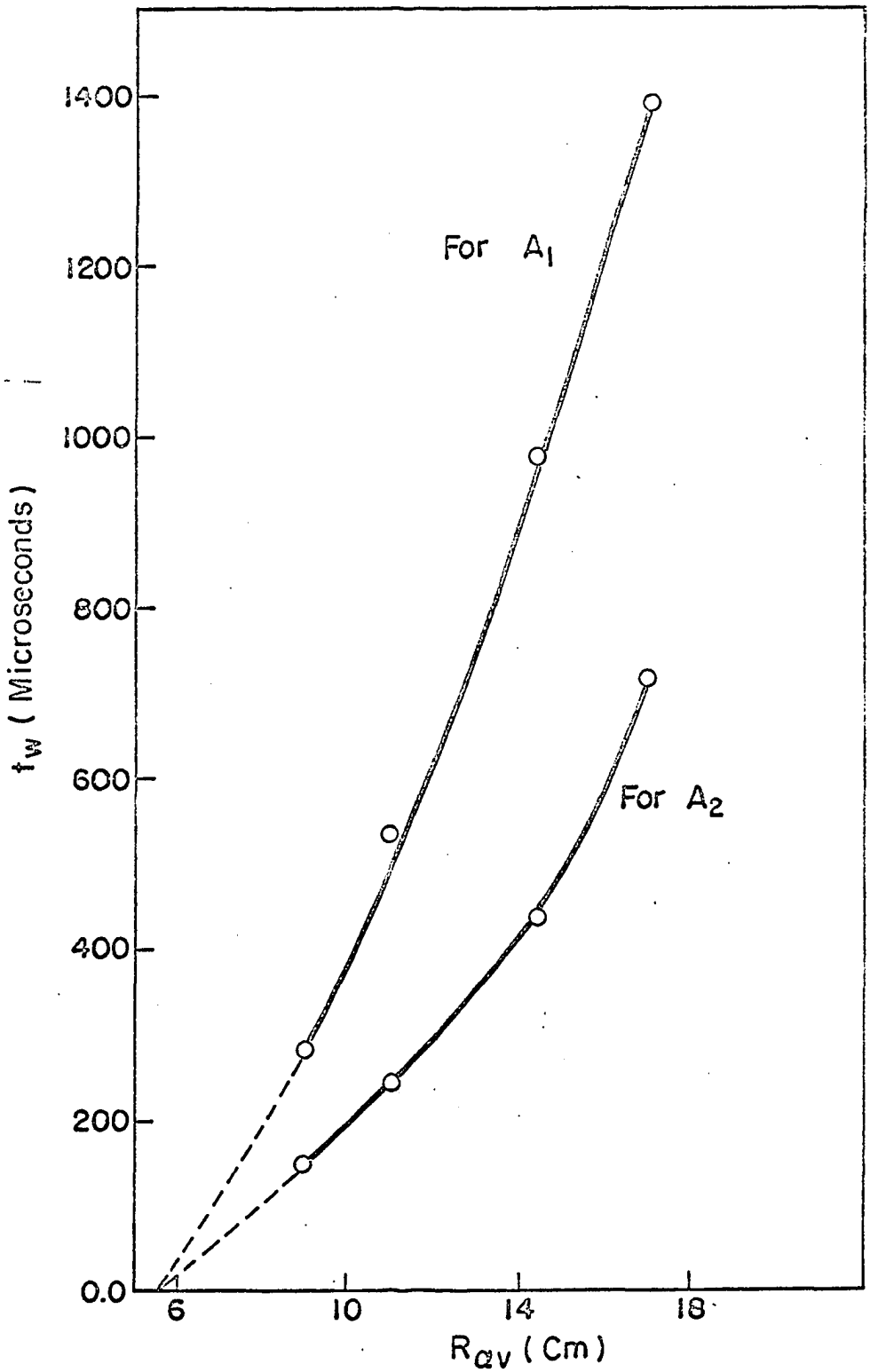
1400
1200
1000
800
600
400
200
0.0
t_w (Microseconds)
For A_1
For A_2
6
10
14
18
R_{av} (Cm)

successive time channels. If the number of counts in a given channel is of the form

$$N_n = A \exp(-\lambda_0 t_n) + BG \quad , \tag{5.8}$$

where BG is the background and assumed to be constant, then the difference between the n^{th} channel and the $(n + 1)^{th}$ channel will not contain the background. The logarithm of the difference is

$$\ln(N_n - N_{n+1}) = -\lambda_0 t_{n+1} + \ln(A(\exp(-\lambda_0 \Delta t)-1)) \tag{5.9}$$

The result is a straight line with a slope of λ_0.

The fundamental decay constants obtained by the above procedure for five small spheres are tabulated in Table 5.4 where $B^2_{g,av} = B^2_{g,z} = B^2_g$. The large variance in this table is probably due to the poor counting statistics for small systems.

3. Determination of the diffusion parameters

The usual fit of the experimental points to the function $\lambda_0 = f(B^2_g)$, i.e.,

$$\lambda_0 = V_o\Sigma_{ao} + D_oB^2_g - CB^4_g + OB^6 \tag{5.10}$$

is done here according to the following procedure (19): consider

Table 5.4. Fundamental decay constant for small spherical geometries

Radius[a] of the sphere, R (cm)	Buckling, B_g^2 (cm^{-2})	λ_0 ($sec.^{-1}$)
7.735 ± .003	0.1470	10633 ± 155
6.348 ± .004	0.2206	12896 ± 214
4.863 ± .001	0.3651	18239 ± 362
4.196 ± .0005	0.4810	22101 ± 460
3.553 ± .0003	0.6553	28050 ± 810

[a] $R = R_{av} = R_z$.

$$\sum_i W_i\lambda_0 = V_o\Sigma_{ao}\sum_i W_i + D_o\sum_i W_iB_g^2 + C\sum_i W_iB_g^4$$

$$\sum_i W_iB_g^2\lambda_0 = V_o\Sigma_{ao}\sum_i W_iB_g^2 + D_o\sum_i W_iB_g^4 + C\sum_i W_iB_g^6$$

$$\sum_i W_iB_g^4\lambda_0 = V_o\Sigma_{ao}\sum_i W_iB_g^4 + D_o\sum_i W_iB_g^6 + C\sum_i W_iB_g^8 \qquad (5.11)$$

where W_i is the inverse of the variance of λ_0 and $\sum_i$ denotes the summation over all the experimental points λ_0 and the corresponding bucklings. The coefficient matrix, A, is given by

$$A = \begin{bmatrix} \sum_i W_i & \sum_i W_iB_g^2 & \sum_i W_iB_g^4 \\ \sum_i W_iB_g^2 & \sum_i W_iB_g^4 & \sum_i W_iB_g^6 \\ \sum_i W_iB_g^4 & \sum_i W_iB_g^6 & \sum_i W_iB_g^8 \end{bmatrix} \qquad (5.12)$$

The inverse elements s_{lm} are obtained by taking the cofactor of lm and dividing by the determinant det(A).

$$s_{lm} = \frac{\text{cofactor of lm}}{\det(A)} \qquad l, m = 1, 2, 3$$

The inverse matrix is denoted by

$$A^{-1} = \begin{bmatrix} s_{11} & s_{12} & s_{13} \\ s_{21} & s_{22} & s_{23} \\ s_{31} & s_{32} & s_{33} \end{bmatrix} \tag{5.13}$$

$$V_o\Sigma_{ao} = s_{11} \sum_i W_i\lambda_0 + s_{12} \sum_i W_i\lambda_0 B_g^2 + s_{13} \sum_i W_i\lambda_0 B_g^4 \tag{5.14}$$

$$D_o = s_{21} \sum_i W_i\lambda_0 + s_{22} \sum_i W_i\lambda_0 B_g^2 + s_{23} \sum_i W_i\lambda_0 B_g^4 \tag{5.15}$$

$$C = s_{31} \sum_i W_i\lambda_0 + s_{32} \sum_i W_i\lambda_0 B_g^2 + s_{33} \sum_i W_i\lambda_0 B_g^4 \tag{5.16}$$

The corresponding standard deviations are given by:

$$d_{(V_o\Sigma_{ao})} = [s_{11} \sum_i W_i e_i^2/(N - 3)]^{1/2} \tag{5.17}$$

$$d_{D_o} = [s_{22} \sum_i W_i e_i^2/(N - 3)]^{1/2} \tag{5.18}$$

$$d_C = [s_{33} \sum_i W_i e_i^2/(N - 3)]^{1/2} \tag{5.19}$$

where N is the number of points used in the least-squares fit

and e_i = λ_0 (calculated) - λ_0 (observed)

It was felt that the use of W_i = 1 yields a more realistic set of parameters for these reasons. 1) Large geometries were not perfect spheres and the radius along the z-axis differs from the average radius. This difference was small for small geometries. 2) Large spheres had wide necks and the water levels at these necks were flat. Hence, there is an uncertainty in the effective center of the sphere. 3) A weighing factor equal to the inverse of the statistical variance of λ_0 tends to weigh more heavily the experimental points of large geometries.

The procedure was applied to the data given in Table 5.1 and 5.4. For spheres with more than one run only values of λ_0 that made the variance of C a minimum were retained. Table 5.5 summarizes the selected data for the best fit in the given range of buckling. Values of λ_0 for spheres where there is a large difference between the average geometric buckling $B^2_{g,av}$ and the radial buckling $B^2_{g,z}$ along the z-axis are omitted from this table. For the rest $B^2_{g,av} = B^2_{g,z} = B^2_g$. The results of the fit for various ranges of bucklings are summarized in the following:

1. Fitting range from 0.045 to 0.365 cm^{-2}.

   $V_o\Sigma_{ao}$ = (4.734 ± 0.036) x 10^3 $sec.^{-1}$

   D_o = (3.8892 ± 0.0442) x 10^4 $cm^2.$ $sec.^{-1}$

Table 5.5. Experimental values of the fundamental decay constant that give the best fit in the indicated buckling range

$B_g^2(cm^{-2})$	$\lambda_o(sec.^{-1})$
0.04504	6465
0.07960	7825
0.11370	9069
0.14700	10372
0.22060	13082
0.36510	18323

$C = (4.590 \pm 1.034) \times 10^3\ cm^4.\ sec.^{-1}$

2. Fitting range from 0.0796 to 0.365 cm^{-2}:

$V_o\Sigma_{ao} = (4.767 \pm 0.068) \times 10^3\ sec.^{-1}$

$D_o = (3.8570 \pm 0.0736) \times 10^4\ cm^2.\ sec.^{-1}$

$C = (3.940 \pm 1.600) \times 10^3\ cm^4.\ sec.^{-1}$

3. Fitting range from 0.045 to 0.2206 cm^{-2}:

$V_o\Sigma_{ao} = (4.718 \pm 0.065) \times 10^3\ sec.^{-1}$

$D_o = (3.9209 \pm 0.1110) \times 10^4\ cm^2.\ sec.^{-1}$

$C = (5.840 \pm 4.039) \times 10^3\ cm^4.\ sec.^{-1}$

It is clear from these results that, at the time $V_o\Sigma_{ao}$ and D_o are not sensitive to the range of fitting, C and its

associated standard error show a large variation. This reflects the usual inherent difficulty of determining the curvature of an unknown function defined by a small set of experimental points having finite standard deviation.

Values of the microscopic absorption cross section for hydrogen calculated on the basis of V_o = 220,000 cm. $sec.^{-1}$ are as follows:

σ_a^H = 321 ± 2.46 mb , fitting range : 0.045-00.365 cm^{-2}.

σ_a^H = 323 ± 4.7 mb , fitting range : 0.0796-0.365 cm^{-2}.

The diffusion length L is deduced from the parameters by using the relation

$$L^2 = -\frac{1}{B_g^2}$$

where B_g^2 is found for the stationary state by solving equation 5.10 with $\lambda_0 = 0$. The result is

$$L^2 = \frac{D_o}{V_o \Sigma_{ao}} \left(1 + \frac{V_o \Sigma_{ao} C}{D_o^2}\right) \qquad (5.20)$$

When $V_o \Sigma_{ao} C \ll D_o^2$ equation 5.20 should yield values of L directly comparable to values measured by stationary methods. The values of L for two ranges of fitting are as follows:

L = 2.887 ± 0.024 cm , fitting range: 0.045 - 0.365 cm^{-2}.

L = 2.860 ± 0.030 cm , fitting range: 0.0796 - 0.365 cm^{-2}.

Table 5.6 shows a comparison between these results and those obtained by other investigators. The values of the diffusion cooling constant obtained here are lower than that obtained by Lopez and Beyster (34) and higher than that obtained by Dio (20). The relatively large standard deviation associated with the present values of C are expected on the basis of the inherent difficulty of determining the spherical parameters and hence the expected uncertainty of buckling. The values of the other parameters are in fair agreement with those reported in Table 5.6.

The fit of the experimental data to the expression

$$\lambda_0 = V_o\Sigma_{ao} + D_oB_T^2 - CB_T^4 \qquad (5.21)$$

was also tried. The values of B_T^2 were calculated according to equation 2.52 by using

$D_o = 38570\ cm^2\ sec^{-1}$ (from the fit to $\lambda_0 = f(B_g^2)$)

$M_2 = 3.34\ cm^{-1}$ (for Nelkin's water)

Table 5.7 shows a comparison between the values of the parameters obtained from this fit and those from the previous one. This table shows:

1. Within the experimental errors, the values of $V_o\Sigma_{ao}$ and D_o are essentially the same for the two fits.
2. There is improvement in the standard error of C.
3. The value of C from the new fit is as high as 1.5 times the value obtained from the other fit.

Table 5.6. Comparison between neutron diffusion parameters for water at 22°C by pulsed method.

Reference	$D_o(cm^2sec^{-1})$	$C(cm^4sec^{-1})$	$\sigma_a^H(mb)$	L(cm)	Range of B_g^2
Present work	38892 ± 442	4590 ± 1034	321 ± 2.46	2.887 ± 0.024	0.045 - 0.365
Present work	38570 ± 736	3940 ± 1600	323 ± 4.7	2.860 ± 0.03	0.0796-0.3651
Lopez and Beyster (34)	36700 ± 370	4852 ± 800	---	2.795 ± 0.016	0.014 - 0.018
Scott et al. (46)	38500 ± 800	---	320 ± 8.0	2.850 ± 0.050	0.006 - 0.018
Antonov et al. (1)	35000 ±1000	4000 ± 1000	329 ±10.0	2.700 ± 0.100	0.09 - 0.93
Dio (20)	35450 ± 600	3700 ± 700	328 ± 6.0	2.715 ± 0.06	0.093 - 0.87

Table 5.7. Comparison between the diffusion parameters obtained from the fit to $\lambda_0 = f(B_T^2)$ and those from $\lambda_0 = f(B_g^2)$ for the range of buckling from 0.0796 to 0.3651 cm^{-2}

	$\lambda_0 = f(B_T^2)$	$\lambda_0 = f(B_g^2)$
$V_o\Sigma_{ao}$ (sec^{-1})	4770 ± 68	4767 ± 68
D_o ($cm^2 . sec^{-1}$)	38493 ± 722	38570 ± 736
C ($cm^4 . sec^{-1}$)	5861 ± 1540	3940 ± 1600

The speculation that follows from these observations is that if the experimental values of the decay constant previously reported are fitted to equation 5.21 a reduction in the uncertainty of the diffusion cooling constant might be achieved.

The question to be imposed at this point is, why the theoretical value of C obtained from the same expression does not agree with the value of the fit. The explanation for this is the fact that in calculating C its g factor given according to equation 2.47 was taken to be 1.776. This value is for two Laguerre polynomials. If higher polynomials could have been taken into consideration, g would have been equal to 2.004, as reported by Perez and Uhrig (42), and one would have obtained a theoretical value of C more close to the value of the fit. Another reason for the discrepancy is the uncer-

Figure 5.7. Least squares fit to data of the fundamental decay constant in spherical geometry

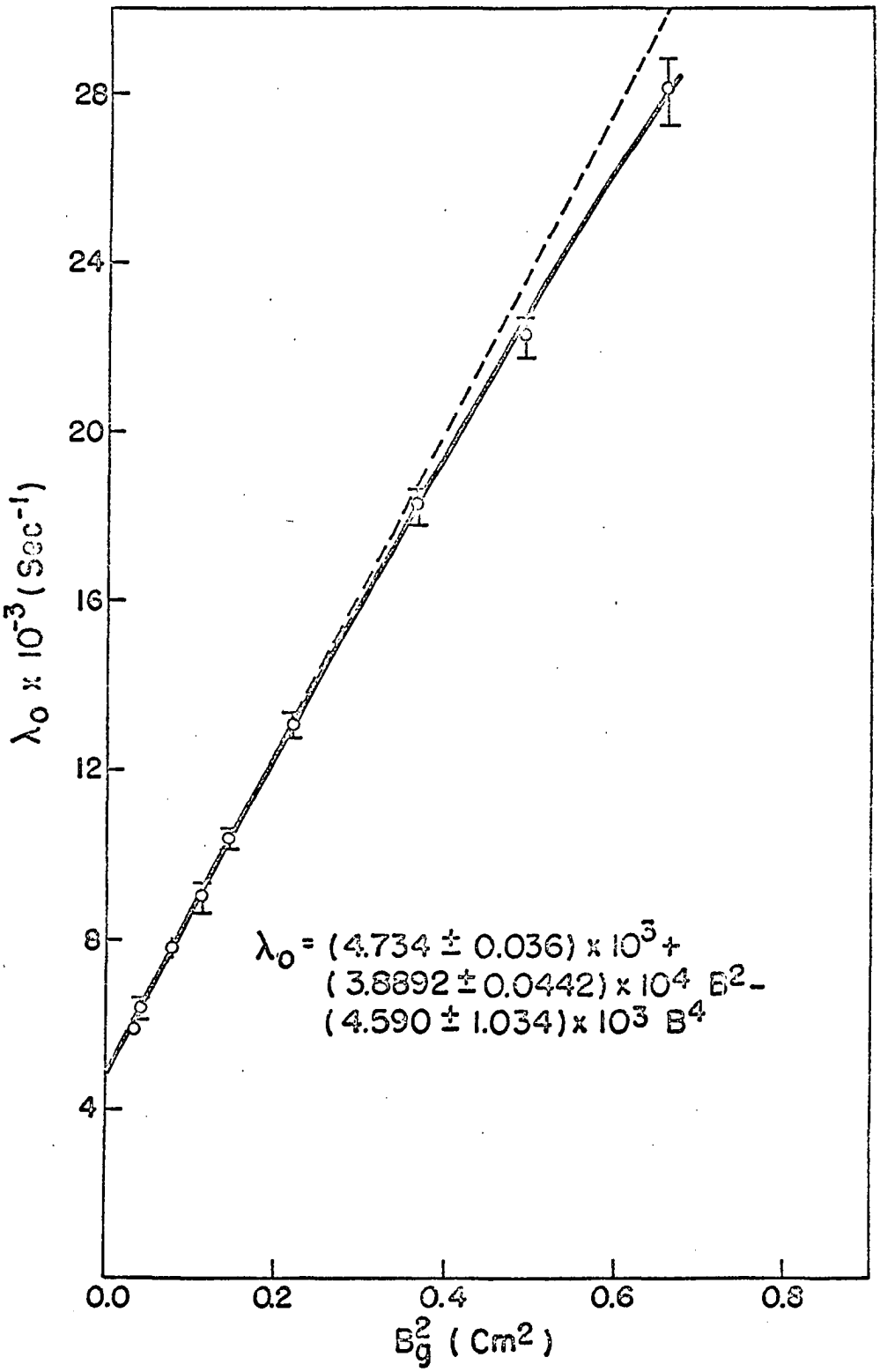
28
24
20
16
12
8
4
$\lambda_o \times 10^{-3}$ (Sec^{-1})
$\lambda_o = (4.734 \pm 0.036) \times 10^3 +$
$(3.8892 \pm 0.0442) \times 10^4 B^2 -$
$(4.590 \pm 1.034) \times 10^3 B^4$
0.0
0.2
0.4
0.6
0.8
B_g^2 (Cm^2)

tainty of M_2 and the low order of P_N approximation used in deriving B_T^2. To correct for the last factor one should use a more realistic model of the Boltzmann's equation like the P_3 approximation.

The disadvantage of the new fit, therefore, is the strong link between theory and experiment and the fact that accurate theoretical predictions are prerequisite for the experiment. To put it more simply, the new fit requires accurate values of M_2 and this so far is obtained from theoretical models.

B. Extrapolation Distances of Pulsed Neutron Experiments

The effect of the uncertainty in the extrapolated end points on the diffusion parameters extracted from pulsed source experiments was emphasized in earlier work (24, 34) and it was clear that more accurate measurements, especially in spherical geometries, were required. Beckurts (2) stated this need quite explicitly. The differences reported between extrapolated end points obtained by flux plotting in pulsed and steady state experiments also called for further investigation. Early pulse measurements in water at about 20°C (8, 18) gave values in the range 0.4 - 0.46 cm which are well above the upper limits now indicated by steady state values (in the range 0.32 - 0.35 cm) (56). To help in resolving these inconsistancies further measurements have been

carried out according to the following procedure:

A computer program was written to perform the least squares fitting of the extrapolation distance data to equation 5.4. A trial value, $d^{(0)}$, of the extrapolation distance, d, was first found graphically from the flux plots. Values of d in the range from $(d^{(0)} - 0.5)$ to $(d^{(0)} + 0.5)$ cm were tried with an increment of 0.05 cm. In each case the amplitudes (A_i), the corresponding flux at the various space points and the sum (S) of the squares of the residuals were computed. The value of d corresponding to the minimum of the function $S = f(d)$ (see Figure 5.8) was as the best fitted value for the given increment d. This value was then taken for $d^{(0)}$ and the procedure repeated with smaller increment until the desired accuracy was reached.

To take into account the statistical fluctuation of d with time, the method has been applied to data of five different spheres recorded at various times after the end of the fast neutron burst. The results of fitting to three harmonics are given in Table 5.8. A unit weighing factor was used in the analysis. The results generally show a relatively large standard deviation of d at both short and long time after the initiation of the neutron pulse. In the former case the deviation could be accounted for by the insufficiency of the three harmonic fit and the random distribution of the count rate about the best fit. The deviation

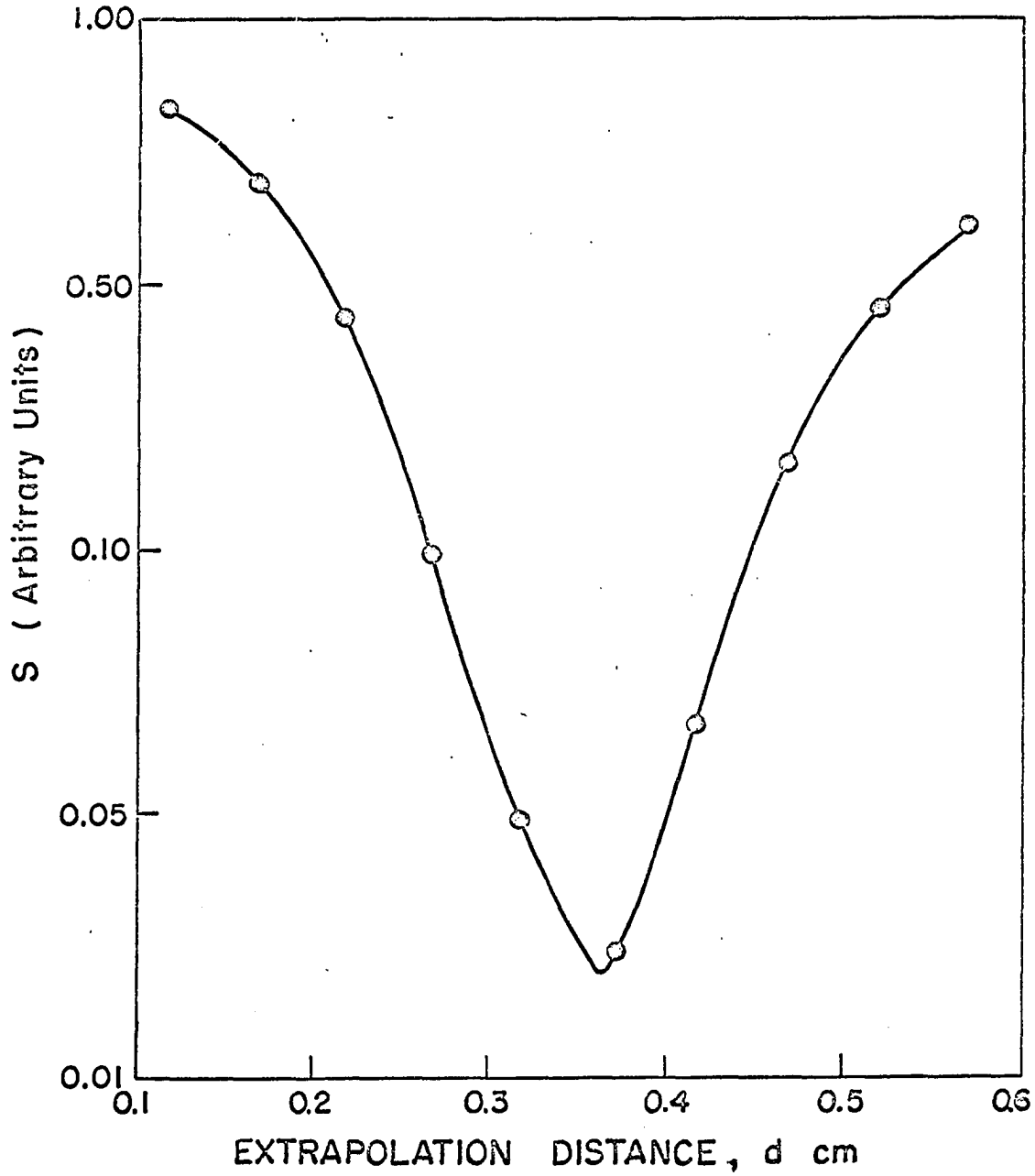

Figure 5.8. Variation of the sum of the squares of the residuals with the trial value of the extrapolation distance for a sphere with R_z = 14.46 cm

Table 5.8. Extrapolation distances for 3 harmonic fit

Number of sphere	R_z (cm)	Number of harmonics	Number of space points	Channel number	A_0	A_1	A_2	$Sx10^{-4}$	d (cm)
1	16.42	3	11	18	18179	-1481	212	13.94	.400
		3	11	24	5340	- 390	- 75	9.98	.415
		3	11	25	4126	93	-127	0.40	.380
2	14.46	3	11	14	22308	- 717	-152	16.43	.291
				15	17894	- 506	-158	6.27	.333
				16	13934	- 244	- 82	4.65	.431
				20	5642	- 74	- 74	3.08	.373
3	10.79	3	5	13	7070	62	-167	1.17	.365
				14	5311	27	- 11	1.37	.338
				15	3833	172	- 37	0.98	.347
				16	2986	148	- .8	1.20	.356
4	8.97	3	5	10	8083	21	36	.054	.340
				11	5625	200	73	.36	.372
				12	4124	201	- 43	.016	.346
				13	3015	- 28	20	.005	.348
				14	2152	16	2.5	.023	.335
				15	1496	92	- 48	.003	.350
5	7.735	3	5	5	37153	-2030	-1436	2.44	.352
				7	13900	- 466	302	4.72	.305
				8	11494	-1306	358	2.15	.370

at longer times would be mainly due to the statistical fluctuation of the count rate data.

To account for the effect of higher harmonics, the same data were fitted to an increasing number of modes until consistent results were obtained. These results are listed in Table 5.9. The standard deviation shown is mainly statistical in nature and does not account for the uncertainty in the value of the radius along the z-axis.

The boundary effect on d was not investigated. However, the space distribution taken for each sphere was such that points beyond a distance from the boundary of the order of one cm were excluded from the analysis. Hence, the boundary effect on the reported values is expected to be negligible.

Recently Walker et al. (56) measured d from flux distribution in pulsed cubical systems. They obtained values of

$$0.38 \pm 0.04 \text{ cm} \qquad \text{for} \qquad B_g^2 = 0.087 \text{ cm}^{-2}$$

and

$$0.35 \pm 0.02 \text{ cm} \qquad \text{for} \qquad B_g^2 = 0.25 \text{ cm}^{-2}$$

These values of d are in agreement with the present results.

Table 5.9. Extrapolation distances for water in spherical geometries at 22°C. The number of space points and harmonics used in the analysis are indicated

Number of sphere	R_z (cm)	R_{av} (cm)	$B^2_{g,z}$ (cm^{-2})	Number of space points	Number of harmonics	$d(b^2_{g,z})$ (cm)
1	16.420 ± 0.08	17.025 ± 0.005	0.0349	11	5	0.392 ± 0.05[a]
2	14.460 ± 0.060	14.412 ± 0.005	0.0449	11	5	0.356 ± 0.45
3	10.790 ± 0.050	10.830 ± 0.004	0.0794	5	4	0.352 ± 0.012
4	8.970 ± 0.030	8.968 ± 0.003	0.1129	5	4	0.347 ± 0.013
5	7.740 ± 0.060	7.735 ± 0.003	0.1510[b]	5	3	0.338 ± 0.033

[a]The error does not include the uncertainty in the radius along the z-axis. It is mainly due to the statistical fluctuation of the value of d with time.

[b]This value was calculated using the value of R_{av} = 7.735 cm.

VI. SUMMARY

A study of neutron thermalization in a sphere of light water was carried out both theoretically and experimentally. The theoretical aspect of the problem was dealt with utilizing the P_1-L_1 approximation. The space dependence was represented by the spherical Bessel functions of zeroth-order. The use of this representation made it possible to avoid the Fourier transform technique which strictly applies to infinite media. The study employed values of the thermalization parameter, M_2, corresponding to the scattering kernels of Mass-1, Mass-18, Brown & St.John and Nelkin. When the time decay constant, λ, was plotted versus the spherical Bessel function variable, B^2, two limiting values of B^2 were obtained. One was $B^2_{1,max}$, below which all decay constants were real and the other one was $B^2_{2,max}$, beyond which no real decay constants existed.

The curve describing the fundamental time eigenvalue in the (λ, B^2) plane had a negative curvature at the origin for all values of M_2 investigated. The amplitude of the curvature increased with decreasing value of M_2. For Nelkin's water, the curvature was in agreement with the experimental results and in disagreement with the findings of Travelli and Calame (52) obtained from a 4-group treatment in the P_1 approximation. These authors found a positive

curvature for the Radkowsky kernel.

The sensitivity to M_2 was also observed in the limiting value, λ_{lim}, of the fundamental decay constant obtained graphically from the (λ, B^2) plots. The values obtained were higher than the limit reported by Corngold and Michael (12) and lower than that obtained by Purohit et al. (45) for the Doppler corrected kernel. λ_{lim} for the Mass-1 kernel was in excellent agreement with that obtained by Ohanian and Daitch (41).

The expansion of the fundamental eigenvalue, λ_0, in power series of B^2 was shown to have a radius of convergence that covers all the buckling ranges available to experiments. On the other hand, λ_1 (the first eigenvalue) had a very small radius of convergence and its expansion in power series of B^2 was shown to be questionable even for large geometries.

The "buckling-dependence" of the diffusion cooling coefficient in the P_1 approximation was suppressed by expanding the fundamental decay constant in power series of B_T^2, a slowly varying function of B^2. The difference between B_T^2 and B^2 was correlated to the difference between the P_1 and the diffusion approximation in the time dependent case. Values of the decay constant obtained from the function $\lambda_0 = f(B_T^2)$ differed by no more than fractions of percent from the corresponding values obtained from the original polynomial given by 2.37.

The thermalization time constant was obtained from the

limiting case of the transcendental quadratic equation in λ_1, as $B^2 = \Sigma_{ao} = 0$. Two cases were considered. A case in which the transport mean free path varied as $\sqrt{E}$ and another in which λ_{tr} was constant. The values of t_{th} for the latter case were about 4 times as large as the corresponding values for the energy dependent case. The result for Nelkin's scattering kernel was in good agreement with the experimental result reported by Möller and Sjöstrand (37).

The concept of buckling for spherical water systems was investigated and found to be valid as long as the fundamental decay constant, K_0, is less than about twenty thousands times the thermalization parameter, M_2. This concept broke down for the mass-18 kernel at values of B^2 greater than 0.5 cm^{-2}.

The neutron spectrum of the asymptotic distribution presented in this work exhibited the diffusion cooling phenomenon shown in the results reported by Clendenen (9) for the high order P_N approximation.

The space transient near the boundary and its effect on the extrapolation distance were studied. The transient effect was negligible beyond a distance from the boundary of the order of 0.5 cm. At the boundary the effect was determined by the neutron spectra.

A calculation of the extrapolation distances for spherical geometry showed that the Marshak's boundary condition used for the outer boundary is not suited for this type of con-

figuration and that it is desirable to work the problem in the "equivalent" slab geometry that suited the indicated boundary condition for the given order of the P_N approximation.

Pulsing data for nine spheres with a buckling range of 0.0351 - 0.6553 cm^{-2} were obtained and analyzed by the method of least squares (32). The amplitudes of higher harmonics showed with time an oscillatory behavior. A possible explanation for this phenomenon was offered.

The data for the fundamental decay constant were fitted to two functions. $\lambda_0 = f(B_g^2)$ and $\lambda_0 = f(B_T^2)$. Within the experimental errors, values of the absorption cross section and the diffusion coefficient D_o obtained from the two fits were almost identical. On the other hand, the diffusion cooling coefficient C obtained from the first fit was much lower than that of the second fit. The new fit gave a relatively improved standard deviation of C.

The extrapolation distances for five spheres were obtained by a least squares fit to the flux distribution in the pulsed experiments. The effect of higher harmonic contamination on the magnitude of the extrapolation length and the rule of the flux variation with time on the fitted values were considered in the analysis.

VII. CONCLUSIONS

1. Based on a comparison between the theoretical considerations of this work and that of Travelli and Calame (52), it is concluded that the P_1-L_1 approximation, with a realistic scattering kernel for light water, predicts the time behavior in pulsed neutron experiments more accurately than few-groups P_1 approximation and that the diffusion cooling phenomenon is best exhibited in the continuous energy representation as was anticipated by Daitch and Ebeoglu (15).
2. In case of light water, the usual expansion of the fundamental decay constant is justifiable on the basis that the value of buckling beyond which a travelling wave phenomenon occurs is of the order of 6 cm^{-2} (or even higher (15)). This value covers all the experimental ranges of interest. The same is not equally applicable to the first eigenvalue, a matter that leads to doubting the method of Purohit (43) in expanding this constant in a power series of B^2.
3. Although the diffusion and the P_1-L_1 approximations might be identical in the time-independent case, they are different from each other when the time dependence is retained. This difference can be correlated with that one between the geometric buckling and the transport buckling

introduced in this thesis.

4. The concept of buckling for a spherical geometry in the energy dependent case is valid as long as the asymptotic region is well established. This is not possible for small systems described by the Mass-18 gas kernel.

5. The sharp variation of the effective buckling and the effective average energy of neutrons in pulsed spheres is due to the diffusion cooling phenomenon in finite media of light water as a result of the energy dependence of the transport mean free path.

6. For reliable values of the extrapolation distances obtained from pulsed spheres one must take into account:

   i. The boundary effect due to the transient distribution. The effect of this transient is negligible for space points far from the boundary by distances of the order of 0.5 cm.

   ii. The statistical variation of the extrapolation distance with time. This could lead to large errors especially at long times after the initiation of the neutron pulse.

   iii. Effect of higher harmonics which could be serious for large geometries.

   In addition, the number and distribution of the space points used in the analysis.

7. A BF_3 detector at a zero of a given higher harmonic might

behave as a point detector in multidimensional systems; while in a sphere it does not behave the same. This is because the count rate per unit length varies along the effective length in case of spherical geometry. As a result, a detector in a sphere is very sensitive to any fluctuation that might occur with time in the flux distribution. A unique feature that has been observed in pulsed spheres is the oscillatory behavior of the amplitudes of higher harmonics with time. The oscillations contribute to the difficulty in determining higher decay constants. Another inherent difficulty with these experiments is the determination of the effective center of the sphere. This results mainly from the neck effect. The water level at the neck is flat especially if the neck is wide. Hence, the upper and lower halves of the sphere are not symmetric. The experiments also depend strongly on the exact determination of the effective center of the detector. Any uncertainty in finding its location is reflected in the radial buckling. In general, a successful experiment in spherical geometry requires:

i. Exact location of the effective center.

ii. A small BF_3 detector.

iii. A sphere for which the average radius is very close to the radius as measured along the z-axis. This, in turn, depends on the degree of the sphericity of the body and the diameter of the neck.

VIII. LITERATURE CITED

1. Antonov, A. V., et al. A study of neutron diffusion in beryllium, graphite and water by the impulse method. Intern. Conf. Peaceful Uses of Atomic Energy, Geneva, Proc. 5: 3. 1955.

2. Beckurts, K. H. Transient effects in space, time and energy. Brookhaven Conf. on Neutron Thermalization Proc. 3: RE-1. 1962.

3. Beyster, J. R., et al. Differential neutron scattering from hydrogenous moderators. U.S. Atomic Energy Commission Report GF-92951 (General Atomic Div., General Dynamics Corp., San Diego, Calif.). 1965.

4. Beyster, J. R., et al. Integral neutron thermalization. U.S. Atomic Energy Commission Report GF-4659 (General Atomic Div., General Dynamics Corp., San Diego, Calif.). 1964.

5. Beyster, J. R., et al. Measurements of neutron spectra in water, polyethylene, and zirconium hydride. Nuclear Science and Engineering 9: 168. 1961.

6. Brown, H. and St.John, D. Neutron energy spectra in water. U.S. Atomic Energy Commission Report DP-64 (Dupont de Nemours(E.I) & Co., Wilmington, Del.). 1956.

7. Calame, G. P. Diffusion parameters of water for various scattering kernels. Nuclear Science and Engineering 19: 189. 1964.

8. Campbell, E. C. and Stelson, P. H. Measurement of thermal-neutron relaxation times in subcritical systems. U.S. Atomic Energy Commission Annual Report ORNL-2204 (Oak Ridge National Lab., Tenn.). 1956.

9. Clendenen, W. W. Temperature dependence of neutron-pulsed parameters in water. Nuclear Science and Engineering 18: 3516. 1964.

10. Cornell, R. G. A new estimation procedure for linear combinations of exponentials. U.S. Atomic Energy Commission Annual Report ORNL-2120 (Oak Ridge National Lab., Tenn.). 1956.

11. Corngold, N. and Michael, P. Some transient phenomena in thermalization; I. Theory. Nuclear Science and Engineering 19: 80. 1964.

12. Corngold, N. and Michael, P. Some transient phenomena in thermalization; II. Implications for experiment. Nuclear Science and Engineering 19: 91. 1964.

13. Corngold, N., Michael, P., and Wollman, W. The time decay constants in neutron thermalization. Brookhaven Conf. on Neutron Thermalization Proc. 4: 1103. 1962.

14. Corngold, N., Michael, P., and Wollman, W. The time decay in neutron thermalization. Nuclear Science and Engineering 15: 13. 1963.

15. Daitch, P. B. and Ebeoglu, D. B. Transients in pulsed moderators. Brookhaven Conf. Neutron Thermalization Proc. 4: 1132. 1962.

16. Davison, B. Neutron transport theory. Oxford Press, London, England. 1957.

17. De Jurene, J. A. Spectral correction analysis of pulsed neutron diffusion parameters. International Atomic Energy Agency Vienna Conf. on Pulsed Neutron Research 1: 323. 1965.

18. De Jurene, J. A., Stookberry and Caroll, E. E. Measurements of extrapolation lengths in pulsed water systems. Brookhaven Conf. on Neutron Thermalization Proc. 3: 895. 1962.

19. Deming, W. E. Statistical adjustment of data. 1st ed. New York, John Wiley and Sons, Inc. 50-55. 1946.

20. Dio, W. H. Über untersuchungen der diffusion thermischer neutronen in wasser und paraffin mit einer gepulsten quelle. Nukleonik 1: 13. 1958.

21. Egelstaff, P., Cocking, S., Royston, R., and Thorson, I. The thermal neutron scattering law for light and heavy water. International Atomic Energy Agency Vienna Conf. on Inelastic Scattering Paper IS/P/10. 1960.

22. Egelstaff, P. and Schofield, P. On the evaluation of the thermal neutron scattering law. Nuclear Science and Engineering 12: 260. 1962.

23. Gelbard, E. M. Application of the simplified spherical harmonics equations in spherical geometry. U.S. Atomic Energy Commission Research and Development Report WAPD-TM-294 (Westinghouse Atomic Power Division-technical memorandum, Pitts.). 1962.

24. Gelbard, E. M. and Davis, J. A. The behavior of extrapolation distances in die-away experiments. Nuclear Science and Engineering 13: 237. 1962.

25. Goldman, D. and Federighi, F. A comparison of calculated and experimental thermal energy exchange cross sections. Am. Nucl. Soc. Trans. 4: 135. 1961.

26. Häfele, W. and Dresner, L. The theory of the diffusion cooling effect in homogeneous and heterogeneous assemblies. U.S. Atomic Energy Commission Annual Report ORNL-2842 (Oak Ridge National Lab., Tenn.). 124. 1959.

27. Honeck, H. C. The calculation of the thermal utilization and disadvantage factor in uranium/water lattices. Nuclear Science and Engineering 18: 49. 1964.

28. Hughes, D. J. and Schwartz, R. B. Neutron cross sections. 2nd ed. BNL-325 (Brookhaven National Laboratory Upton, Long Island, N.Y.). 1958.

29. Inönu, E. The effect of boundary region in the determination of the extrapolation length from experiments with critical cylinders. U.S. Atomic Energy Commission Annual Report ORNL-3016 (Oak Ridge National Lab., Tenn.). 188. 1960.

30. Kazarnovsky, M. V., Stepanov, A. V., and Shapiro, F. L. Neutron thermalization and diffusion in heavy media. Intern. Conf. Peaceful Uses Atomic Energy, Geneva, Proc. 2: P/2148. 1958.

31. Koppel, J. Y. and Young, J. A. Neutron scattering by water taking into account the anisotropy of the molecular vibrations. Nuclear Science and Engineering 19: 412. 1964.

32. Lanczos, C. Applied analysis. New York, N.Y., Prentice-Hall, Inc. 1958. 1956.

33. Lapidus, L. Digital computation for chemical engineers. New York, McGraw-Hill Book Company, Inc. 1962.

34. Lopez, W. M. and Beyster, J. R. Measurement of neutron diffusion parameters in water by the pulsed neutron method. Nuclear Science and Engineering 12: 190. 1962.

35. Mani, G. S. The slowing down relaxation time for neutrons in moderators. J. Nuclear Energy 7: 220. 1958.

36. McMurray, H. L., Russel, G. J., and Brugger, R. M. Slow neutron scattering by water. Nuclear Science and Engineering 25: 248. 1966.

37. Möller, E. and Sjöstrand, N. G. Measurement of the slowing-down and thermalization time of neutrons in water. Ark. Fys. 27: 531. 1964.

38. Nelkin, M. S. The diffusion cooling of neutrons in a finite moderator. J. Nuclear Energy 8: 48. 1958.

39. Nelkin, M. S. The decay of a thermalized neutron pulse. Nuclear Science and Engineering 7: 210. 1960.

40. Nelkin, M. S. The scattering of slow neutrons by water. Phys. Rev. 119: 791. 1960.

41. Ohanian, M. J. and Daitch, P. B. Eigenfunction analysis of thermal neutron spectra. Nuclear Science and Engineering 19: 343. 1964.

42. Perez, R. B. and Uhrig, R. E. Propagation of neutron waves in moderating media. Nuclear Science and Engineering 17: 90. 1963.

43. Purohit, S. N. Neutron thermalization and diffusion in pulsed media. Nuclear Science and Engineering 9: 157. 1961.

44. Purohit, S. N. Neutron thermalization in a crystalline medium in incoherent approximation. Brookhaven Conf. on Neutron Thermalization Proc. 1: 203. 1962.

45. Purohit, S. N. and Sjostrand, N. G. Neutron thermalization parameters. International Atomic Energy Agency Vienna Conf. on Pulsed Neutron Research 1: 289. 1965.

46. Scott, F. R., Thomson, D. B., and Wright, W. Thermal neutron capture cross sections of hydrogen, boron and silver. Phys. Rev. 95: 582. 1954.

47. Shapiro, C. S. Time eigenvalues and degenerate kernels in neutron thermalization. U.S. Atomic Energy Commission Report BNL-8433 (Brookhaven National Lab., Upton, N.Y.). 1964.

48. Singwi, K. S. The theory of diffusion cooling of neutrons in a finite solid moderator assembly. J. Nuclear Energy 11: 19. 1959.

49. Star, E. and Koppel, J. Determination of diffusion hardning in water. Brookhaven Conf. on Neutron Thermalization Proc. 3: 1012. 1962.

50. Texas Nuclear Corporation. Instruction manual: Model 9400 neutron generator series. Austin, Texas, author. ca. 1964.

51. Texas Nuclear Corporation. Instruction manual for pulsing systems. Austin Texas, author. ca. 1964.

52. Travelli, A. and Calame, G. P. Thermal-neutron space-time decay constant in various order P_N approximations. Nuclear Science and Engineering 20: 414. 1964.

53. Vértes, P. Some problems concerning the theory of pulsed neutron experiments. Nuclear Science and Engineering 16: 363. 1963.

54. von Dardel, G. F. A study of the interaction of neutrons with moderating materials. Phys. Rev. 94: 1272. 1954.

55. von Dardel, G. F. and Sjöstrand, N. G. Diffusion parameters of thermal neutrons in water. Phys. Rev. 96: 1245. 1954.

56. Walker, J., Brown, J. B. C., and Wood, J. Extrapolation distances for pulsed neutron experiments. International Atomic Energy Agency Vienna Conf. on Pulsed Reutron Research 1: 49. 1965.

57. Weinberg, A. M. and Wigner, E. P. The physical theory of neutron chain reactors. University of Chicago Press, Chicago, Illinois. 1958.

58. Wigner, E. and J. Wilkins, Jr. Effect of temperature of the moderator on the velocity distribution of neutrons with numerical calculations for hydrogen as moderator. U.S. Atomic Energy Commission Report AECD-2275 (Division of Technical Information Extension, AEC). 1944.

59. Williams, M. M. R. Space-energy seperability in pulsed neutron systems. Brookhaven Conf. on Neutron Thermalization Proc. 4: 1331. 1962.

60. Wood, J. Time and space eigenvalues of the Boltzmann equation. International Atomic Energy Agency Vienna Conf. on Pulsed Neutron Research 1: 219. 1965.

61. Zinn, W. H. Diffraction of neutrons by a single crystal. Phys. Rev. 71: 752. 1947.

IX. ACKNOWLEDGMENT

I wish to express my gratitude to Distinguished Professor of Engineering Dr. Glenn Murphy, Head of the Department of Nuclear Engineering, for his continuous interest, helpfulness and criticism during the progress of this work.

X. APPENDIX

The computation in the theoretical chapter employed values of the total scattering cross section and the average of the scattering cosine obtained by McMurry *et al.* (36). Table A.1 and A.2 show a comparison between values for the McMurry-Russell model and those obtained from different sources.

Table A.1. Comparison of total scattering cross sections.[a]

		(bσ(E)/molecule)				
E(ev)	Observed[b]	MR[c]	N[d]	N-KY[e]	KY[e]	FG[f]
0.002	200	202	210	224	206	212
0.005	164	166	165	174	165	143
0.025	107	107	106	105	105	86.2
0.050	83	82	77.7	79	82	76.7
0.100	70.1	67.3	69.1	70	72	67.1
0.150	63.1	61.0	62.3	64	64	62.4

[a]The data were compiled by McMurry *et al.* (36).

[b]Data for E < 0.1 ev are from Hughes and Schwartz (28). For E > 0.1 ev, data are from Beyster *et al.* (3).

[c]MR refers to calculations by McMurry, Russell and Brugger (36).

[d]N refers to Nelkin's model.

[e]N-KY and KY refer to calculations by Koppel and Young (31) who used the Nelkin model and a model that corrects for the vibrational anisotropy.

[f]FG refers to the free gas model.

Table A.2. Comparison[a] of average scattering cosines ($\bar{\mu}$)

E(ev)	Observed	MR[a]	N	N-KY[b]	KY[b]	FG[c]
0.002	---	0.017	0.035	0.023	---	0.101
0.005	0.033	0.048	0.071	0.060	---	0.145
0.025	0.140	0.180	0.190	0.180	0.160	0.258
0.050	0.220	0.270	0.280	0.260	0.240	0.316
0.100	0.290	0.350	0.350	0.320	0.300	0.365
0.150	0.340	0.380	0.380	0.350	0.340	0.392

[a]MR refers to McMurry, Russell, and Brugger (36) who compiled the data in this table.

[b]N-KY and KY refer to calculations by Koppel and Young (31) who used the Nelkin model and a model that corrects for the vibrational anisotropy.

[c]FG refers to the free gas model.

From Table A.1, it is seen that the N and MR calculations agree well with the experimental data. The MR model uses higher effective masses, and this accounts for the $\bar{\mu}$ values being smaller than those of the N model.

The absorption cross section used in calculating the decay constant was obtained by Gelbard and Davis (24) for the Radkowsky kernel. In the quoted paper

$$V_o\Sigma_{ao} = 4876 \text{ sec.}^{-1} \text{ (for the } P_3 \text{ calculation).}$$